AD-A148 415 SECONDARY FLOW IN CASCADES(U) CINCINNATI UNIV OH DEPT 1/1
OF AEROSPACE ENGINEERING AND APPLIED MECHANICS A HAMED
JUN 84 UC-ASE-AH-101 AFOSR-TR-84-0912 AFOSR-80-0242
UNCLASSIFIED F/G 20/4 NL

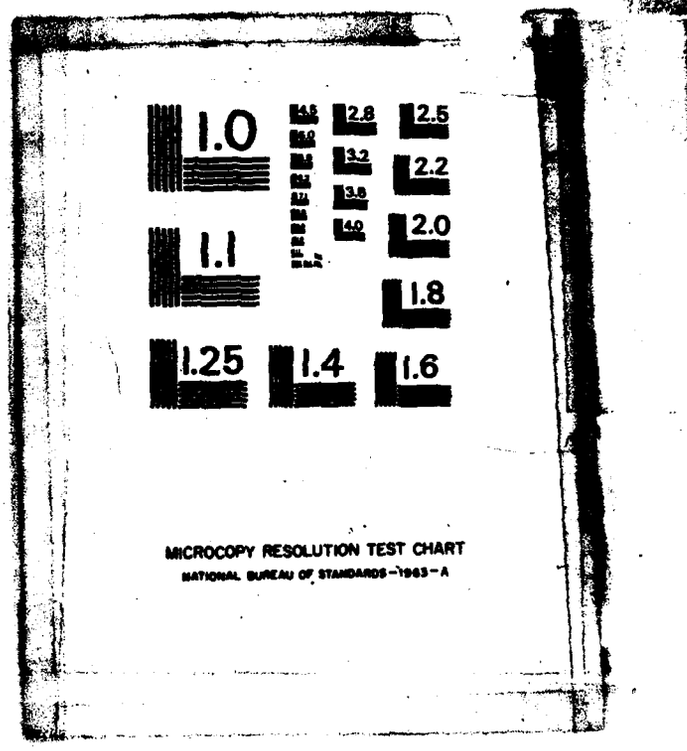
1.0
1.1
1.25
1.4
1.6
2.0
2.2
2.5
2.8
3.2
3.6
4.0
MICROCOPY RESOLUTION TEST CHART
NATIONAL BUREAU OF STANDARDS-1963-A

(12)

AFOSR-TR- 84-0912

SECONDARY FLOW IN CASCADES

A. Hamed

University of Cincinnati
Cincinnati, Ohio 45221

June 1984

Final Scientific Report
July 1, 1980 Through December 31, 1983

Grant AFOSR-80-0242

Prepared for

Directorate of Aerospace Sciences
Air Force Office of Scientific Research
Bolling Air Force Base
Washington, D.C. 20332

Approved for Public Release Distribution Unlimited

Qualified requesters may obtain additional copies from the Defense Technical Information Service.

UNCLASSIFIED

SECURITY CLASSIFICATION OF THIS PAGE (When Data Entered)

REPORT DOCUMENTATION PAGE	READ INSTRUCTIONS BEFORE COMPLETING FORM
1. REPORT NUMBER: AFOSR-TR- 84-0912	2. GOVT ACCESSION NO.: AD-A148415
3. RECIPIENT'S CATALOG NUMBER	
4. TITLE (and Subtitle): SECONDARY FLOW IN CASCADES	5. TYPE OF REPORT & PERIOD COVERED: Final Scientific Report; July 1980-31 Dec
	6. PERFORMING ORG. REPORT NUMBER: UC-ASE-AH-101
7. AUTHOR(s): A. Hamed	8. CONTRACT OR GRANT NUMBER(s): AFOSR-80-0242
9. PERFORMING ORGANIZATION NAME AND ADDRESS: University of Cincinnati, Cincinnati, Ohio 45221	10. PROGRAM ELEMENT, PROJECT, TASK AREA & WORK UNIT NUMBERS: 61102F, 2307/A4
11. CONTROLLING OFFICE NAME AND ADDRESS: Directorate of Aerospace Sciences, Air Force Office of Scientific Research, Bolling Air Force Base, DC	12. REPORT DATE: June 1984
	13. NUMBER OF PAGES: 80
14. MONITORING AGENCY NAME & ADDRESS (if different from Controlling Office)	15. SECURITY CLASS. (of this report): UNCLASSIFIED
	15a. DECLASSIFICATION/DOWNGRADING SCHEDULE

16. DISTRIBUTION STATEMENT (of this Report)

Approved for public release; distribution unlimited.

17. DISTRIBUTION STATEMENT (of the abstract entered in Block 20, if different from Report)

Unlimited

18. SUPPLEMENTARY NOTES

19. KEY WORDS (Continue on reverse side if necessary and identify by block number)

Secondary Flow, Rotational Flow, Three dimensional Flow
Internal Flow

20. ABSTRACT (Continue on reverse side if necessary and identify by block number)

This report covers research work which was conducted at the Univ. of Cincinnati over a period of three years to investigate the secondary flow phenomena in internal flow fields analytically and experimentally. The work was sponsored by the Air Force Office of Scientific Research and its main objective was to develop computational procedures for internal three-dimensional rotational flow fields and to obtain experimental measurements

DD FORM 1 JAN 73 1473 EDITION OF 1 NOV 65 IS OBSOLETE S/N 0102-LF-014-6601

UNCLASSIFIED (over)

SECURITY CLASSIFICATION OF THIS PAGE (When Data Entered)

Block 20 cont

of the three velocity components of the rotational flow in a curved duct with shear inlet velocity profile.

(cont on p 7)

FORWARD

This technical report covers an analytical and experimental [illegible] of secondary flow in curved passages for period [illegible] through December 31, 1983. The research was [illegible] by the Air Force Office of Scientific Research under [illegible].

The grant was monitored by Dr. James Wilson and Captain [illegible], Program Managers, Directorate of Aerospace [illegible], Air Force Office of Scientific Research, United States Air Force, Bolling Air Force Base, DC.

This Final Report supersedes all the previous interim [illegible] and includes all the technical papers both published and [illegible] preparation, which were written under this research [illegible].

ACKNOWLEDGEMENT

The principal investigator wishes to express sincere appreciation to the program managers Dr. J. Wilson and Capt. M. Francis for their continued interest, help to obtain equipment and valuable suggestions during the course of this work. With the help of this grant we have been able to develop our Laser Doppler Velocimeter and data aquisition systems for measureing complex internal flow fields.

TABLE OF CONTENTS

ABSTRACT

[illegible] measurements of the three velocity components were [illegible] for the flow in a curved rectangular duct with an [illegible] velocity profile. The results provide the needed information to develop analytical models of internal flows with strong secondary velocities. In addition, new analytical models [illegible] developed for predicting three dimensional rotational flows in curved passages, with inlet total pressure distortion. The agreement between the computed results and the experimental [illegible] suggest that these solutions model the important three dimensional flow field characteristics.

PROFESSIONAL PERSONNEL

A. Hamed	-	Professor
W. Tabakoff	-	Professor
S. Abdallah	-	Graduate Research Assistant
C. AbouGhantous	-	Graduate Research Assistant
C. Cheng	-	Graduate Research Assistant
M. Malak	-	Graduate Research Assistant
J. Cupito	-	Mechanic

ADVANCED DEGREES AWARDED

M.S. Degree to M. Malak, Thesis Title:

"An Investigation Of The Trailing Edge Condition In The Finite Element Solution Of Inviscid Flow In Cascade And Single Airfoil".

Ph.D. Degree to S. Abdallah, Dissertation Title:

"An Inviscid Solution For The Secondary Flow In Curved Passages".

PUBLICATIONS GENERATED UNDER THIS RESEARCH GRANT

[illegible], S., and Hamed, A., "Inviscid Solution for the Secondary [illegible] in Curved Ducts", AIAA Journal, Vol. 19, No. 8, 1981, pp. 993-[illegible].

[illegible], A., and Abdallah, S., "The Elliptic Solution of the Secondary Flow Problem," Journal of Engineering for Power, Vol. 105, 1983, pp. 330-335.

Hamed, A. and Liu, "Three-Dimensional Rotational Compressible Flow [illegible] in Variable Area Channels," AIAA Paper No. 83-0259, and [illegible] for publication in the AIAA Journal.

Hamed, A. and Abdallah, S., "Internal Three-Dimensional Viscous Flow Solution Using the Streamlike Function," AIAA Paper No. 84-1633, June 1984.

Hamed, A. and Abdallah, S., "The Elliptic Solution of 3-D Internal Viscous Flow Using the Streamlike Function," Recent Advances in Numerical Methods in Fluids Vol. III on Computational Methods in Viscous Flows, Pineridge Press, 1984.

Hamed, A. and Malak, M., "LDV Measurements of Three-Dimensional Flow Development in a Curved Rectangular Duct With Inlet Shear Profile," AIAA Paper No. 84-1601, June 1984.

RESEARCH OBJECTIVES

The main objective of this research work was to investigate the secondary flow phenomena analytically and experimentally. The experimental work was conducted to obtain measurements for the three velocity components using Laser Doppler Velocimeter (LDV) in a curved duct with inlet shear velocity profile. The purpose of the analytical work was to develop a formulation and a numerical procedure for the solution of internal three dimensional rotational flow fields.

ACCOMPLISHED WORK

Since all six technical papers, which were generated under AFOSR sponsorship are attached in this report, only the important contributions will be summarized here.

The first phase of the analytical work was aimed at developing a numerical computational procedure for inviscid incompressible rotational flow using a marching technique. The governing equations for the through flow velocity and vorticity components and for the streamlike functions in the cross-sectional planes were derived from the conservation of mass and momentum. The numerical results were obtained for the rotational flow field in a curved rectangular duct with constant cross sectional area and curvature, and compared with available experimental data. This work was published in the AIAA Journal, Vol. 19, No. 8, 1981, pp. 993-999 (Appendix 1).

The next step in the analytical work was to develop an elliptic numerical solution for internal inviscid rotational flows. The equation of conservation of mass for three dimensional flows was identically satisfied through the definition of three two-dimensional streamlike functions on sets of orthogonal surfaces. An iterative procedure was developed for the numerical solution of the governing equations for the through flow vorticity, total pressure and streamlike functions. The results of the numerical flow computations were compared with the experimental data and with the results of other analytical studies. This work was presented as ASME Paper No. 82-GT-242 at the 27th International Gas Turbine Conference in London, England, April 1982, and later published in the Journal of Engineering for Power, Vol. 105, 1983, pp. 530-535 (Appendix 2). The analysis was then generalized to compressible flows in curved ducts with variable cross-sectional area, using orthogonal curvilinear coordinates. The results of the numerical computations were compared with the experimental measurements in Stanitz duct. This work was presented as AIAA Paper Number 83-0259 at the AIAA 21st Aerospace Sciences Meeting at Reno, Nevada, January 10-13, 1983, (Apendix 3), and is accepted for publication in the AIAA Journal.

The final phase of the analytical study was to determine the suitability of the streamlike function vorticity formulation for obtaining elliptic solutions for three dimensional viscous flows. The results of the computations were presented for the three dimensional viscous flow in a square duct.

The computed results were found in agreement with the experimentally measured through flow velocity profiles. In addition the viscous elliptic influence was reflected in the computed axial and cross velocity components upstream of the duct inlet. This work was presented as AIAA Paper No. 84-1633, at the AIAA 17th Fluid Dynamics, Plasma Dynamics and Lasers Conference at Snowmass, Colorado June 25-27, 1984 (Appendix 4). It will also appear in Recent Advances in Numerical Methods in Fluids Volume III on Computational Methods in Viscous Flows, Pineridge Press, 1984, (Appendix 5).

The experimental work was conducted to obtain measurements of the three velocity components of the flow in a curved rectangular duct, using Laser Doppler Velocimeter. A nearly linear inlet shear velocity profile was produced using a grid of parallel wires with variable spacing, resulting in secondary velocities as high as 25% of the mean inlet velocity. This work was presented as AIAA Paper No. 84-1601 at the AIAA 17th Fluid Dynamics, Plasma Dynamics and Lasers Conference at Snowmass, Colorado, June 25-27, 1984 (Appendix 6).

(cont'd 1473B)

SUMMARY OF SIGNIFICANT RESULTS

Two formulations were developed for modeling inviscid three-dimensional rotational flow fields in curved passages. The first, for a very efficient marching solution with hyperbolic equations governing the development of through flow velocity and vorticity profiles along the duct. In the second formulation, a new approach was developed to satisfy the conservation of mass in three dimensional flows by defining two dimensional streamlike functions on fixed orthogonal surfaces in the flow field. The first formulation leads to a faster numerical solution in which the influence of the pressure field on the three dimensional flow can be sensed upstream only through the curvilinear coordinate system. The second formulation on the other hand is more complex since it models the elliptic influence of the three dimensional pressure field. Computer time savings are realized through the two dimensionality of the equations for the streamlike functions and their Dirichlet boundary conditions. Agreement between the computed results and the experimental data was very good in both cases.

The streamlike function vorticity formulation was also tested for its ability to model viscous flow effects and their elliptic influence in a square duct. The viscous elliptic solution predicted the influence of the duct on the flow field upstream of the inlet. In addition, the computed results were in very good agreement with the experimentally measured through

profiles inside the duct.

, LDV measurements of the three velocity components, in a curved rectangular duct with an inlet shear profile. The experiment was designed such that the measurements can be used to validate both viscous and inviscid codes for internal three dimensional flow fields with strong vortex and high secondary flow velocities due to inlet total pressure distortions. A grid of wires with variable spacing used to produce a nearly linear inlet velocity profile. Strong secondary velocities of magnitudes up to 25% of the mean inlet velocity, were measured in the curved duct.

TECHNICAL APPLICATIONS

The experimental data for the three velocity components in , obtained in this research work, provide detailed description of the secondary flow pattern. This information can be used in the development of appropriate flow models for the mathematical analysis of internal flow. In addition, the presented analytical work can be used in both inviscid and viscous three dimensional flow computations to model the various secondary flow generating mechanisms in turbomachines.

Appendix 1

Inviscid Solution for the Secondary Flow in Curved Ducts

AIAA 80-1116R
[redacted] Solution for the Secondary Flow in Curved Ducts

S. Abdallah and A. Hamed

Reprinted from AIAA Journal
Volume 19, Number 8, August 1981, Page 983

AMERICAN INSTITUTE OF AERONAUTICS AND ASTRONAUTICS • 1290 AVENUE OF THE AMERICAS • NEW YORK, NEW YORK, 10104

Inviscid Solution for the Secondary Flow in Curved Ducts

S. Abdallah* and A. Hamed†
University of Cincinnati, Cincinnati, Ohio

This paper presents an analytical formulation and a numerical solution for three-dimensional rotational flow in curved ducts. The formulation is based on calculating the through flow vorticity and velocity components from the momentum equation, using a marching technique. The secondary velocities are determined from the simultaneous solution of the continuity and vorticity equations. These equations are transformed through the use of the streamline function formulation into a single Poisson equation with Dirichlet boundary conditions. A numerical solution is obtained for the flow with large inlet velocity gradient in a 90-deg curved duct with constant radius of curvature. The results are presented and compared with the existing analytical and experimental data.

Nomenclature

C	= constant defined in Eqs. (17) and (18)
H	= duct height
P	= total pressure divided by the density
r,θ,z	= cylindrical polar coordinates
R_i,R_o	= duct's inner and outer radii
q_r,q_θ,q_z	= velocity components in r, θ, and z directions
V	= flow velocity
ξ	= vorticity component in θ direction
χ	= streamline function
Subscript	
I	= conditions at the duct inlet

Introduction

A STREAMWISE vorticity is known to develop in cascades and bends through the turning of shearing flow, with nonuniform inlet velocity profile. The transverse velocities, associated with the vorticity, have a significant effect on the losses and flow turning angles. The secondary flow theory was developed by Hawthorne[1] to explore this phenomenon. He developed expressions for the change in the streamwise vorticity component for steady inviscid, incompressible flow. Using his theory, Hawthorne[2] also derived expressions for the distributed secondary circulation, the trailing shed, and the trailing filament circulations at turbomachinery cascade exit. Following Hawthorne, other investigators derived generalized vorticity equations to include effects that are not in Hawthorne's expression. A. G. Smith[3] derived an expression for the streamwise vorticity in rotating axes, while Lakshminarayana and Horlock[4] gave a general vorticity equation, valid for compressible, stratified, and viscous flow. The application of Hawthorne's equations for streamwise vorticity calculations, requires prior knowledge of the resulting flowfield. Consequently, some approximations usually have been involved in the application of Hawthorne's equation for the streamwise vorticity calculation.

A first-order estimate of the streamwise vorticity generation in cascades and bends can be obtained for small perturbations using Squire and Winter's formula.[5] A related streamfunction[6,7] usually is used to calculate the associated transverse velocities and turning angles. These secondary velocities are superimposed on the primary two-dimensional flowfield at the cascade exit. L. H. Smith[8] defined the secondary vorticity as the difference between the actual streamwise vorticity and the primary vorticity that would exist if there were an infinite number of blades. Horlock[9] demonstrated that the three-dimensional flows resulting from the superposition of the primary and secondary flows, according to this definition, is the same as that obtained from the traditional secondary flow theory.

The purpose of the present investigation is to study the secondary flow phenomenon associated with the distributed secondary vorticity. The rotational flow in curved ducts is considered to investigate this phenomenon without the additional turbomachinary effects of stagnation point, tip clearance, trailing edge, and spanwise pressure gradient. The works of Stuart and Hetherington[10] and of Fagan[11] represent the two related analytical studies in the literature. In their study, Stuart and Hetherington[10] developed an iterative scheme that is based on an extension of the two variable streamline curvature method to a three-variable problem. In their approach, two numerical values are calculated for the same through flow velocity by integrating two sets of first-order equations for the streamline curvatures. The difference between the two values was introduced as a source term in two pseudocontinuity equations, which were used, in turn, to calculate the two secondary velocity components. The boundary conditions were not compatible with this scheme in which a duplicate variable is used for the forward velocity, and the continuity equation is integrated twice. The authors rectified this situation by deriving two integral boundary conditions for the duplicate forward velocities from the two continuity equations after dropping the source term. Fagan[11] on the other hand used Wu's technique[12] on two families of stream surfaces. On these surfaces the inviscid flow governing equations are combined to obtain Poisson type equations. The stream surfaces in this case are skewed and warped because of the streamwise vorticity. This analysis was used successfully in cases of small disturbances, but Fagan reported difficulties in highly rotational flow, because of the warpage of the stream surfaces which was more than 90 deg. Corkscrew coordinates that rotate at a specified rate were introduced in Ref. 11 to resolve this problem.

This paper presents a new analytical formulation and an efficient numerical technique for the solution of the rotational flow in curved ducts. Through cross differentiation, the pressure terms are cancelled from the

Presented as Paper 80-1116 at the AIAA/SAE/ASME 16th Joint Propulsion Conference, Hartford, Conn., June 30-July 2, 1980; submitted July 15, 1980; revision received Jan. 29, 1981.

*Graduate Research Assistant, Dept. of Aerospace Engineering and Applied Mechanics. Member AIAA.

†Professor, Dept. of Aerospace Engineering and Applied Mechanics. Member AIAA.

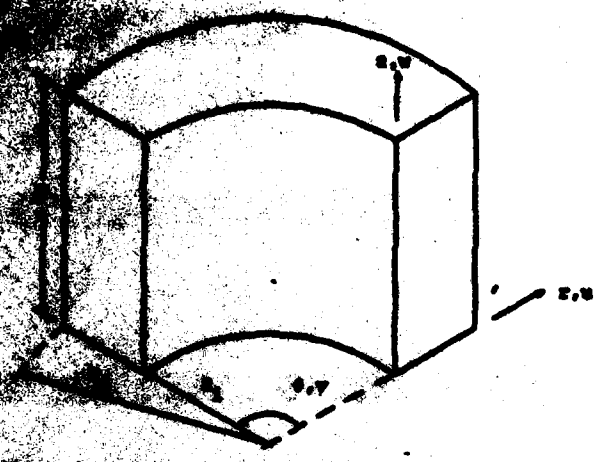

Fig. 1 Duct geometry, $R_i = 0.320$ m, $R_o = 0.488$ m, and $H = 0.254$ m.

[illegible] equation. Helmholtz equation is also used, [illegible] as two hyperbolic equations in the through flow [illegible] and velocity. These two equations are solved [illegible] using a marching procedure starting at the duct [illegible]. The continuity and vorticity equations are solved [illegible] to determine the other two velocity components in the cross planes. There are two fundamental [illegible] between the present method and the marching [illegible] previously by the same authors.[13] The first is [illegible] the present investigation, the through flow velocity is [illegible] directly from the momentum equations, while [illegible] is computed from an algebraic equation involving the velocity and vorticity components. In addition, a [illegible] is used in the simultaneous solution of the [illegible] equations, in which the streamlike [illegible] is used to combine these two equations into a [illegible] equation with Dirichlet boundary conditions. It has been possible through this present formulation to [illegible] effectively the computational time and storage required in the numerical solution.

Numerical results are obtained in a rectangular curved duct. The results of the computations are presented and compared [illegible] experimental data,[15] and with the numerical results of Ref. 11.

Analysis

The governing equations are derived from the basic equations of conservation of mass and momentum for steady, [illegible], and incompressible flow. The equations are written in cylindrical polar coordinates, to match the duct geometry of Fig. 1.

Momentum equations:

$$u\left(\frac{\partial u}{\partial r}+\frac{u}{r}-\frac{1}{r}\frac{\partial w}{\partial \theta}\right)-w\xi=\frac{\partial P}{\partial r} \tag{1}$$

$$w\left(\frac{1}{r}\frac{\partial w}{\partial \theta}-\frac{\partial u}{\partial z}\right)-u\left(\frac{\partial w}{\partial r}+\frac{w}{r}-\frac{1}{r}\frac{\partial u}{\partial \theta}\right)=\frac{1}{r}\frac{\partial P}{\partial \theta} \tag{2}$$

$$u\xi-v\left(\frac{1}{r}\frac{\partial w}{\partial \theta}-\frac{\partial u}{\partial z}\right)=\frac{\partial P}{\partial z} \tag{3}$$

Continuity equation:

$$\frac{\partial u}{\partial r}+\frac{u}{r}+\frac{1}{r}\frac{\partial v}{\partial \theta}+\frac{\partial w}{\partial z}=0 \tag{4}$$

where ξ is the θ component of the vorticity defined as

$$\xi=\frac{\partial u}{\partial z}-\frac{\partial w}{\partial r} \tag{5}$$

In the preceding equations u, v, and w are the velocity components in the r, θ, and z directions, respectively, and P is the total pressure divided by the density. The total pressure is eliminated from Eqs. (1-3) using cross differentiation. The resulting equations that are solved for ξ and v are

$$u\frac{\partial \xi}{\partial r}+\frac{v}{r}\frac{\partial \xi}{\partial \theta}+w\frac{\partial \xi}{\partial z}=\left(\frac{1}{r}\frac{\partial w}{\partial \theta}-\frac{\partial u}{\partial z}\right)\frac{\partial v}{\partial r}+\frac{\xi}{r}\frac{\partial v}{\partial \theta}$$
$$+\left(\frac{\partial v}{\partial r}+\frac{v}{r}-\frac{1}{r}\frac{\partial u}{\partial \theta}\right)\frac{\partial w}{\partial z}+\left[u\xi-v\left(\frac{1}{r}\frac{\partial w}{\partial \theta}-\frac{\partial u}{\partial z}\right)\right]/r \tag{6}$$

$$u\frac{\partial v}{\partial r}+\frac{v}{r}\frac{\partial v}{\partial \theta}+w\frac{\partial v}{\partial z}=\left\{w\left(u\frac{\partial \xi}{\partial r}+\frac{v}{r}\frac{\partial \xi}{\partial \theta}+w\frac{\partial \xi}{\partial z}\right)\right.$$
$$+\left[u\left(\frac{\partial v}{\partial r}-\frac{v}{r}\right)-v\left(\frac{\partial u}{\partial r}+\frac{\partial w}{\partial z}\right)\right]\left(\frac{\partial v}{\partial r}+\frac{v}{r}-\frac{1}{r}\frac{\partial u}{\partial \theta}\right)$$
$$\left.+w\xi\left(\frac{\partial u}{\partial r}+\frac{\partial w}{\partial z}\right)+w\left(\frac{1}{r}\frac{\partial w}{\partial \theta}-\frac{\partial u}{\partial z}\right)\left(\frac{v}{r}-\frac{\partial v}{\partial r}\right)\right\}$$
$$+\left(\frac{\partial v}{\partial r}+\frac{v}{r}-\frac{1}{r}\frac{\partial u}{\partial \theta}\right) \tag{7}$$

The reader is referred to the Appendix for the derivation of Eqs. (6) and (7).

Initial and Boundary Conditions

Referring to Fig. 1, the following initial and boundary conditions are used

$$v(r,0,z)=v_i \tag{8}$$

$$\xi(r,\theta,z)=0 \tag{9}$$

$$u(R_i,\theta,z)=0 \tag{10a}$$

$$u(R_o,\theta,z)=0 \tag{10b}$$

$$w(r,\theta,0)=0 \tag{11a}$$

$$w(r,\theta,H)=0 \tag{11b}$$

Equations (4-7) with the boundary conditions Eqs. (8-11) form a closed system that is solved for the variables u, v, w, and ξ.

Method of Solution

The streamlike function formulation[14] is used for the simultaneous solution of Eqs. (4) and (5) with the boundary conditions Eqs. (10) and (11). The method of solving Eqs. (4) and (5) for the velocity components u and w will be briefly outlined here. More details about this method can be found in Ref. 14. Equations (4) and (5) are first rewritten in the following form:

$$\frac{\partial}{\partial r}(ru)+\frac{\partial}{\partial z}(rw)=-\frac{\partial v}{\partial \theta} \tag{12}$$

and

$$\frac{\partial}{\partial z}(u)-\frac{\partial}{\partial r}(w)=\xi \tag{13}$$

A stream function χ is defined to satisfy Eq. (12) identically. The velocity components v and w in terms of χ are

$$v = -\frac{1}{r}\frac{\partial \chi}{\partial z} + \frac{1}{r}\int_{z_1}^{z}\left(-\frac{\partial w}{\partial \theta}\right)dz \tag{14}$$

$$w = -\frac{1}{r}\frac{\partial \chi}{\partial r} \tag{15}$$

When Eqs. (14) and (15) are substituted into Eq. (13), one obtains

$$\frac{\partial^2 \chi}{\partial r^2} - \frac{1}{r}\frac{\partial \chi}{\partial r} + \frac{\partial^2 \chi}{\partial z^2} = r\zeta + \frac{\partial}{\partial z}\int_{z_1}^{z}\frac{\partial w}{\partial \theta}dz \tag{16}$$

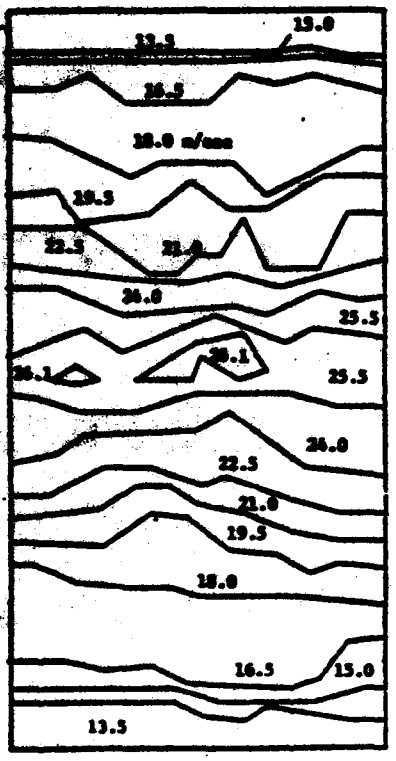

Fig. 2 Inlet velocity contours, experimental data.[18]

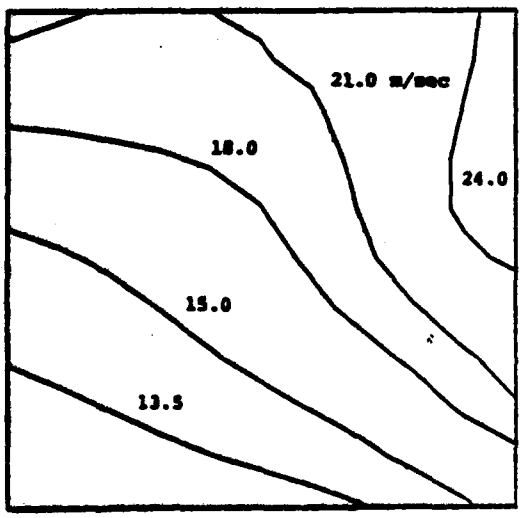

Fig. 3 Velocity contours at $\theta = 30$ deg.

The boundary conditions, Eqs. (10) and (11) are rewritten in terms of the streamlike function χ as follows:

$$\chi(R_i, z) = C \tag{17a}$$

$$\chi(R_o, z) = \int_z \int_{R_i}^{R_o} \frac{\partial w}{\partial \theta} dr dz + C \tag{17b}$$

and

$$\chi(r, \theta) = \chi(r, H) = C \tag{18}$$

Equation (16) is solved using the S.O.R. method, with the boundary conditions Eqs. (17) and (18). In the numerical solution the integrals in Eqs. (14), (16), and (17b) are evaluated using the trapezoidal rule.

Lax's scheme[17] is used to solve the hyperbolic Eqs. (6) and (7) with initial conditions Eqs. (8) and (9). A forward-difference quotient is used to advance the solution in θ direction and the derivatives with respect to r and z are approximated using central finite-difference formulas. Two important integral relations must be satisfied by the solution to this system of equations (6), (7), and (16). The first integral relation represents the global condition for the conservation of mass:

$$\iint_A v dr dz = Q \tag{19}$$

where A is the duct cross-sectional area and Q is the volume flux rate. Due to truncation error, the numerical solution for v may not satisfy condition Eq. (19) exactly; consequently, a uniform correction is introduced in the source term representing the right-hand side of Eq. (12) to satisfy Eq. (19).

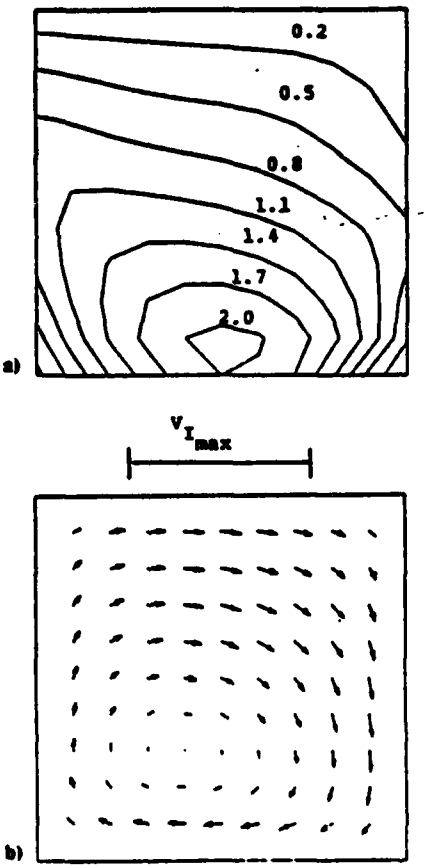

Fig. 4 Secondary vorticity and velocities at $\theta = 30$ deg; a) secondary vorticity, b) secondary velocities.

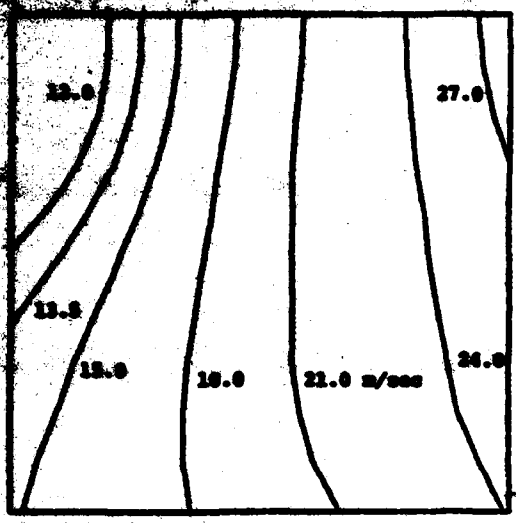

Fig. 6 Velocity contours at $\theta = 60$ deg.

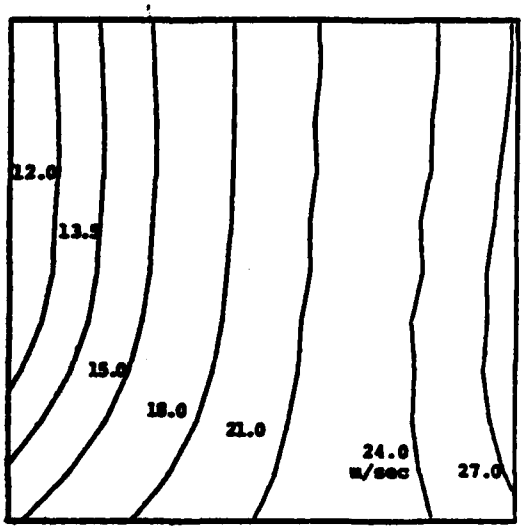

Fig. 7 Velocity contours at $\theta = 90$ deg.

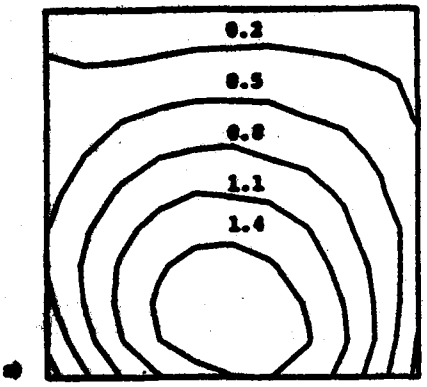

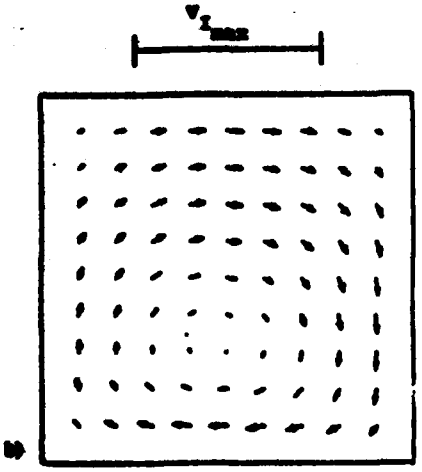

Fig. 8 Secondary vorticity and velocities at $\theta = 60$ deg; a) secondary vorticity, b) secondary velocities.

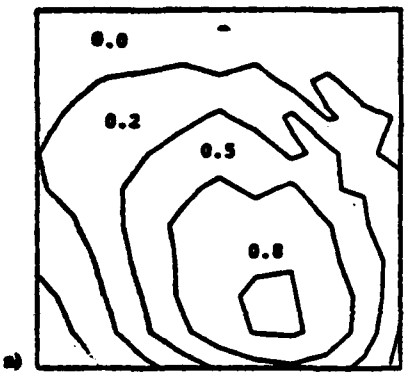

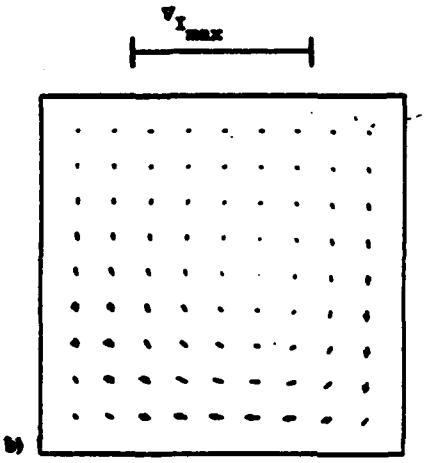

Fig. 9 Secondary vorticity and velocities at $\theta = 90$ deg; a) secondary vorticity, b) secondary velocities.

The second integral relation equates the circulation at each cross-sectional plane with the flux of the through flow vorticity ξ.

$$\iint_A \xi \, dr\,dz = \int_S V_s \, dS \tag{20}$$

where V_s represents the velocity tangent to the contour S containing the area A. The following boundary conditions for ξ determine a unique solution for Eq. (6) and satisfy the condition Eq. (20).

$$\xi = \frac{1}{r}\frac{\partial^2 \chi}{\partial r^2} - \frac{1}{r^2}\frac{\partial \chi}{\partial r} \qquad \text{at } r = R_i, R_o \tag{21}$$

and

$$\xi = \frac{1}{r}\frac{\partial^2 \chi}{\partial z^2} + \frac{1}{r}\frac{\partial}{\partial z}\int_{R_i}^{r}\left(-\frac{\partial v}{\partial \theta}\right)dr \quad \text{at } z = 0,\ H$$

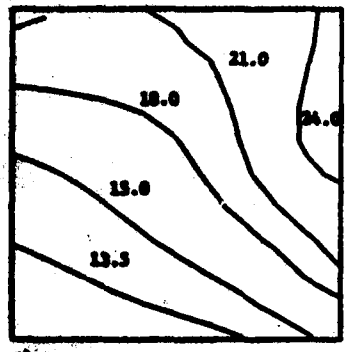

a)

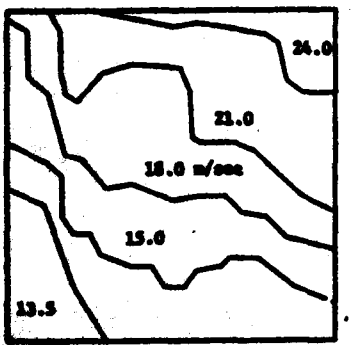

b)

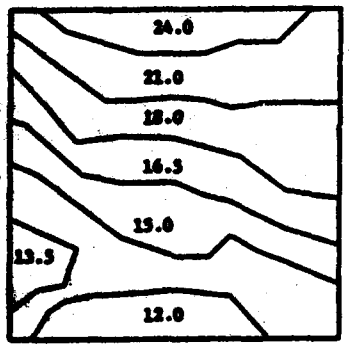

c)

Fig. 9 Velocity contours at $\theta = 30$ deg, lower half: a) present results, b) experimental data of Ref. 15, and c) numerical results of Ref. 16.

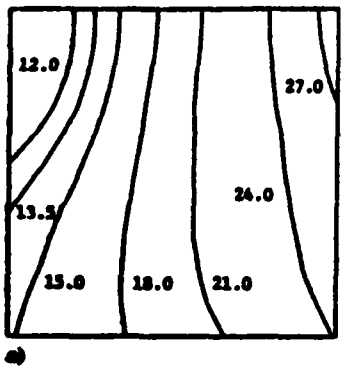

a)

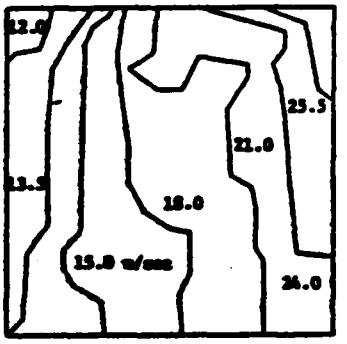

b)

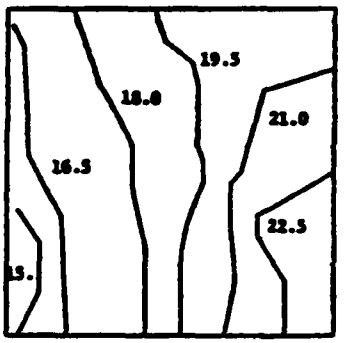

c)

Fig. 10 Velocity contours at $\theta = 60$ deg, lower half: a) present results, b) experimental data of Ref. 15, and c) numerical results of Ref. 11.

The solution to Eq. (7) on the duct solid boundaries is obtained using the two-dimensional form of Lax's scheme.[17] A stable linear extrapolation procedure is used to calculate the boundary conditions for v along the duct corners.

Results and Discussion

The numerical solution of the governing equations is obtained in a 90 deg turning duct with rectangular cross section. The experimental data of Ref. 15 provides flow measurements at the 30-, 60-, and 90-deg turning angles of a rectangular duct with a 0.375-m (15 in.) mean radius and a 0.125×0.25 m (5×10 in.) cross section. The duct geometry and dimensions are shown in Fig. 1. Since the experimental data of Ref. 15 is obtained for a flowfield with substantial inlet velocity variation, it can be very useful in the assessment of the present analysis. The same data was used for comparison with the numerical results in Refs. 10, 11, and 16. The experimentally measured inlet velocity profile of Ref. 15 is reproduced in Fig. 2. In this figure, the values labeling the velocity contours are in meters per second. It can be seen from this figure that the variations in the profile are greater in the low velocity regions compared to the nearly uniform velocity at the centerline. In addition, it may be observed that the variation in the r direction is not too significant. The inlet velocity profile of Fig. 2 was found too noisy to be used directly in the numerical solution. Therefore, the experimental data is simulated with a parabolic variation in the z direction to obtain the numerical results. Due to the symmetry of the inlet profile the computations are carried out only in the lower half of the duct. The results in Ref. 10 were also presented in the lower half, while Refs. 11 and 16 presented their results and comparison with the experimental data in the upper half of the duct. The governing equations were nondimensionalized before the numerical solution, so that all results, except the velocity contours, are presented in nondimensional form. The duct inner radius R_i and the maximum flow velocity at inlet $V_{z_{max}}$ were used in the normalization. The numerical computations were carried out in double precision on the AMDAHL 470. The results presented here were generated using an $11 \times 11 \times 45$ grid.

The results are presented in the form of velocity and secondary vorticity contours, and vectors showing the magnitude and direction of the secondary velocities. The velocity contours at the 30-, 60- and 90-deg turning angles are shown in Figs. 3, 5, and 7, respectively. It can be seen from these figures that the rotation of the velocity contours, which were parallel and horizontal at inlet, is very significant in the

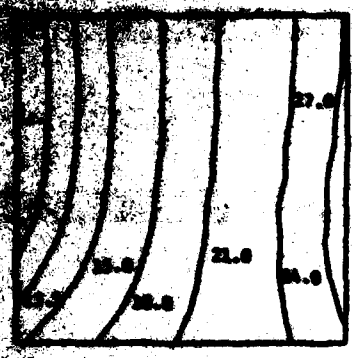

a)

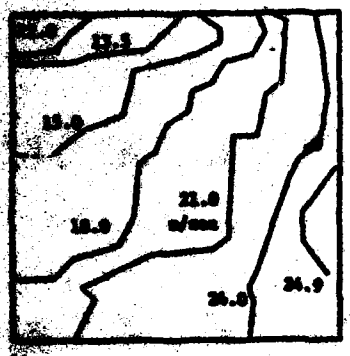

b)

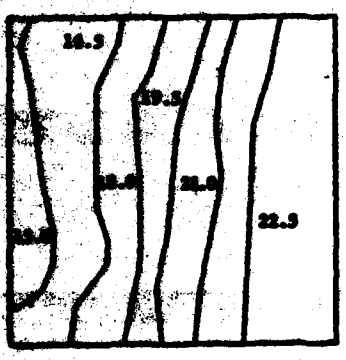

c)

Fig. 11 Velocity contours at $\theta = 90$ deg, lower half: a) present results, b) experimental data of Ref. 15, and c) numerical results of Ref. 11.

first 60 deg of the duct. The contours become nearly vertical before their rotation rate starts to decrease for turning angles greater than 60 deg.

The secondary vorticity and the corresponding secondary velocities are shown in Figs. 4, 6, and 8, at 30-, 60-, and 90-deg turning angles. A comparison of Figs. 4a, 6a, and 8a reveals that the generated secondary vorticity reaches a maximum at the 30-deg cross section. It is important to recognize that with a symmetric inlet velocity profile, the secondary vorticity is asymmetric and therefore vanishes at the plane of symmetry. It can be observed from these figures that the vortex center has moved toward the outer radius between the 30- and the 90-deg turning angles. Figure 8a shows a larger region of low secondary vorticity near the plane of symmetry at the 90-deg cross section. This region also extends to the inner corner where negative vorticity starts to develop. The corresponding variations in secondary velocities can be seen in Figs. 6b, 7b, and 8b. It can be seen from these figures that, while the secondary velocities are comparable in magnitude at the 30- and 60-deg duct cross sections, they are significantly smaller at the 90-deg duct cross section. The secondary velocities are particularly very small near the plane of symmetry at the 90-deg section. This is the region of very low secondary vorticity in Fig. 8. In this same region, all the velocity contours of Fig. 7 remain practically vertical with no significant rotation. It can be noticed from these figures, that between 30- and 90-deg cross sections, the center of rotation has moved outward and upward. The center of rotation is different from the vortex center in Figs. 4, 6, and 8. This difference can be attributed to the source term in the continuity equation which is caused by the variation in the through flow velocity component in θ direction.

The computed velocity contours at the 30-, 60-, and 90-deg cross sections are shown with the experimental data of Ref. 15 and the inviscid flow analysis of Ref. 11 in Figs. 9-11 for comparison. It can be seen from these figures that the present analysis predicts the rotation of the velocity contours accurately at 30- and 60-deg turning angles, and in the high velocity region at the 90-deg turning angle. The agreement between the analysis and the experimental data is very significant in the high velocity regions, where the viscous effects are not dominant. In addition, the present analysis predicts the experimentally measured low velocity regions at the inner wall as can be seen at the inner corner in Fig. 9 and the centerline of the cross section in Fig. 10. The translation of this low velocity region from the corner at the 30-deg cross section to the centerline at the 60-deg cross section is not predicted by the analysis of Ref. 11.

The computer time used in the solution of the present study is significantly less than the computer time in Refs. 10, 11, and 16. Fagan,[11] using the total of six stream surfaces with 200 nodal points per surface, reported a CPU time of 1500-2100 s on the IBM 370/155. Stuart and Hetherington[10] reported a CPU time of 840 s on the IBM 360/65 using a $9\times8\times15$ grid. Roscoe[16] used an $8\times8\times16$ grid to obtain his solution, and reported a CPU time of 550 s on CDC 7600. In the present analysis, the CPU time was 20 s on AMDAHL 470 V/6-II using an $11\times11\times45$ grid in the numerical solution.

Conclusion

The present analysis of internal rotational flows leads to a very efficient numerical scheme for predicting the secondary flow phenomenon. The analysis is applied to the rotational flow in a 90-deg bend with rectangular cross section. From the comparison of the computed results with the experimental data, it can be concluded that the physics of the secondary flow problem are well represented in the analysis. The present formulation can be adapted with some modifications to variable area ducts and turbomachinery passages.

Appendix

Derivation of Eq. (6)

Differentiating Eq. (1) with respect to z and Eq. (3) with respect to r and subtracting, one obtains

$$u\frac{\partial\xi}{\partial r}+w\frac{\partial\xi}{\partial z}+\xi\left(\frac{\partial u}{\partial r}+\frac{\partial w}{\partial z}\right)-\frac{\partial v}{\partial r}\left(\frac{1}{r}\frac{\partial w}{\partial\theta}-\frac{\partial v}{\partial z}\right)$$
$$-v\frac{\partial}{\partial r}\left(\frac{1}{r}\frac{\partial w}{\partial\theta}-\frac{\partial v}{\partial z}\right)-\frac{\partial v}{\partial z}\left(\frac{\partial v}{\partial r}+\frac{v}{r}-\frac{1}{r}\frac{\partial u}{\partial\theta}\right)$$
$$-v\frac{\partial}{\partial z}\left(\frac{\partial v}{\partial r}+\frac{v}{r}-\frac{1}{r}\frac{\partial u}{\partial\theta}\right)=0 \qquad \text{(A1)}$$

the divergence of the vorticity vector is identically equal to zero. This can be expressed in terms of u, v, and w and ξ as follows:

$$\frac{\partial}{\partial r}\left(\frac{1}{r}\frac{\partial w}{\partial\theta}-\frac{\partial v}{\partial z}\right)+\frac{1}{r}\left(\frac{1}{r}\frac{\partial w}{\partial\theta}-\frac{\partial v}{\partial z}\right)$$
$$+\frac{\partial}{\partial z}\left(\frac{\partial v}{\partial r}+\frac{v}{r}-\frac{1}{r}\frac{\partial u}{\partial\theta}\right)+\frac{1}{r}\frac{\partial\xi}{\partial\theta}=0 \qquad \text{(A2)}$$

[illegible] Eq. (A8) and the continuity Eq. (4) into Eq. [illegible] one obtains

$$+\frac{\partial}{\partial r}+\frac{v}{r}\frac{\partial}{\partial\theta}+w\frac{\partial}{\partial z}-\left(\frac{1}{r}\frac{\partial w}{\partial\theta}-\frac{\partial v}{\partial z}\right)\frac{\partial w}{\partial r}+\frac{1}{r}\frac{\partial w}{\partial\theta}$$

$$+\left(\frac{\partial}{\partial r}+\frac{v}{r}-\frac{1}{r}\frac{\partial}{\partial\theta}\right)\frac{\partial w}{\partial z}+\left[w\xi-v\left(\frac{1}{r}\frac{\partial w}{\partial\theta}-\frac{\partial v}{\partial z}\right)\right]/r \quad \text{(A5)}$$

[illegible] (A5) represents the θ component of Helmholtz [illegible]

[illegible]

The total derivative operator is defined as follows:

$$\frac{D}{Dt}(\ )=\vec{V}\cdot\nabla(\ ) \quad \text{(A4)}$$

[illegible] derivative operator to Eq. (1), one obtains

$$\vec{V}\cdot\nabla\left[v\left(\frac{\partial w}{\partial r}+\frac{v}{r}-\frac{1}{r}\frac{\partial u}{\partial\theta}\right)-w\xi\right]=\vec{V}\cdot\nabla\frac{\partial P}{\partial z} \quad \text{(A5)}$$

The total pressure term is eliminated from the right-hand side of Eq. (A5) using the momentum equation as follows:

$$\vec{V}\cdot\nabla\frac{\partial P}{\partial r}=\vec{V}\cdot\frac{\partial}{\partial r}\nabla P+\frac{v}{r^2}\frac{\partial P}{\partial\theta}$$

$$=\frac{\partial}{\partial r}(\vec{V}\cdot\nabla P)-\frac{\partial\vec{V}}{\partial r}\cdot\nabla P+\frac{v}{r^2}\frac{\partial P}{\partial\theta} \quad \text{(A6)}$$

The first term on the right-hand side is equal to zero from the momentum equation. Therefore, using Eqs. (A5) and (A6), we obtain

$$\vec{V}\cdot\nabla\left[v\left(\frac{\partial w}{\partial r}+\frac{v}{r}-\frac{1}{r}\frac{\partial u}{\partial\theta}\right)-w\xi\right]=-\frac{\partial\vec{V}}{\partial r}\cdot\nabla P+\frac{v}{r^2}\frac{\partial P}{\partial\theta} \quad \text{(A7)}$$

Using the momentum equations, the pressure gradients in the right-hand side of Eq. (A7) is expressed in terms of the velocity components u, v, and w and the vorticity ξ as follows:

$$-\frac{\partial\vec{V}}{\partial r}\cdot\nabla P+\frac{v}{r^2}\frac{\partial P}{\partial\theta}=-\frac{\partial u}{\partial r}\left[v\left(\frac{\partial w}{\partial r}+\frac{v}{r}-\frac{1}{r}\frac{\partial u}{\partial\theta}\right)-w\xi\right]$$

$$+\left(\frac{v}{r}-\frac{\partial w}{\partial r}\right)\left[w\left(\frac{1}{r}\frac{\partial w}{\partial\theta}-\frac{\partial v}{\partial z}\right)-u\left(\frac{\partial w}{\partial r}+\frac{v}{r}-\frac{1}{r}\frac{\partial u}{\partial\theta}\right)\right]$$

$$-\frac{\partial w}{\partial r}\left[u\xi-v\left(\frac{1}{r}\frac{\partial w}{\partial\theta}-\frac{\partial v}{\partial z}\right)\right] \quad \text{(A8)}$$

Helmholtz equation is used to eliminate the second-order derivatives on the left-hand side of Eq. (A5) as follows:

$$\vec{V}\cdot\nabla\left(\frac{\partial w}{\partial r}+\frac{v}{r}-\frac{1}{r}\frac{\partial u}{\partial\theta}\right)=\left(\frac{1}{r}\frac{\partial w}{\partial\theta}-\frac{\partial v}{\partial z}\right)\frac{\partial w}{\partial r}$$

$$+\xi\frac{1}{r}\frac{\partial w}{\partial\theta}+\left(\frac{\partial w}{\partial r}+\frac{v}{r}-\frac{1}{r}\frac{\partial u}{\partial\theta}\right)\frac{\partial w}{\partial z} \quad \text{(A9)}$$

Substituting Eqs. (A8) and (A9) into Eq. (A7) and simplifying, one obtains

$$u\frac{\partial w}{\partial r}+\frac{v}{r}\frac{\partial w}{\partial\theta}+w\frac{\partial w}{\partial z}=\left\{w\left(u\frac{\partial\xi}{\partial r}+\frac{v}{r}\frac{\partial\xi}{\partial\theta}+w\frac{\partial\xi}{\partial z}\right)\right.$$

$$+\left[u\left(\frac{\partial w}{\partial r}-\frac{v}{r}\right)-v\left(\frac{\partial u}{\partial r}+\frac{\partial w}{\partial z}\right)\right]\left(\frac{\partial v}{\partial r}+\frac{v}{r}-\frac{1}{r}\frac{\partial u}{\partial\theta}\right)$$

$$+w\xi\left(\frac{\partial u}{\partial r}+\frac{\partial w}{\partial z}\right)+w\left(\frac{1}{r}\frac{\partial w}{\partial\theta}-\frac{\partial v}{\partial z}\right)$$

$$\left.\times\left(\frac{v}{r}-\frac{\partial w}{\partial r}\right)\right\}\Big/\left(\frac{\partial v}{\partial r}+\frac{v}{r}-\frac{1}{r}\frac{\partial u}{\partial\theta}\right) \quad \text{(A10)}$$

Acknowledgment

This research was sponsored under AFOSR Contract 80-0242.

References

[1] Hawthorne, W. R., "Secondary Circulation in Fluid Flow," *Proceedings of the Royal Society Ser. A*, Vol. 206, 1951, pp. 374-387.

[2] Hawthorne, W. R., "Rotational Flow Through Cascades. Part I—The Components of Vorticity," *Quarterly of the Journal of Mechanics and Applied Mathematics*, Vol. VIII, Pt. 3, 1955, pp. 266-279.

[3] Smith, A. G., "On the Generation of the Streamwise Component of Vorticity for Flows in Rotating Passages," *The Aeronautical Quarterly*, Vol. 8, Nov. 1957, pp. 569-583.

[4] Lakshminarayana, B. and Horlock, J. H., "General Expressions for Secondary Vorticity Using Intrinsic Coordinates," *Journal of Fluid Mechanics*, Vol. 59, Part 1, June 1973, p. 97.

[5] Squire, H. B. and Winter, K. G., "The Secondary Flow in a Cascade of Aerofoils in a Non-Uniform Stream," *Journal of Aeronautical Sciences*, Vol. 18, 1951, p. 271.

[6] Hawthorne, W. R., "Some Formulae for the Calculation of Secondary Flow in Cascades," Aeronautical Research Council, ARC Rept. 17519, 1955.

[7] Bardon, M. F., Moffat, W. C., and Randall, J. L., "Secondary Flow Effects on Gas Exit Angles in Rectilinear Cascades," *Journal of Engineering for Power*, Vol. 97, Jan. 1975, pp. 93-100.

[8] Smith, L. H., "Secondary Flow in Axial-Flow Turbomachinery," *Transactions of ASME*, Vol. 77, Oct. 1955, pp. 1065-1076.

[9] Horlock, J. H., "Discussion of the Paper by Dixon, S. L., entitled 'Secondary Vorticity in Axial Compressor Blade Rows,' " NASA SP 304, *Fluid Mechanics, Acoustics and Design of Turbomachines*, Pt. I, 1976, pp. 169-201.

[10] Stuart, A. R. and Hetherington, R., "The Solution of the Three Variable Duct Flow Equations," NASA SP 304, *Fluid Mechanics, Acoustics and Design of Turbomachines*, Pt. I, 1974, pp. 135-150.

[11] Fagan, J. R., "Three-Dimensional Subsonic Duct Flow Analysis," Detroit Diesel Allison, Div. of General Motors Corp., EDR7451, 1972.

[12] Wu, C. H., "A General Theory of Three Dimensional Flow in Subsonic and Supersonic Turbomachines of Axial, Radial and Mixed Flow Types," NACA TN2604, 1952.

[13] Hamed, A. and Abdallah, S., "Three-Dimensional Rotational Flow in Highly Curved Ducts Due to Inlet Vorticity," AIAA Paper 78-146, 1978.

[14] Hamed, A. and Abdallah, S., "Streamlike Function: A New Concept in Flow Problems Formulation," *Journal of Aircraft*, Vol. 16, Dec. 1979, pp. 801-802.

[15] Joy, W., "Experimental Investigation of Shear Flow in Rectangular Bends," M.S. Thesis, Massachusetts Institute of Technology, 1950.

[16] Roscoe, D. F., "The Numerical Solution of the Navier-Stokes Equations for a Three-Dimensional Laminar Flow in Curved Pipes Using Finite Difference Methods," *Journal of Engineering Mathematics*, Vol. 12, Oct. 1978, pp. 303-323.

[17] Lax, P. D., "Weak Solutions of Nonlinear Hyperbolic Equations and Their Numerical Computation," *Communications on Pure and Applied Mathematics*, Vol. VII, 1954, pp. 159-193.

Reprinted from July 1983, Vol. 105, Journal of Engineering for Power

The Elliptic Solution of the Secondary Flow Problem

S. Abdallah
Research Associate,
Applied Research Laboratory,
Pennsylvania State University,
State College, Pa. 16802

A. Hamed
Professor,
Department of Aerospace Engineering and Applied Mechanics,
University of Cincinnati,
Cincinnati, Ohio 45221
Mem. ASME

This paper presents the elliptic solution of the inviscid incompressible secondary flow in curved passages. The three-dimensional flow field is synthesized between 3 sets of orthogonal nonstream surfaces. The two-dimensional flow field on each set of surfaces is considered to be resulting from a source/sink distribution. The distribution and strength of these sources are dependent on the variation in the flow properties normal to the surfaces. The dependent variables in this formulation are the velocity components, the total pressure, and the main flow vorticity component. The governing equations in terms of these dependent variables are solved on each family of surfaces using the streamlike function formulation. A new mechanism is implemented to exchange information between the solutions on the three family surfaces, resulting into a unique solution. In addition, the boundary conditions for the resulting systems of equations are carefully chosen to insure the existence and uniqueness of the solution. The numerical results obtained for the rotational inviscid flow in a curved duct are discussed and compared with the available experimental data.

Introduction

Three-dimensional flow calculations in turbomachines constitute a complex mathematical problem. The fact that the three velocity components change greatly in passing through a turbomachine limits the two-dimensional approximations to a few special cases. A major contribution in this field is Wu's general theory [1], for the inviscid flow calculations. In this theory the flow field is determined from two-dimensional solutions, which are obtained on two intersecting families of stream filaments with variable thickness. The governing equations are satisfied on the mean surfaces of these stream filaments, which are referred to as the S_1 (blade-to-blade) and the S_2 (meridional) surfaces. The correct solution of one family of surfaces requires some data from the other and, consequently, an iterative process between the solutions on these two families of surfaces is involved. Many investigators have applied Wu's theory to obtain solution on the S_1 or S_2 surfaces. Two techniques have been used in these studies; namely, the matrix method and the streamline curvature method.

Marsh [2], Katsanis [3, 4], Smith [5], Bosman and El-Shaarawi [6], and Malanik [7], used the matrix method to obtain solutions on the S_1 and S_2 surfaces. Katsanis developed computer programs for a meridional solution [3] and also for solution on a blade-to-blade surface of revolution [4] with a tube thickness proportional to the blade height. In [3] and [4], a representative mean averaged S_2 stream surface is used, and the S_1 surfaces are generated by rotating the streamlines in the S_2 surface about the axis of revolution.

The streamline curvature method has been used by Wilkinson [8] to obtain blade-to-blade solutions. The same method, has also been used by Novak and Hearshy [9] and by Katsanis [10, 11] to obtain meridional and blade-to-blade solutions. The assumptions and approximations used for the stream surface shape and stream filament thickness distribution in the S_1 and S_2 solution using this method are mainly similar to those discussed previously in connection with the matrix method.

Several problems are encountered in computing a synthesized three-dimensional turbomachine flow field from the solutions on the S_1 and S_2 surfaces. These problems are related to the exchanged information between the two solutions, concerning the stream surface shape and the stream filament thickness. Novak and Hearshy [9] pointed out that the S_2 filament thickness, as calculated from the blade-to-blade solution, is not constant upstream and downstream of the blade row. This is in contradiction with the requirement that the flow must be treated as axisymmetric in these regions. They also discussed the effect of the lean of the S_2 mean stream surface extending upstream and downstream of the blades, where the net angular momentum changes must be zero. Stuart and Hetherington [12] tried to use a technique similar to Wu's in their solution for rotational flow in a 90-deg bend, by synthesizing the three-dimensional flow field through the iterations between two-dimensional solutions. They were unable to reach convergence in the iterative numerical solution and had to abandon this approach. They speculated that the information conveyed between the two solutions was not sufficient to produce convergence.

The assumption that the S_1 stream surface is a body of revolution was common in all applications of Wu's theory in turbomachines [2–12]. This assumption is valid if the flow is irrotational. In general, the S_1 surface is twisted and skewed due to the presence of the secondary velocities. These

Contributed by the Gas Turbine Division of The American Society of Mechanical Engineers and presented at the 27th International Gas Turbine Conference and Exhibit, London, England, April 18–22, 1982. Manuscript received at ASME Headquarters December 18, 1981. Paper No. 82-GT-242.

Appendix 2

The Elliptic Solution of the Secondary Flow Problem

transverse velocities exist due to the streamwise vorticity which is generated by the turning of a nonuniform flow with a vorticity component in the curvature plane [13, 14]. The nonuniformities of inlet velocities in turbomachines are associated with the hub and the tip boundary layers. Stream surface warpage pose additional mathematical difficulties in the solution of the rotational flow. Fagan [15] could not obtain a solution for highly rotational flow in curved ducts using Wu's approach. He resolved the problems encountered when the stream surfaces warpage approaches 90 deg through using a corkscrew coordinate system that operates at a specified angular rate.

In reference [16], Abdallah and Hamed developed an effective method for the solution of three-dimensional rotational flow in curved ducts, in which the throughflow velocity and vorticity components were computed using a marching technique in the main flow direction. This led to a very efficient numerical solution whose results compared favorably with the experimental data for duct flows. However, because of the marching technique used in computing the through flow velocity, the influence of the downstream conditions on the flow characteristics is not modeled. This effect, although not significant in duct flow, may be quite important in turbomachinery applications. Barber and Langston [17] contrasted the blade row and duct flow problems and discussed the importance of the elliptic solution to the flow in blade rows.

This investigation represents an elliptic solution for the internal nonviscous incompressible rotational flow in curved passages. The streamlike function method, which was developed by the authors [18] for the efficient numerical solution of the continuity and rotationality equations is implemented in the present problem formulation. The dependent variables in this formulation are the three streamlike functions, the total pressure, and the throughflow vorticity component. The equations of motion are satisfied on three arbitrary sets of orthogonal surfaces. On these surfaces, two-dimensional Poisson equations are derived, for the streamlike functions, with source terms representing the flow three-dimensionality. The source terms are dependent upon the variation of the flow properties in the direction normal to these surfaces. Because of the dependency of the solution on each set of surfaces on the solutions for the remaining two sets of surfaces, an iterative process is involved in the solution. The three flow velocity components are determined by the source terms and the three streamlike function derivatives. The total pressure and through flow vorticity are computed from Bernoulli and Helmholtz equations, respectively.

The initial and boundary conditions for a closed system of equations are carefully chosen to insure the existence and uniqueness of the solution. The no-flux condition at the solid boundaries leads to Dirichlet boundary conditions for the streamlike functions. Downstream, the derivatives of the flow properties in the throughflow direction is set to zero. A Poisson type equation with Neumann boundary conditions is derived and solved for the static pressure at the inlet plane, which is then used together with the inlet velocity profile to determine the inlet total pressure profile.

Numerical resutls are obtained for the case of rotational flow in a curved duct with rectangular cross sections. The results are discussed and compared with the experimental data.

Mathematical Formulation

For simplicity and to be able to compare with existing experimental results in ducts [19], the cylindrical polar coordinates are used in the following presentation. The basic equations for nonviscous incompressible flow are expressed in terms of the three velocity components, the total pressure and the throughflow vorticity components as follows:

Conservation of mass

$$\frac{1}{r}\frac{\partial}{\partial r}(ru)+\frac{1}{r}\frac{\partial v}{\partial \theta}+\frac{\partial w}{\partial z}=0 \tag{1}$$

Conservation of momentum in r-direction

$$v\left[\frac{\partial v}{\partial r}+\frac{v}{r}-\frac{1}{r}\frac{\partial u}{\partial \theta}\right]-w\xi=\frac{\partial P}{\partial r} \tag{2}$$

Conservation of momentum in z-direction

$$u\xi-v\left[\frac{1}{r}\frac{\partial w}{\partial \theta}-\frac{\partial v}{\partial z}\right]=\frac{\partial P}{\partial z} \tag{3}$$

where P is the total pressure divided by the density, and (u,v,w) are the three velocity components in (r,θ,z)-directions. The throughflow vorticity component, ξ, can be written in terms of the cross velocities, u and w, as follows

$$\xi=\frac{\partial u}{\partial z}-\frac{\partial w}{\partial r} \tag{4}$$

Bernoulli's Equation.

Bernoulli's equation is used instead of the momentum equation in the θ-direction.

$$u\frac{\partial P}{\partial r}+\frac{v}{r}\frac{\partial P}{\partial \theta}+w\frac{\partial P}{\partial z}=0. \tag{5}$$

Helmholtz Equation.

$$u\frac{\partial \xi}{\partial r}+\frac{v}{r}\frac{\partial \xi}{\partial \theta}+w\frac{\partial \xi}{\partial z}$$

$$=\eta\frac{\partial v}{\partial r}+\frac{\xi}{r}\frac{\partial v}{\partial \theta}+\zeta\frac{\partial v}{\partial z}+\frac{1}{r}(u\xi-v\eta) \tag{6}$$

Nomenclature

A = duct cross-sectional area
C = contour enclosing A
dC = incremental distance along C
n = outward normal to the contour, C
P = total pressure divided by the density
P_s = inlet static pressure divided by the density
(r,θ,z) = cylindrical polar coordinates
r_1,z_1 = arbitrary integration reference points on the r- and z-coordinates, respectively
S_1,S_2 = blade-to-blade and meridional stream surfaces, respectively
(u,v,w) = velocity components in (r,θ,z) directions, respectively
χ = streamlike function
ξ = main flow vorticity component in θ-direction
$(\Delta r,\Delta\theta,\Delta z)$ = space increments in (r,θ,z) directions

Subscripts

h = horizontal surfaces
I = inlet conditions
v = vertical surfaces
c = cross-sectional surfaces

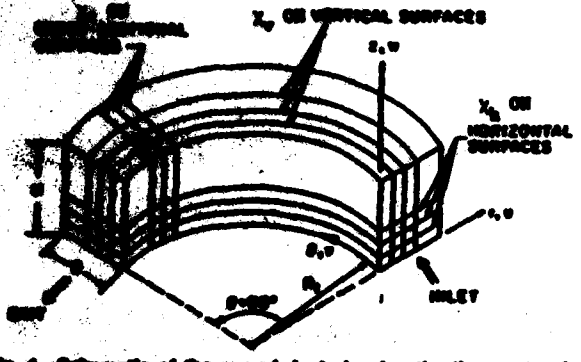

Fig. 1 Schematic of the curved duct showing the three sets of orthogonal surfaces and the corresponding streamlike functions

where

$$\eta = \frac{1}{r}\frac{\partial w}{\partial \theta} - \frac{\partial v}{\partial z}$$

and

$$\xi = \frac{\partial u}{\partial r} + \frac{u}{r} - \frac{1}{r}\frac{\partial w}{\partial \theta}$$

The governing equations (1–4) are satisfied on three families of orthogonal surfaces, c, h and v, as shown in Fig. 1. The combined elliptic solutions on these surfaces provide the three velocity components, u, v and w, whereas the hyperbolic equations (5) and (6) are solved for P and ξ, respectively.

The streamlike function formulation, developed by the authors [16] is utilized in the present problem for the purpose of obtaining an economical numerical solution to equations (1–6). Three separate streamlike functions, χ_h, χ_v, and χ_c, are defined for the three sets of orthogonal surfaces shown in Fig. 1, to identically satisfy the principal of conservation of mass, given by equation (1).

The streamlike function, χ_h, is defined on the horizontal surfaces as follows

$$\frac{1}{r}\frac{\partial \chi_h}{\partial \theta} = u_h + \frac{1}{r}\int_{r_1}^{r} r\frac{\partial w_v}{\partial z}\,dr \tag{7a}$$

$$\frac{\partial \chi_h}{\partial r} = -v_h \tag{7b}$$

where r_1 is the radial coordinate of an arbitrary integration reference surface, and the subscripts h and v refer to the solutions on the horizontal and vertical surfaces, respectively.

The streamlike function, χ_v, is defined on the vertical surface as follows

$$\frac{1}{r}\frac{\partial \chi_v}{\partial \theta} = -w_v - \int_{z_1}^{z}\frac{1}{r}\frac{\partial}{\partial r}(ru_h)\,dz \tag{8a}$$

$$\frac{\partial \chi_v}{\partial z} = v_v \tag{8b}$$

where z_1 is the axial coordinate of an arbitrary integration reference surface.

The streamlike function, χ_c, is defined on the cross planes as follows

$$\frac{\partial \chi_c}{\partial z} = -u_c + \frac{1}{r}\int_{r_1}^{r} r\frac{\partial w_v}{\partial z}\,dr \tag{9a}$$

$$\frac{\partial \chi_c}{\partial r} + \frac{\chi_c}{r} = w_c - \int_{z_1}^{z}\frac{1}{r}\frac{\partial}{\partial r}(r u_h)\,dz \tag{9b}$$

where the subscript, c, refers to the solution on the cross-sectional surfaces.

The governing equations for these stream functions are obtained by substituting equations (7a,b) into equation (2), equations (8a,b) into equation (3) and equations (8a,b) into equation (4), leading to the following equations

$$\frac{\partial^2 \chi_h}{\partial r^2} + \frac{1}{r}\frac{\partial \chi_h}{\partial r} + \frac{1}{r^2}\frac{\partial^2 \chi_h}{\partial \theta^2} = -\left[w\xi + \frac{\partial P}{\partial r}\right]/v + \frac{1}{r}\frac{\partial}{\partial \theta}\int_{r_1}^{r} r\frac{\partial w_v}{\partial z}\,dr + \left[\frac{\partial w_v}{\partial r} + \frac{w_v}{r} - \frac{1}{r}\frac{\partial u_c}{\partial \theta}\right] \tag{10}$$

$$\frac{\partial^2 \chi_v}{\partial z^2} + \frac{1}{r^2}\frac{\partial^2 \chi_v}{\partial \theta^2} = -\left[u\xi - \frac{\partial P}{\partial z}\right]/v - \frac{1}{r}\frac{\partial}{\partial \theta}\int_{z_1}^{z}\frac{1}{r}\frac{\partial}{\partial r}(ru_h)\,dz + \left[\frac{1}{r}\frac{\partial w_c}{\partial \theta} - \frac{\partial v_h}{\partial z}\right] \tag{11}$$

$$\frac{\partial^2 \chi_c}{\partial r^2} + \frac{1}{r}\frac{\partial \chi_c}{\partial r} - \frac{\chi_c}{r^2} + \frac{\partial^2 \chi_c}{\partial z^2} = -\xi + \frac{1}{r}\frac{\partial}{\partial z}\int_{r_1}^{r} r\frac{\partial w_v}{\partial z}\,dr - \frac{\partial}{\partial r}\int_{z_1}^{z}\frac{1}{r}\frac{\partial}{\partial r}(ru_h)\,dz + \left[\frac{\partial u_h}{\partial z} - \frac{\partial w_v}{\partial r}\right] \tag{12}$$

The elliptic equations (10), (11), and (12) are solved on the horizontal, vertical, and cross-sectional surfaces for χ_h, χ_v and χ_c, respectively. The solution on one set of surfaces is influenced by the solutions on the other two sets of surfaces through the source terms. Consequently, an iterative process between the three families of surfaces is involved. The three-dimensional solution is obtained by adding the computed velocity components in each of the solutions as follows

$$u = u_h + u_c \tag{13a}$$

$$v = v_h + v_v \tag{13b}$$

$$w = w_v + w_c \tag{13c}$$

It can be easily shown that the velocity components as determined by equation (13) represent a unique solution.

Boundary Conditions. The inlet conditions for ξ and P are given by

$$\xi = 0 \tag{14}$$

$$P = P_s + \frac{1}{2}v_i^2 \tag{15}$$

where P_s is the inlet static pressure divided by the density. The static pressure distribution at the duct inlet cross section is computed from the numerical solution of the following equation

$$\frac{\partial^2 P_s}{\partial r^2} + \frac{1}{r}\frac{\partial P_s}{\partial r} + \frac{\partial^2 P_s}{\partial z^2} = \sigma \tag{16}$$

where

$$\sigma = \frac{\partial}{\partial r}\left[-\frac{v}{r}\frac{\partial u}{\partial \theta} + \frac{v^2}{r}\right] - \frac{\partial}{\partial z}\left[\frac{v}{r}\frac{\partial w}{\partial \theta}\right] + \frac{1}{r}\left(\frac{v^2}{r} - \frac{v}{r}\frac{\partial u}{\partial \theta}\right)$$

With the following boundary conditions

$$\frac{\partial P_s}{\partial r} = \frac{v^2}{r} \quad \text{at} \quad r = R_i, R_o \tag{17a}$$

$$\frac{\partial P_t}{\partial z}=0 \quad \text{at} \quad z=0, H \tag{17b}$$

The existence and uniqueness of the solution to equation (16), with the boundary conditions (17a) and (17b), requires that the integration of the following condition

$$\iint_A \nabla P_t \cdot \mathbf{n}\, dr\, dz=\int_C r\frac{\partial P_t}{\partial n}\, dC \tag{18}$$

where A is the duct inlet cross-sectional area, n is the outward normal to the contour, C, enclosing the area, A, and dC is the incremental distance along C. The derivation of Poisson's equation may be based on satisfying the continuity equation at the inlet plane, and its solution is unique within an arbitrary constant.

In addition, Bernoulli and Helmholtz equations take the following forms at the duct boundaries

$$\frac{v}{r}\frac{\partial P}{\partial \theta}+w\frac{\partial P}{\partial z}=0 \quad \text{at} \quad r=R_i, R_o, \tag{19a}$$

$$u\frac{\partial P}{\partial r}+\frac{v}{r}\frac{\partial P}{\partial \theta}=0 \quad \text{at} \quad z=0, H \tag{19b}$$

$$\frac{v}{r}\frac{\partial \xi}{\partial \theta}+w\frac{\partial \xi}{\partial z}=\frac{1}{r}\frac{\partial w}{\partial \theta}\frac{\partial v}{\partial r}+\frac{\xi}{r}\frac{\partial v}{\partial \theta}+\frac{v}{r}\frac{\partial v}{\partial z}-\frac{1}{r}v\left[\frac{1}{r}\frac{\partial w}{\partial \theta}-\frac{\partial v}{\partial z}\right] \quad \text{at} \quad r=R_i, R_o \tag{20a}$$

and

$$u\frac{\partial \xi}{\partial r}+\frac{v}{r}\frac{\partial \xi}{\partial \theta}=\frac{\xi}{r}\frac{\partial v}{\partial \theta}-\frac{1}{r}\frac{\partial u}{\partial \theta}\frac{\partial v}{\partial z}+\frac{1}{r}\left[u\xi+2v\frac{\partial v}{\partial z}\right] \quad \text{at} \quad z=0, H \tag{20b}$$

The corner values for P and ξ are calculated using a stable extrapolation process, similar to the method used in [16].

The Boundary Conditions for the Streamlike Functions. The following inlet and exit flow conditions for the flow velocities as well as the no-flux condition at the duct boundaries, are used to determine the boundary conditions for the three streamlike functions

At inlet

$$u=0 \tag{21a}$$

$$v=v_i \tag{21b}$$

$$w=0 \tag{21c}$$

At $r=R_i, R_o$

$$u=0 \tag{22}$$

At $z=0, H$

$$w=0 \tag{23}$$

At exit

$$\frac{1}{r}\frac{\partial u}{\partial \theta}=0 \tag{24a}$$

$$\frac{1}{r}\frac{\partial w}{\partial \theta}=0 \tag{24b}$$

$$\frac{1}{r}\frac{\partial v}{\partial \theta}=0 \tag{24c}$$

In addition, the following condition is used to uniquely determine χ_b, χ_c, and χ_v:

$$\frac{\partial \chi_v}{\partial r}+\frac{\chi_v}{r}+\frac{1}{r}\frac{\partial \chi_c}{\partial \theta}+\frac{\partial \chi_b}{\partial z}=0 \tag{25}$$

Equations (21–25) are used together with equations (7–9) and equations (13), to obtain the following boundary conditions for χ_v, χ_c, and χ_b. The integration reference surfaces for the integrals in equations (7–9) are chosen here to be represented by $r_1 = R_i$ and $z_1 = 0$, respectively.

At inlet

$$\chi_v=0 \tag{26a}$$

$$\chi_b=-\int_{R_i}^{r} v_i\, dr \tag{26b}$$

$$\frac{1}{r}\frac{\partial \chi_c}{\partial \theta}=\frac{\partial}{\partial z}\int_{R_i}^{r} v_i\, dr \tag{26c}$$

At $r=R_i$

$$\chi_b=0 \tag{27a}$$

$$\chi_c=0 \tag{27b}$$

$$\frac{\partial \chi_v}{\partial r}+\frac{\chi_v}{r}=0 \tag{27c}$$

At $r=R_o$

$$\chi_b=-\int_{R_i}^{R_o} v_i\, dr \tag{28a}$$

$$\chi_c=0 \tag{28b}$$

$$\frac{\partial \chi_v}{\partial r}+\frac{\chi_v}{r}=\frac{\partial}{\partial z}\int_{R_i}^{R_o} v_i\, dr \tag{28c}$$

At $z=0, H$

$$\chi_v=0 \tag{29a}$$

$$\chi_c=0 \tag{29b}$$

$$\frac{\partial \chi_b}{\partial z}=0 \tag{29c}$$

At exit

$$\frac{1}{r}\frac{\partial \chi_b}{\partial \theta}=0 \tag{30a}$$

$$\frac{1}{r}\frac{\partial \chi_c}{\partial \theta}=0 \tag{30b}$$

$$\frac{1}{r}\frac{\partial \chi_v}{\partial \theta}=0 \tag{30c}$$

The governing equations (5), (6), (10), (11) and (12) with the conditions given by equations (14), (15), and (26–30) form a closed system which is solved for the variables χ_b, χ_c, χ_v, ξ, and P.

Results and Discussions

The results of the computations of the secondary flow in curved ducts caused by total pressure inlet distortion are presented. The iterative solution procedure is based on the use of successive over relaxation method for the solution of the three streamlike function equations, and Lax's [20] marching scheme for the total pressure and through flow vorticity equations. The results are presented and compared with the experimental measurements of Joy [19] for the flow in a curved duct with constant curvature and rectangular cross section. Joy [19] obtained flow measurements in a curved rectangular duct of 0.125 × 0.25-m (5 × 10-in.) cross section, 0.375-m (15-in.) mean radius, and 90 deg turning angle. A large velocity gradient was produced in the experiment using screens placed before the curved portion of the duct, which resulted in a nearly symmetrical velocity profile at inlet to the bend. The velocity contours in the lower half of the duct are shown in Fig. 2. The computations were carried out in the lower half of the duct to take advantage of the symmetry. The

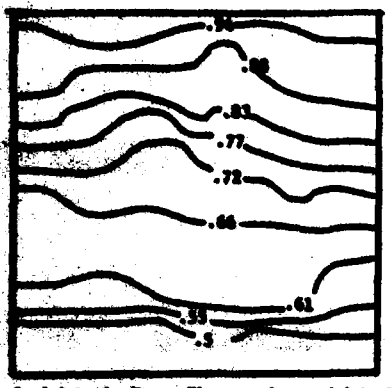

Fig. 2 Inlet velocity profile, experimental data, [19]

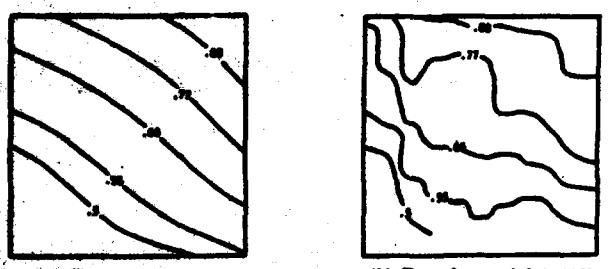

(a) Computed results (b) Experimental data [19]

Fig. 3 Velocity contours at $\theta = 30$ deg

results of the computations are compared with Joy's flow measurements at 30, 60, and 90 deg turning angles. The magnitudes of the flow velocities in Figs. 2–5 are normalized with respect to the maximum inlet velocity. It can be seen from these figures that the computed results are in good agreement with the experimental measurements at the 30 and 90 deg turning angles. There is a lack of agreement however with the experimental results at the 60 deg turning angle inner wall near the duct centerline. Other investigators [12, 15] comparing with the same experimental results speculated viscous boundary layer separation there and attributed the lack of agreement to it. The analysis otherwise predicts the measured contour rotation caused by the secondary flow development. The computed static pressure contours at 0, 30, 60 and 90 deg turning angles are presented in Figs. 6. These contours show that the static pressure is not constant over the cross sections even at zero duct turning angle. The static pressure gradient in the radial direction is necessary to balance the centrifugal forces. Joy [19] did not obtain static pressure measurements that could be compared with the present results; however, static pressure contours similar to those of Fig. 6*a*, were measured by Brunn [20] in a curved duct at zero turning angles. The effect of the secondary flow development on the pressure distribution is demonstrated in these figures by the variation in the shape of the contours with the duct turning angle. The computations were carried out using a uniform ($9 \times 9 \times 31$) grid in the r-, z-, and θ-directions, respectively. The convergence of the iterative procedure was very fast, as shown in Fig. 7, which presents the average of the absolute value of the error in the calculation of u_h, the through velocity component from the χ_h solution. The exchange of information from the solutions on the vertical and cross-sectional surfaces to this surface does not start until the second iteration, which leads to maximum error that consequently decreases very rapidly. The solution was obtained using double precision with 50 outer iterations and 120 iterations in the solution of the differential equations for χ_r, χ_θ, and χ_z on all 49 surfaces and required 4.5 min on AMDAHL 470. The authors have not attempted to optimize the

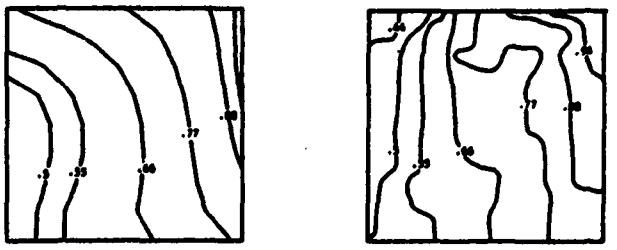

(a) Computed results (b) Experimental data [19]

Fig. 4 Velocity contours at $\theta = 60$ deg

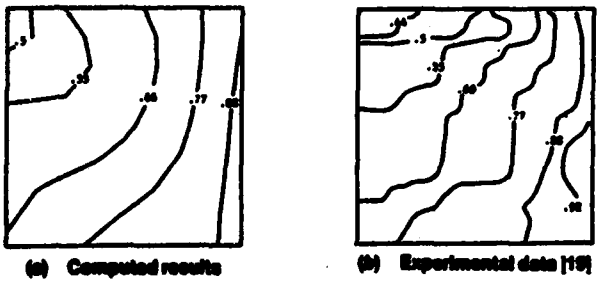

(a) Computed results (b) Experimental data [19]

Fig. 5 Velocity contours at $\theta = 90$ deg

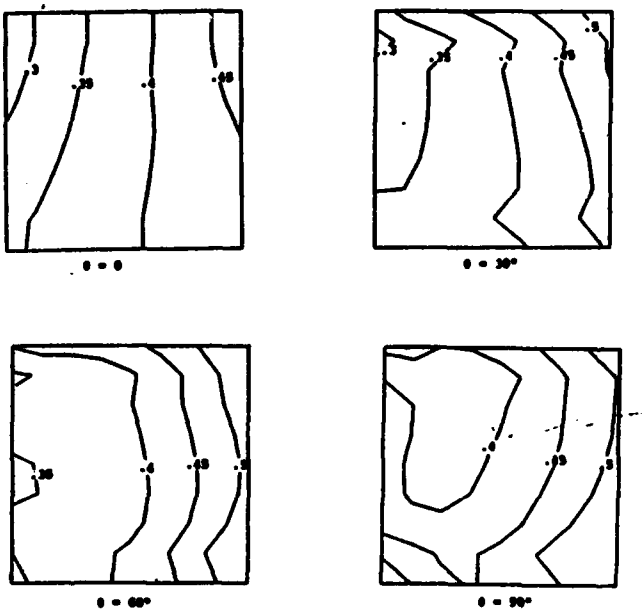

Fig. 6 Static pressure coefficient contours at $\theta = 0$, 30, 60 and 90 deg

CPU time through changing the number of iterations in the solution of Poisson's equations with the outer iteration cycles, or to reduce the CPU time through the use of noniterative methods [21, 22] in the code. At present, direct Poisson solvers codes are being studied for incorporation into the numerical solution. This is expected to lead to considerable CPU time savings when it is combined with the streamlike function formulation and its corresponding Dirichlet boundary conditions.

Conclusions

It can be concluded that the present analysis can predict the inviscid secondary flow development caused by inlet total pressure distortion and the results of the computations compare with the experimental measurements. Through the elliptic solution, the influence of the downstream conditions

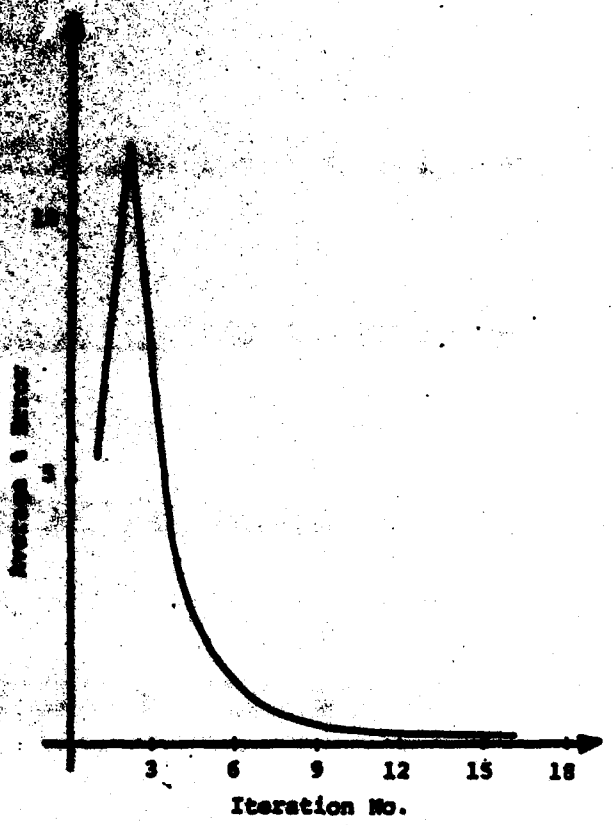

Fig. 7 Typical error variation for u_θ solutions

on the flow is included. The solution is very efficient due to the use of the streamlike function in the formulation. In addition, convergence is very fast because of the interaction mechanism between the three solutions on the three sets of orthogonal surfaces.

Acknowledgment

This research was sponsored by the U.S. Air Force Office of Scientific Research under contract No. 80-0242.

References

1 Wu, C. H., "A General Theory of Three Dimensional Flow in Subsonic and Supersonic Turbomachines of Axial, Radial and Mixed-Flow Types," NACA TN-2604, 1952.

2 Marsh, H., "A Digital Computer Program for the Through Flow Fluid Mechanics in an Arbitrary Turbomachine Using a Matrix Method," Aero. Research Council R&M 3509, 1968.

3 Katsanis, T., "Revised Fortran Program for Calculating Velocities and Streamlines on the Hub-Shroud Midchannel Stream Surface of an Axial-, Radial- or Mixed-Flow Turbomachine or Annular Duct. I: User's Manual," NASA TND-8430, July 1977.

4 Katsanis, T., "Computer Program for Calculating Velocities and Streamlines on a Blade-to-Blade Stream Surface of a Turbomachine," NASA TND-8525, 1968.

5 Smith, D. J. L., "Computer Solutions of Wu's Equations for Compressible Flow Through Turbomachines," NASA SP-304, Fluid Mechanics Acoustics and Design of Turbomachinery, Part I, pp. 43–74, 1974.

6 Bosman, C., and El-Shaarawi, M. A. I., "Quasi-Three-Dimensional Numerical Solution of Flow in Turbomachines," ASME Paper No. 76-FE-23, 1976.

7 Katsanis, S., "The Calculation of the Quasi-Three-Dimensional Flow in an Axial Gas Turbine," ASME, Journal of Engineering for Power, Apr. 1973, pp. 283–294.

8 Wilkinson, D. H., "Calculation of Blade-to-Blade Flow in Turbomachines by Streamline Curvature," Aeronautical Research Council R&M No. 3704, 1972.

9 Novak, R. A., and Hearsey, R. M., "A Nearly Three-Dimensional Intrablade Computing System for Turbomachinery," ASME, Journal of Fluids Engineering, Mar. 1977, pp. 154–166.

10 Katsanis, T., "Fortran Program for Calculating Transonic Velocities on a Blade-to-Blade Stream Surface of a Turbomachine," NASA TND-5427, Sept. 1969.

11 Katsanis, T., "Use of Arbitrary Quasi-Orthogonals for Calculating Flow Distribution in the Meridional Plane of a Turbomachine," NASA TND-2809, May 1965.

12 Stuart, A. R., and Hetherington, R., "The Solution of the Three Variable Duct Flow Equations," Fluid Mechanics, Acoustics and Design of Turbomachinery, pt. 1, NASA SP-304, 1974, pp. 135–153.

13 Hawthorne, W. R., "Secondary Circulation in Fluid Flow," Proc. Roy. Soc. A, Vol. 206, 1951, p. 374.

14 Squire, H. B., and Winter, K. G., "The Secondary Flow in a Cascade of Airfoils in a Nonuniform Stream," Journal of Aeronautical Sciences, Vol. 18, 1951, pp. 247–274.

15 Fagan, J. R., "Three-Dimensional Subsonic Duct Flow Analysis," Detroit Diesel Allison, Division of General Motors Corp., EDR7451, 1972.

16 Abdallah, S., and Hamed, A., "Inviscid Solution for the Secondary Flow in Curved Ducts," AIAA Journal, Vol. 19, Aug. 1981, pp. 999–999.

17 Stother, T., and Langston, L. S., "Three-Dimensional Modeling of Cascade Flow," AIAA Paper 79-0047, 1979.

18 Hamed, A., and Abdallah, S., "Streamline Function: A New Concept in Flow Problems Formulation," Journal of Aircraft, Vol. 16, No. 12, Dec. 1979, pp. 801–802.

19 Joy, W., "Experimental Investigation of Shear Flow in Rectangular Bends," M.S. thesis, Massachusetts Institute of Technology, 1950.

20 Lax, P. D., "Weak Solutions of Nonlinear Hyperbolic Equations and Their Numerical Computation," Communications on Pure and Applied Mathematics, Vol. 7, 1954, pp. 159–193.

21 Brown, H. H., "An Experimental Investigation of Secondary Flow Losses in Bends with Rectangular Cross Sections," CUED/A-Turbo/TR 95, University of Cambridge, Department of Engineering, 1979.

22 Dorr, F. W., "The Direct Solution of the Discrete Poisson Equation on Rectangle," SIAM Review, Vol. 12, No. 2, Mar. 1970, pp. 248–263.

23 Sweet, R. A., "A Cyclic Reduction Algorithm for Solving Block Tridiagonal Systems of Arbitrary Dimension," SIAM Journal on Numerical Analysis, Vol. 14, No. 4, Sept. 1977, pp. 706–720.

Appendix 3

Three Dimensional Rotational Compressible Flow Solution in Variable Area Channels

83

Rotational Compressible
in Variable Area Channels

and C. [illegible], Univ. of Cincinnati,

AIAA 21st Aerospace Sciences Meeting

January 10-13, 1983/Reno, Nevada

THREE-DIMENSIONAL ROTATIONAL COMPRESSIBLE FLOW SOLUTION IN VARIABLE AREA CHANNELS†

A. Hamed* and C. Liu**
Department of Aerospace Engineering and Applied Mechanics
University of Cincinnati
Cincinnati, Ohio 45221

Abstract

This paper presents the analytical formulation and numerical solution of compressible inviscid rotational flow in a variable area duct. The three dimensional flow field is synthesized from the streamlike function solution on three sets of orthogonal surfaces in the passage. This leads to a very economical elliptic solution that is adaptable to turbomachinery applications since it simulates the downstream conditions and channel area variation. The computed results for compressible rotational flow with shear inlet velocity in variable area curved ducts are presented to determine the influence of the area variation and the effects of compressibility on the three-dimensional flow field.

Nomenclature

h	total enthalpy
h_1, h_2, h_3	metric coefficients
P	total pressure
p	static pressure
S	entropy
T	total temperature
V_1, V_2, V_3	velocity components
x_1, x_2, x_3	orthogonal curvilinear coordinates
ρ	density
σ	source term
χ	streamlike function
$\Omega_1, \Omega_2, \Omega_3$	vorticity components

Subscripts

c	cross sectional
h	horizontal
I	inlet
max	maximum
r	reference point
v	vertical

Introduction

Recent developments of computational methods for three dimensional flows in turbomachine blade passages and curved ducts include both viscous and inviscid flow models. The parabolic methods[1,2] were first developed for the solution of internal viscous flows. These methods are based on the assumption of the small influence of the downstream pressure field on the upstream flow conditions, which leads to parabolic governing equations. The use of marching techniques leads to a very efficient solution but it also limits its application to flow in ducts with mild curvature. Later partially parabolic methods[3,4] were developed in which the diffusion of mass, momentum and energy in the streamwise direction were still neglected but the elliptic influence was transmitted upstream through the pressure field.

Numerical methods have also been developed for the solution of inviscid flows[5-16]. The approaches used in the numerical solution are considerably different depending on the flow model and the problem formulation. Earlier quasi-three dimensional methods[5-8] consisted of an interactive procedure between two dimensional flow solutions on blade to blade and hub to tip stream surfaces. These efficient two dimensional solvers allowed for arbitrarily superimposed loss models[9,10] but for most of the solutions, the blade to blade stream surface was taken as a surface of revolution[8-9]. The attempts to extend these methods to rotational flow were not successful[11] because the stream surfaces become twisted and warped. It was found that the iterative procedure between the two solutions does not converge in this case through the exchanged information during iterations in the form of stream surface shape and stream filament thickness. Time dependent techniques have been developed for the solution of three dimensional rotational flows[12,13] and were used in flow field calculations[14]. Aside from the time dependent technique, two other methods[15,16] were developed for the solution of internal

† This research was supported by the Air Force Office of Scientific Research, under Grant No. 80-0242.

* Professor, Department of Aerospace Engineering and Applied Mechanics, University of Cincinnati, Cincinnati, Ohio. Associate Fellow AIAA.

**Visiting Scientist. Senior Engineer, The Shenyang Aeroengine Research Institute

inviscid rotational flows. Lancor and Stone[15] developed a very simple model for the solution of oligraphic flow fields by splitting the velocity vector into irrotational and rotational parts. They used a single function to describe the rotational part, for this special class of problems, in which the rothalpy and entropy gradients are orthogonal to the vorticity vector.

Abdallah and Hamed[16] presented a method for the elliptic solution of three dimensional rotational incompressible inviscid flow in which the velocity vector is synthesized from two dimensional solutions of three streamlike functions on three sets of orthogonal surfaces. Aside from incompressibility, no additional assumptions were imposed that might limit the analysis to a special class of problems. The present work represents an extension of that analysis to compressible flow fields with generalized channel geometries using orthogonal curvilinear body fitted coordinates. The problem formulation leads to a very efficient solution since the governing equations for the streamlike functions consist of Poisson's equations with Dirichlet boundary conditions while the governing equations for total pressure, total enthalpy and streamwise vorticity are hyperbolic. The convergence of this three-dimensional solution is very fast[16] and does not suffer from the problems encountered with the traditional quasi-three-dimensional methods in the presence of streamwise vorticity.

Analysis

The governing equations used in the numerical solution of the compressible three dimensional inviscid rotational internal flow are derived from the basic equations of conservation of mass momentum and energy in orthogonal curvilinear body fitted coordinates. In the analysis, hyperbolic equations are derived for the through flow vorticity, the total enthalpy, while elliptic equations are derived for three sets of streamlike functions which are defined on fixed orthogonal surfaces. The details of the analysis for incompressible flow can be found in reference 16. In the following derivations, the same approach is applied to compressible flow using orthogonal curvilinear coordinates.

The Streamlike Function Formulation

The equation of conservation of mass for compressible flow in curvilinear coordinates is given by

$$\frac{\partial}{\partial x_1}(h_2h_3\rho V_1) + \frac{\partial}{\partial x_2}(h_1h_3\rho V_2) + \frac{\partial}{\partial x_3}(h_1h_2\rho V_3) = 0 \qquad (1)$$

where V_1, V_2 and V_3 are the velocity components in the directions of the x_1, x_2, x_3 coordinates, respectively, ρ is the flow density and h_1, h_2, h_3 are the metric coefficients of the orthogonal curvilinear coordinates.

The equation of conservation of mass is identically satisfied through the definition of three streamlike functions[17] χ_h, χ_v and χ_c. The streamlike function χ_h is defined such that its derivatives on the surface x_3 = constant are related to the two velocity components V_{1h}, V_{2h} as follows:

$$\frac{\partial}{\partial x_1}(h_3\chi_h) = h_1h_3\rho V_{2h} + \int_{x_{2r}}^{x_2} \frac{\partial}{\partial x_3}(h_1h_2\rho V_{3v})\,dx_2 \qquad (2a)$$

and

$$\frac{\partial}{\partial x_2}(h_3\chi_h) = -h_2h_3\rho V_{1h} \qquad (2b)$$

The following definition of the second streamlike function χ_v is given in terms of its derivatives on the surface x_2 = constant:

$$\frac{\partial}{\partial x_1}(h_2\chi_v) = -h_1h_2\rho V_{3v} - \int_{x_{3r}}^{x_3} \frac{\partial}{\partial x_2}(h_1h_3\rho V_{2h})\,dx_3 \qquad (3a)$$

and

$$\frac{\partial}{\partial x_3}(h_2\chi_v) = h_2h_3\rho V_{1v} \qquad (3b)$$

The third streamlike function χ_c is similarly defined as follows:

$$\frac{\partial}{\partial x_3}(h_1\chi_c) = -h_1h_3\rho V_{2c} + \int_{x_{2r}}^{x_2} \frac{\partial}{\partial x_3}(h_1h_2\rho V_{3v})\,dx_2 \qquad (4a)$$

and

$$\frac{\partial}{\partial x_2}(h_1\chi_c) = h_1h_2\rho V_{3c} - \int_{x_{3r}}^{x_3} \frac{\partial}{\partial x_2}(h_1h_3\rho V_{2h})\,dx_3 \qquad (4b)$$

The integrals on the right hand sides of equations (2) through (4) represent source terms which are dependent upon the flow crossing the three sets of fixed orthogonal surfaces. The superposition of the velocity components in the above streamlike function definitions gives the three gas velocity components V_1, V_2 and V_3, which identically satisfy the conservation of mass equation (1)

$$V_1 = V_{1h} + V_{1v} \tag{5a}$$

$$V_2 = V_{2h} + V_{2c} \tag{5b}$$

$$V_3 = V_{3v} + V_{3c} \tag{5c}$$

Governing Equations

The equations of conservation of momentum and energy in a stationary passage are given by:

$$\vec{\nabla} \times (\vec{\Omega}) = \nabla H - T \nabla S \tag{6}$$

and

$$\vec{\nabla} \cdot \vec{W} = 0 \tag{7}$$

where

$$\vec{\Omega} = \nabla \times \vec{\nabla} \tag{8}$$

It is known that temperature gradients generate secondary flow only when it is accompanied by gradients in the velocity and entropy such that gradient in stagnation pressure exists[18]. Therefore, in the present analysis the momentum equation is expressed in terms of the total pressure, P, which is used as one of the flow variables in the solution.

$$\vec{\nabla} \times (\nabla \times \vec{\nabla}) = \frac{\nabla^2}{2} \frac{\nabla H}{H} + \frac{P}{\rho} \frac{\nabla P}{P} \tag{9}$$

Two hyperbolic equations can be derived for the total pressure P and the through flow vorticity Ω_1 from equation (9). The following equation for the total pressure can be obtained through taking the dot product of the velocity vector with equation (6)

$$\vec{\nabla} \cdot \nabla P = 0 \tag{10}$$

The following equation can also be derived for the through flow vorticity development from the momentum equation:

$$\vec{\nabla} \cdot \nabla \left(\frac{\Omega_1}{\rho}\right) = \frac{\vec{\Omega}}{\rho} \cdot \nabla V_1 + \frac{1}{\rho h_1 h_2} \frac{\partial h_1}{\partial x_2} (\Omega_1 V_2 - \Omega_2 V_1)$$

$$+ \frac{1}{\rho h_1 h_3} \frac{\partial h_1}{\partial x_3} (\Omega_1 V_3 - \Omega_3 V_1)$$

$$+ \frac{1}{\rho^3} \frac{1}{h_2 h_3} \left[\frac{\partial \rho}{\partial x_2} \frac{\partial P}{\partial x_3} - \frac{\partial \rho}{\partial x_3} \frac{\partial P}{\partial x_2}\right] \tag{11}$$

It is clear that the above equation also represents the x_1 component of Helmholtz equation which can be written in the following form for inviscid compressible flow

$$(\vec{\nabla} \cdot \nabla) \frac{\vec{\Omega}}{\rho} = \left(\frac{\vec{\Omega}}{\rho} \cdot \nabla\right) \vec{\nabla} - \frac{1}{\rho} \nabla \times \left(\frac{1}{\rho} \nabla P\right) \tag{12}$$

In the above equations Ω_1, Ω_2 and Ω_3 are three vorticity components which can be expressed in terms of the velocity derivatives from the definition of the vorticity vector (equation 8).

The elliptic governing equations for the streamlike functions χ_h, χ_v and χ_c can be obtained from the substitution of equations (2) through (5) into the x_2 and x_3 components of equation (9) and the x_1 component of equation (8) respectively.

$$\frac{\partial}{\partial x_1} \left[\frac{h_2}{h_1 h_3} \frac{\partial}{\partial x_1} (h_3 \chi_h)\right] + \frac{\partial}{\partial x_2} \left[\frac{h_1}{h_2 h_3} \frac{\partial}{\partial x_2} (h_3 \chi_h)\right]$$

$$= h_1 h_2 \sigma_h \tag{13}$$

$$\frac{\partial}{\partial x_3} \left[\frac{h_1}{h_2 h_3} \frac{\partial}{\partial x_3} (h_2 \chi_v)\right] + \frac{\partial}{\partial x_1} \left[\frac{h_3}{h_1 h_2} \frac{\partial}{\partial x_1} (h_2 \chi_v)\right]$$

$$= h_1 h_3 \sigma_v \tag{14}$$

$$\frac{\partial}{\partial x_2} \left[\frac{h_3}{h_1 h_2} \frac{\partial}{\partial x_2} (h_1 \chi_c)\right] + \frac{\partial}{\partial x_3} \left[\frac{h_2}{h_1 h_3} \frac{\partial}{\partial x_3} (h_1 \chi_c)\right]$$

$$= \sigma_c \tag{15}$$

where

$$\sigma_h = -\frac{\rho}{V_1} \left[\frac{V^2}{2H h_2} \frac{\partial H}{\partial x_2} + \frac{P}{\rho P h_2} \frac{\partial P}{\partial x_2} - V_3 \Omega_1\right]$$

$$+ \frac{V_2}{h_1} \frac{\partial \rho}{\partial x_1} - \frac{V_1}{h_2} \frac{\partial \rho}{\partial x_2}$$

$$+ \frac{1}{h_1 h_2} \left[\frac{\partial}{\partial x_2} (h_1 \rho V_{1v}) - \frac{\partial}{\partial x_1} (h_2 \rho V_{2c})\right]$$

$$+ \frac{1}{h_1 h_2} \frac{\partial}{\partial x_1} \left[\frac{h_2}{h_1 h_3} \int_{x_{2r}}^{x_2} \frac{\partial (\rho h_1 h_2 V_{3v})}{\partial x_3} dx_2\right] \tag{16a}$$

and

$$\sigma_v = \frac{\rho}{V_1} \left[\frac{V^2}{2H h_3} \frac{\partial H}{\partial x_3} + \frac{P}{\rho P h_3} \frac{\partial P}{\partial x_3} + V_2 \Omega_1\right]$$

$$- \frac{V_3}{h_1} \frac{\partial \rho}{\partial x_1} + \frac{V_1}{h_3} \frac{\partial \rho}{\partial x_3}$$

$$- \frac{1}{h_1 h_3} \frac{\partial}{\partial x_3} (\rho h_1 V_{1h}) + \frac{1}{h_1 h_3} \frac{\partial}{\partial x_1} (\rho h_3 V_{3c})$$

$$- \frac{1}{h_1 h_3} \frac{\partial}{\partial x} \left[\frac{h_3}{h_1 h_2} \int_{x_{3r}}^{x_3} \frac{\partial (\rho h_1 h_3 V_{2h})}{\partial x_2} dx_3\right] \tag{16b}$$

and

$$\Omega_c = \rho h_2 h_3 \Omega_1 - \left[\frac{\partial}{\partial x_2}(\rho h_3 V_{3v}) - \frac{\partial}{\partial x_3}(\rho h_2 V_{2h})\right]$$

$$- \frac{\partial}{\partial x_2}\left[\frac{h_3}{h_1 h_2}\int_{x_{3r}}^{x_3} \frac{\partial}{\partial x_2}(\rho h_1 h_3 V_{2h})\, dx_3\right]$$

$$+ \frac{\partial}{\partial x_3}\left[\frac{h_2}{h_1 h_3}\int_{x_{2r}}^{x_2} \frac{\partial}{\partial x_3}(\rho h_1 h_2 V_{3v})\, dx_2\right]$$

$$+ h_3 V_3 \frac{\partial \rho}{\partial x_2} - h_2 V_2 \frac{\partial \rho}{\partial x_3} \qquad (16c)$$

Solution Procedure

The analytical formulation results in two-dimensional Poisson's equations for the streamlike functions. These equations are obtained from satisfying the equations of motion on three sets of orthogonal surfaces represented by constant values of the coordinates x_1, x_2 and x_3 as shown in Fig. 1. The source term in the resulting equations are dependent upon the variation of the flow properties and on the flux in the direction normal to these surfaces. An iterative procedure is used in the numerical solution because of the dependency of the source term in each set of streamlike function equations on the solutions obtained for the remaining two sets.

The iterative procedure for the numerical computations consists of the use of a marching technique[16] in the solution of equations (7), (10) and (11) along the through flow direction x_1, and a successive over relaxation method for the solution of the two dimensional elliptic equations (13), (14) and (15) for the streamlike functions. The flow density, which is allowed to lag one iteration in the numerical computations is determined from the local total pressure, total stagnation enthalpy, and from the flow velocity:

$$\rho = \frac{P}{RT}\left[1 - \frac{V^2}{2H}\right]^{(1/\gamma-1)} \qquad (17)$$

The boundary conditions for the streamlike functions are carefully chosen to insure the uniqueness of the solution.[16] Dirichlet boundary conditions are determined for the streamlike functions from the requirement of zero flux at the duct boundaries.[17] The x_1 derivatives of the flow velocities are set equal to zero at the duct exit, while the Dirichlet boundary conditions for the streamlike functions at $x_1 = 0$, are expressed in terms of integrals of the inlet flux. The total pressure, total temperature and through flow vorticity profiles are required at the duct inlet to start the marching solution. More details about the numerical procedure can be found in reference 16.

Results and Discussion

The results of the numerical computations are presented in an accelerating rectangular elbow and compared with existing experimental measurements [19]. The duct was designed by Stanitz,[20] using inviscid incompressible two dimensional analysis to avoid boundary layer separation. This experimental data was also used for comparison with results of the numerical analysis by other investigators.[15,21] The experimental measurements were obtained for different inlet total pressure profiles to investigate the effects of secondary flow. The inlet total pressure profiles were generated using perforated plates of different heights as spoilers. Figure 2 shows the duct geometry and the computational grid in the x_1 and x_2 directions. Due to symmetry, the flow computations were performed in the lower half of the duct using a (9 x 13 x 55) grid in the x_3, x_2 and x_1 directions, respectively. Figure 3 shows the inlet velocity profiles which were used in the numerical calculations with no variation in the x_2 direction. The experimental measurements for 2.5 inch spoiller which were obtained half way between the pressure and suction surfaces are shown in the same figure. The results of the computations are presented in non-dimensional form in Figs. 4 through 8. The flow velocities are normalized with respect to the maximum inlet velocity, $V_{I_{max}}$, while the pressures are normalized with respect to the critical pressure, which corresponds to a tank gauge pressure of 20 inches water in the experimental measurements.

The orthogonal curvilinear body fitted coordinates for the flow computations were generated numerically using the code developed by Davis[22] which is based on the Schwartz-Kristoffel transformation. The values of the orthogonal coordinate in the transformed plane were between 0 and 1 in the x_2 direction and 0 and 6.791 in the x_1 direction. The computational grid is uniform in the x_3 direction where half the duct height is equal to 1.875 times the duct exit width. The convergence of the numerical solution was fast with CPU time of 3.5 minutes for 25 outer iterations on AMDAHL 370. The inner iterations did not exceed 25 in all the iterative solutions for χ_h, χ_v and χ_c solutions on all 77 surfaces.

The results are presented first for the computed static pressure coefficient distribution over the duct curved walls and are compared with the experimental measurements. Complete spanwise static pressure distributions over the pressure and suction surfaces of the elbow were reported by Stanitz et al [19], for the flow with nominal exit Mach number of 0.26.

Figures 4 and 5 show the computed static pressure coefficient distribution over the duct curved boundaries at two

[illegible]. The static pressure [illegible] is defined as the difference between the local static pressure, p_s, and the [illegible] pressure normalized by the [illegible] pressure:

$$C_p = \frac{p_s - p}{p_t - p_s}$$

[illegible] pressure coefficient obtained [illegible] the experimental measurements with [illegible] code is also shown in the same [illegible]. These figures show good agreement [illegible] the present results and the [illegible] measurements over most of the [illegible] surface and the first half of the suction surface. From these figures, one can see a discrepancy between the [illegible] analysis and the experimental [illegible] over half of the suction [illegible] near the duct exit. Similar [illegible] were reported in the computed [illegible] of the inviscid solution of [illegible] 13 and were attributed to viscous dissipation effects. This is confirmed by Stanitz studies[19] which show that secondary flow begins to roll up half way along the duct length towards the suction surface.

Figure 6 shows the computed total pressure contours at the cross sectional surfaces corresponding to M_1 = 1, 23, 31 and 43. These cross sections correspond to ℓ/s = 0, 2.0, 3.0 and 4.5 in Stanitz data[19]. One can follow the development of the secondary flow through the rotation of the Hamrelli surfaces which were parallel to the end walls at the duct inlet.

Figure 7 shows the streamwise vorticity contours at different cross sectional surfaces corresponding to M_1 = 23, 31 and 43 respectively. The streamwise vorticity is normalized with respect to the ratio of the maximum inlet velocity to the duct exit width. The computed results predict an initial increase in the through flow vorticity components in the first half of the duct length from its zero value at inlet, then a decrease in Ω_1, towards the duct exit. The region of maximum through flow vorticity near the end wall is seen to move across the passage from the pressure surface towards the suction surface. It is interesting to observe that through flow vorticity development spreads across the passage and is not limited to the end wall. This is not surprising since one can see from Fig. 3 that the shear flow occupies about half the area at the duct inlet.

Conclusions

A method is presented for the analysis of internal three dimensional compressible inviscid rotational flow. The streamlike function formulation leads to a very economical elliptic solution that is suitable for turbomachinery applications. The analysis is general and applicable to flow fields with both total pressure and total temperature gradients. The results of the computations are presented for the flow in an accelerating rectangular elbow with shear inlet velocity profile and 90° turning angle. The analysis predicts the secondary flow development and the computed results are in agreement with the experimental measurements in the regions where the viscous dissipation effects are not significant.

References

1. Patankar, S.V., Spalding, D.B., "A Calculation Procedure for Heat, Mass and Momentum Transfer in 3-D Parabolic Flows," Int. J. Heat and Mass Transfer, Vol. 15, p. 1787, 1972.

2. Briley, W.R., "Numerical Method for Predicting 3-D Steady Viscous Flow in Ducts," J. Comp. Phys., Vol. 14, p. 8, 1974.

3. Pratap, V.S., Spalding, D.B., "Fluid Flow and Heat Transfer in 3-D Duct Flows," Int. J. Heat and Mass Transfer, Vol. 19, pp. 1183-1188, 1976.

4. Dodge, P.R., "A Numerical Method for 2-D and 3-D Viscous Flows," AIAA Paper No. 76-425, 1976.

5. Wu, C.H., "A General Theory of Three Dimensional Flow in Subsonic and Supersonic Turbomachines of Axial, Radial and Mixed-Flow Types," NACA TN-2604, 1952.

6. Smith, D.J.L., "Computer Solutions of Wu's Equations for Compressible Flow Through Turbomachines," NASA SP-304, Fluid Mechanics Acoustics and Design of Turbomachinery, Part I, pp. 43-74, 1974.

7. Bosman, C. and El-Shaarawi, M.A.I., "Quasi Three-Dimensional Numerical Solution of Flow in Turbomachines," ASME Paper No. 76-FE-23, 1976.

8. Biniaris, S., "The Calculation of the Quasi-Three-Dimensional Flow in an Axial Gas Turbine," J. of Engineering for Power, April 1975, pp. 283-294.

9. Katsanis, T., "Fortran Program for Calculating Transonic Velocities on a Blade-to-Blade Stream Surface of a Turbomachine," NASA TND-5247, Sept. 1969.

10. Katsanis, T., "Revised Fortran Program for Calculating Velocities and Streamlines on the Hub-Shroud Midchannel Stream Surface of an Axial-, Radial- or Mixed-Flow Turbomachine or Annular Duct. I: User's Manual," NASA TND-8430, July 1977.

11. Stuart, A.R. and Hetherington, R., "The Solution of the Three Variable Duct Flow Equations," NASA SP-304, Fluid Mechanics, Acoustics and Design of Turbomachinery, Part I, 1974, pp. 139-153.

12. Denton, J.D., "A Time Marching Method for Two and Three Dimensional Blade-to-Blade Flows," ARC R&M 3775, 1975.

13. Pandolfi, M. and Colasurdo, G., "Three-Dimensional Inviscid Compressible Rotational Flows - Numerical Results and Comparisons with Analytical Solutions," ASME Flow in Primary Non-rotating Passages in Turbomachines," ASME Symposium, pp. 141-149, 1979.

14. Barber, T. and Langston, L.S., "Three Dimensional Modelling of Cascade Flow," AIAA Paper 79-0047, 1979.

15. Lacor, C. and Hirsch, Ch., "Rotational Flow Calculations in Three Dimensional Blade Passages," ASME Paper No. 82-GT-316, 1982.

16. Abdallah, S. and Hamed, A., "The Elliptic Solution of the Secondary Flow Problem," ASME Paper No. 82-GT-242, 1982.

17. Hamed, A. and Abdallah, S., "Stream-like Function: A New Concept in Flow Problems Formulation," Journal of Aircraft, Vol. 16, No. 12, December 1979, pp. 801-802.

18. Lakshminarayana, B., "Effects of Inlet Temperature Gradients on Turbomachinery Performance," J. of Engineering for Power, Vol. 97, No. 1, pp. 64-74, 1975.

19. Stanitz, J.D., Osborn, W.M., Mizisin, J., "An Experimental Investigation of Secondary Flow in an Accelerating, Rectangular Elbow with 90° of Turning," NACA TN 3015, October 1953.

20. Stanitz, J.D., "Design of 2-D Channels with Prescribed Velocity Distributions Along the Channel Walls, I-Relaxation Solutions," NACA TN 2593, Jan. 1952.

21. Moore, J., Moore, J.G., "A Calculation Procedure for Three Dimensional Viscous Compressible Duct Flow," (Parts I and II), J. of Fluids Engineering, Vol. 101, pp. 415-428, 1979.

22. Davis, R.T., "Grid Generation for Finite Difference Schemes," VKI Lecture Series (1981-5) on Computational Fluid Dynamics.

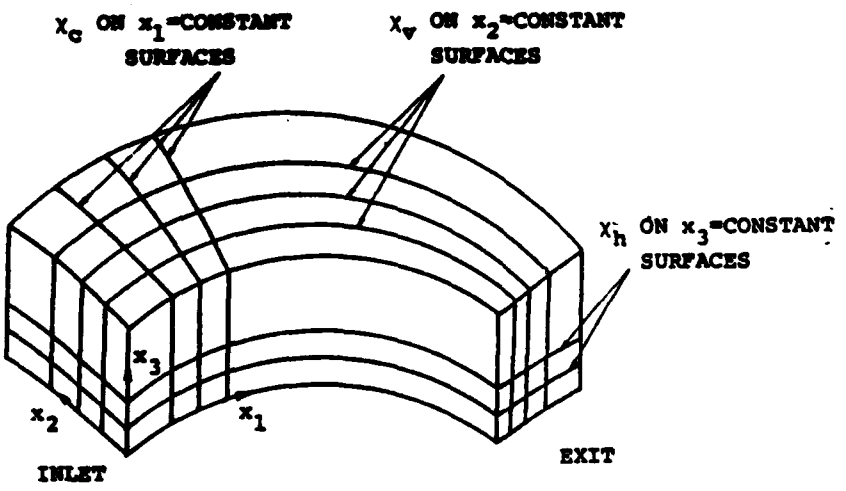

Fig. 1. Schematic of the Curved Ducts Showing The Three Sets of Orthogonal Surfaces and the Corresponding Streamlike Functions.

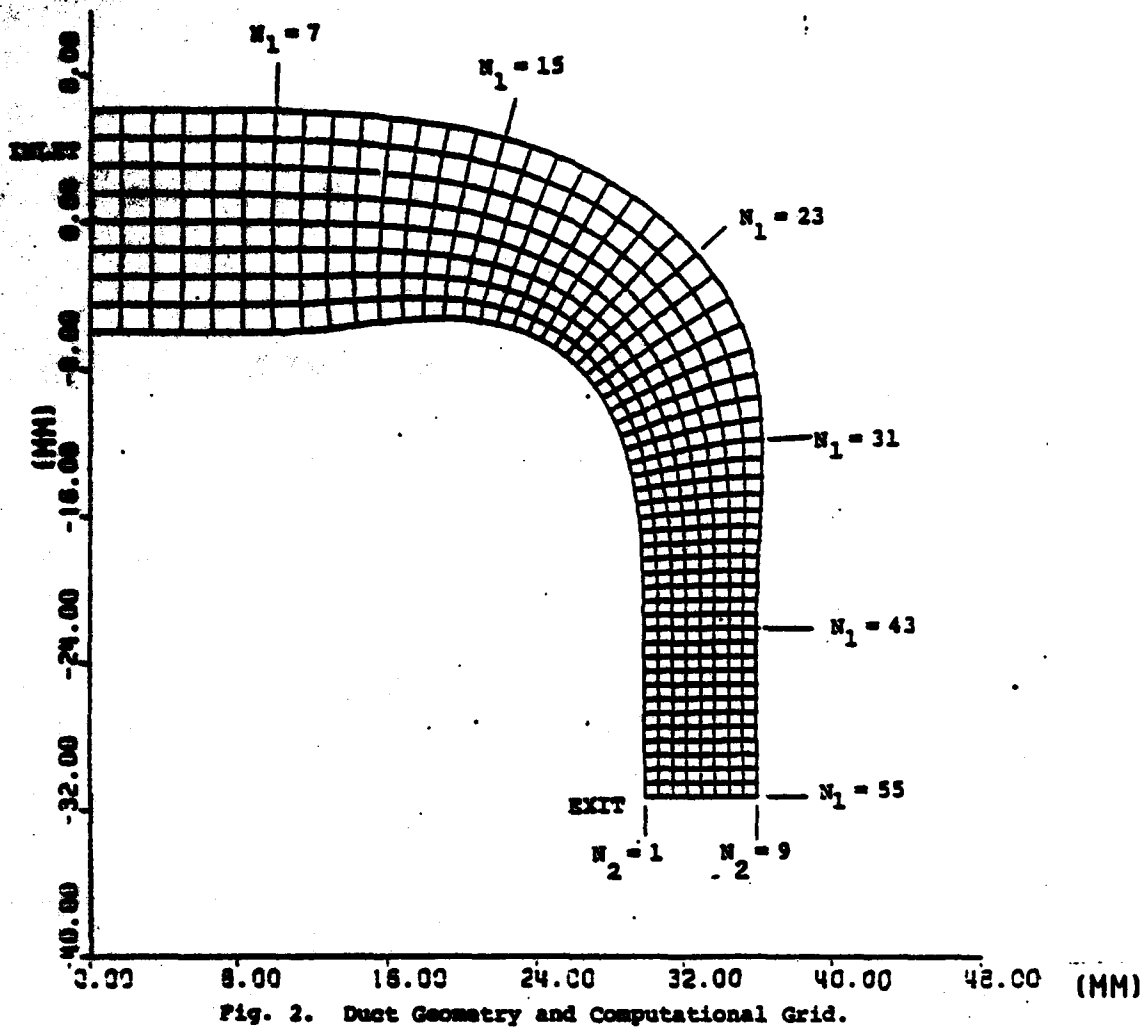

Fig. 2. Duct Geometry and Computational Grid.

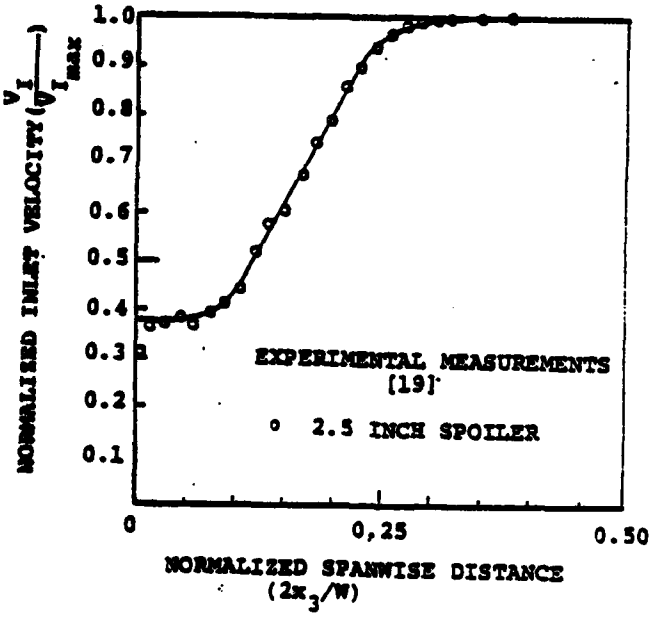

Fig. 3. Inlet Velocity Profile.

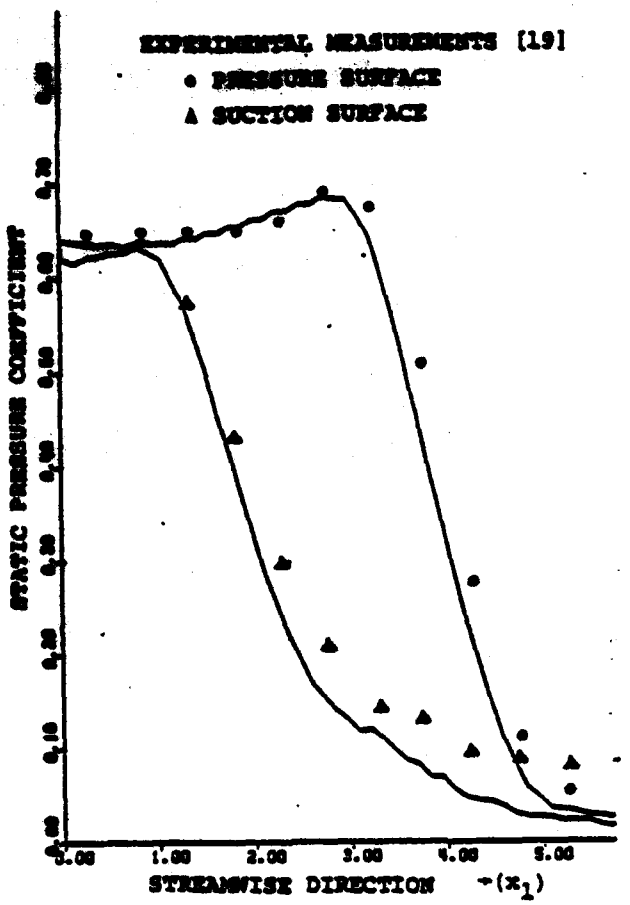

Fig. 4. Pressure Distribution Near End Wall (N_3 = 3).

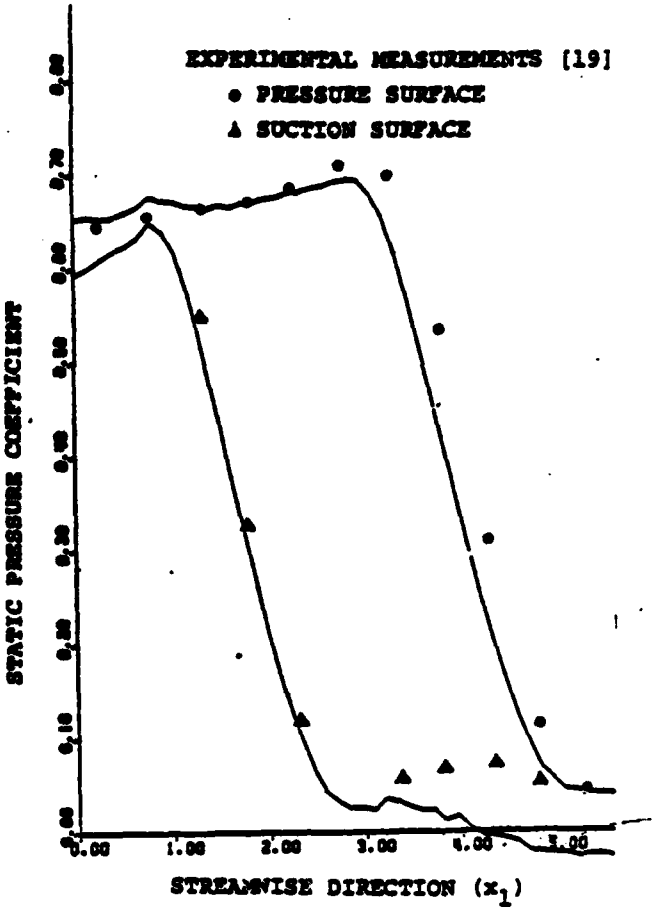

Fig. 5. Static Pressure Distribution Near Mid-Span (N_3 = 11).

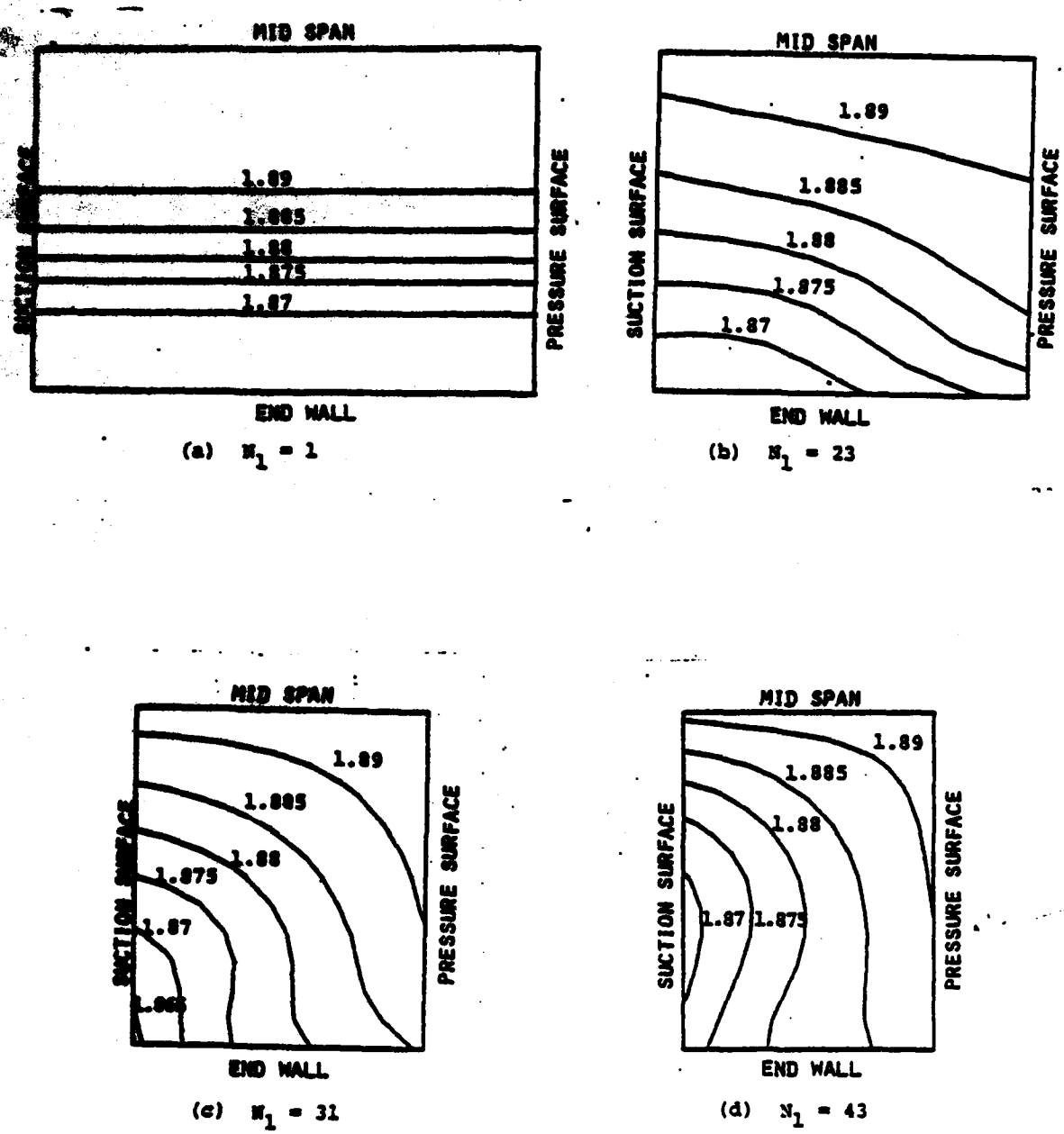

Fig. 6. Normalized Total Pressure Contours in the Cross Sectional Surfaces.

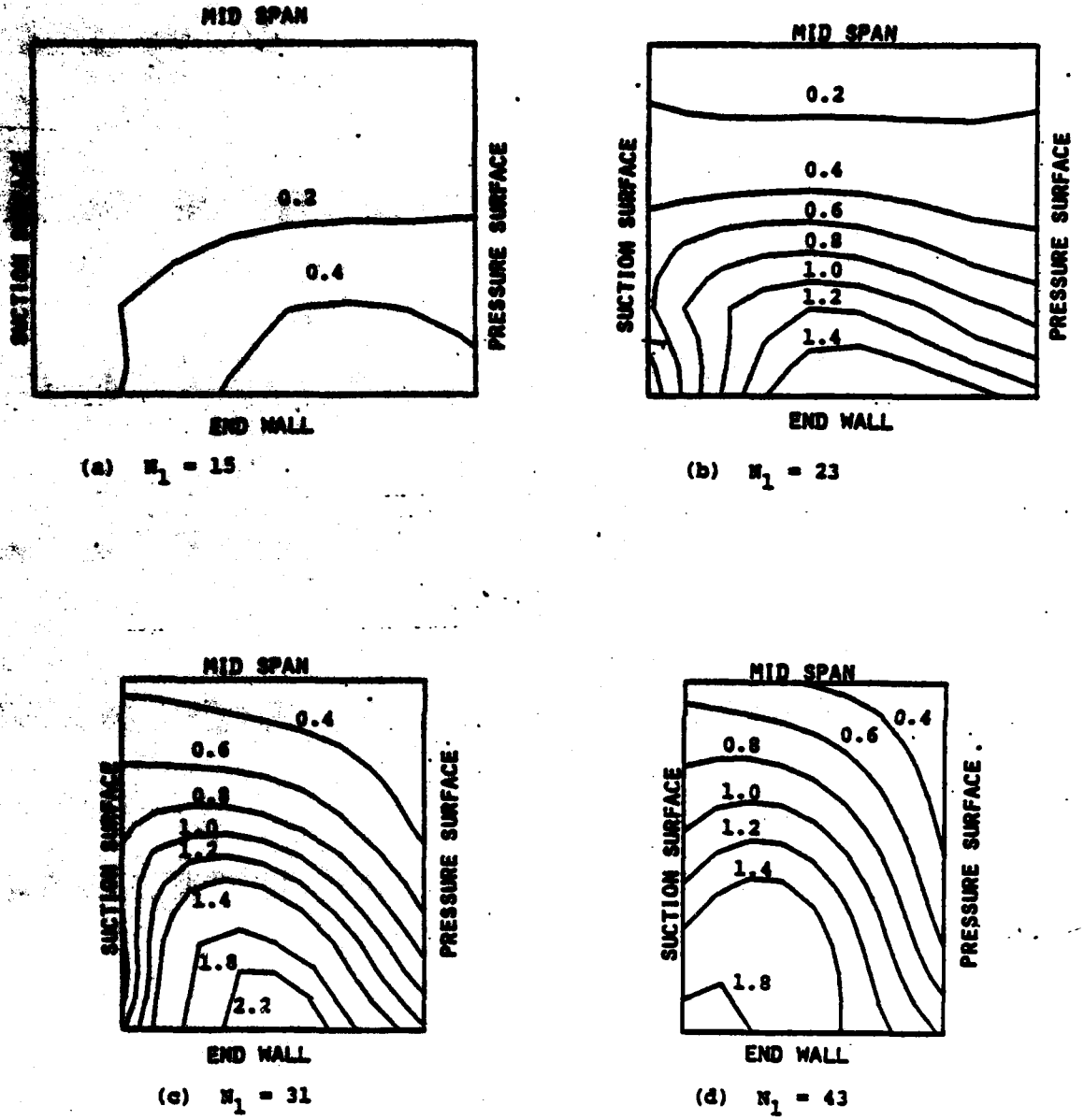

Fig. 7. Normalised Through Flow Vorticity Contours in the Cross Sectional Surfaces.

Appendix 4

Internal Three-Dimensional Viscous Flow Solution Using the Streamlike Function

AIAA-84

AIAA-84-1633

Three-Dimensional Viscous Solution Using the Stream Function

A. Hamed, University of Cincinnati, Cincinnati, OH, and S. Abdallah, Pennsylvania State University, State College, PA

AIAA 17th Fluid Dynamics, Plasma Dynamics, and Lasers Conference

June 25-27, 1984/Snowmass, Colorado

INTERNAL THREE-DIMENSIONAL VISCOUS FLOW SOLUTION USING THE STREAMLIKE FUNCTION

A. Hamed*
Department of Aerospace Engineering and Applied Mechanics
University of Cincinnati
Cincinnati, Ohio 45221

and

Y. Abdallah**
Applied Research Laboratory
Pennsylvania State University
State College, Pennsylvania 16801

Abstract

This paper presents a new method for the three-dimensional elliptic solution of [illegible] equations. It is based on the [illegible] vorticity formulation which was developed by the authors to study the development of secondary velocities and streamwise vorticity for inviscid flows in curved ducts. This formulation is generalized for viscous flows and used to predict the development of internal three dimensional flow fields. The computed results are presented and compared with experimental measurements for the three-dimensional viscous flow in a straight duct.

Nomenclature

H	duct height
L	duct length
Re	Reynolds number
t	time
u,v,w	velocity components in x, y and z directions
$\vec{V}$	velocity vector
V_∞	normalizing velocity at inlet
x,y,z	Cartesian coordinates
X_1, X_2, X_3	streamlike functions
ν	kinematic viscosity
$\vec{\Omega}$	vorticity vector
η, ξ, ζ	vorticity components in x, y and z directions

Introduction

A large number of numerical methods have been developed over the years for the solution of internal viscous flow fields. The earliest solutions[1-3] were obtained for the parabolized Navier-Stokes equations. Several successful implicit iterative solution procedures[4-8] have since been developed for the numerical solution of the parabolized Navier-Stokes equations in primitive variables for incompressible,[8] compressible,[4-7] supersonic,[4] laminar[4,5,8] and turbulent[6,7] internal flows. The only elliptic influence which is accounted for in the parabolized solution is that due to the potential pressure field. Partially parabolized solution procedures[5-7] were subsequently developed for the numerical solution of viscous flow fields in which pressure is the dominant transmitter of influences in the upstream direction.[5] These flows are still characterized by the absence of recirculation in the primary flow direction and by high Reynolds number, so that the viscous diffusion and thermal conduction are significant only in the lateral direction. The solution procedure remains unchanged for the main and lateral momentum equations, but the pressure correction equation at each marching step contains terms that link the pressure correction in a given lateral plane to upstream and downstream pressure corrections. In both methods, the velocity components are obtained from the momentum equations, and the continuity equation is only satisfied indirectly by the pressure field. This indirect approach to satisfying the continuity equation is common to all parabolized[1-4] and partially parabolized[5-7] methods.

The full Navier-Stokes equations are required to model flows with significant separation or shear layers not aligned with one of the coordinates. In addition, the parabolized and partially parabolized methods are not suitable for obtaining solutions to flow fields in which viscous phenomena significantly affect pressure distribution. Several methods have been developed for the solution of the time dependent form of the governing equations.[8-10] These methods can be very expensive, when used in the solution of viscous three dimensional flow fields,[10] but have been demonstrated to predict complex three dimensional phenomena such as the horseshoe vortex in turbine blade passages. The numerical solution to the full steady state Navier-Stokes equations in primitive variables was reported in reference 11 for natural convection and reference 12 for laminar flow in curved

---

* Professor, Associate Fellow AIAA.
** Research Associate, Member AIAA.

ducts. The results of the through flow computations[12] were shown to be dependent on the difference scheme for the continuity equation, especially in the prediction of the secondary flow development. The numerical solution fluttered on the inside of the bend, suffered a loss of mass and failed to fully converge,[11] and the author suggested that more attention to the non-linearities of the flow may possibly alleviate the last two problems. Other methods developed for the elliptic solution of the steady state full Navier-Stokes equations are based on the extension of the well-known 2-D stream function vorticity formulation to three dimensions.[13,14] Aziz and Hellums[13] defined a vector potential to identically satisfy the equation of conservation of mass in three dimensional flow fields. The vector potential vorticity formulation has been used to solve the problem of laminar natural convection.[13,14] In this formulation, the resulting governing equations consist of three 3-D Poisson equations for the vector potential and three vorticity transport equations. The main advantage of this formulation, in two dimensions, namely the smaller size of the governing equations is actually reversed in three dimensions, since three-dimensional differential equations have to be solved for the three components of the vector potential.

One can conclude from the preceding discussions that existing space-elliptic solvers of the 3-D Navier-Stokes equations are very costly in terms of CPU time and storage requirements. In addition, some of these methods which were developed for simple convection problems have not been very successful in through flow calculations. The presented work represents a new formulation for the 3-D Navier-Stokes equations that leads to an elliptic solution. The formulation is based on the use of the 2-D streamlike functions[15] to identically satisfy the equation of conservation of mass for 3-D rotational flows.[16,17] The governing equations consist of the vorticity transport equation and 2-D Poisson equations for the streamlike functions. The present method is very general, in that inviscid flow solutions can be obtained in the limit when $Re \to \infty$. In fact, numerical solutions have been obtained for inviscid rotational incompressible[16] and compressible[17] flows in curved ducts and it was demonstrated that the method can predict significant secondary flow and streamwise vorticity development due to inlet vorticity. The following work represents the generalization of this formulation to internal three-dimensional viscous flow problems.

Analysis

The governing equations consist of the vorticity transport equation and the equation of conservation of mass, which are written in the following dimensionless form, for incompressible viscous flow:

$$(\vec{\nabla}\cdot\nabla)\vec{\Omega} = (\vec{\Omega}\cdot\nabla)\vec{\nabla} - \frac{1}{Re}\nabla^2\vec{\Omega} \qquad (1)$$

and

$$\nabla\cdot\vec{\nabla} = 0 \qquad (2)$$

In the above equations $R = V^*D/\nu$ when the velocities are normalized by V^*, the space dimensions by D and the vorticity by V^*/D.

The solution to the three dimensional viscous flow is obtained in terms of the three vorticity components and three streamlike functions[15] which are defined to identically satisfy the equation of conservation of mass for general three-dimensional rotational flow fields. Unlike the traditional stream function solutions which must be obtained on stream surfaces, the following streamlike function velocity relations permit the definition of these two dimensional functions $\chi_1(x,y)$, $\chi_2(y,z)$, $\chi_3(x,z)$ on fixed non-stream surfaces in the flow field.

Streamlike Functions Velocity Relations

The streamlike function formulation was developed by the authors[15] to model internal three dimensional flow fields.[16] More details and general definitions in curvilinear coordinates of the streamlike function can be found in reference 17. For the sake of simplicity, the equations will be presented here for incompressible flow using Cartesian coordinates.

Definition of χ_1

$$\frac{\partial\chi_1}{\partial y} = u_1 + \int_{x_o}^{x} \frac{\partial w_2}{\partial z}\,dx\,, \qquad (3a)$$

$$\frac{\partial\chi_1}{\partial x} = -v_1 \qquad (3b)$$

Definition of χ_2

$$\frac{\partial\chi_2}{\partial y} = -w_2 - \int_{z_o}^{z} \frac{\partial u_1}{\partial x}\,dz \qquad (4a)$$

$$\frac{\partial\chi_2}{\partial z} = v_2 \qquad (4b)$$

Definition of χ_3

$$\frac{\partial\chi_3}{\partial z} = -u_3 + \int_{x_o}^{x} \frac{\partial w_2}{\partial z}\,dx\,, \qquad (5a)$$

$$\frac{\partial\chi_3}{\partial x} = w_3 - \int_{z_o}^{z} \frac{\partial u_1}{\partial x}\,dz\,, \qquad (5b)$$

[illegible] u, v
[illegible] y and z directions are

$$u = u_1 + u_2 \quad v = v_1 + v_2 \quad \text{and} \quad w = w_2 + w_3 \tag{6}$$

[illegible] that equations
[illegible] equation of conserve-
[illegible], one can use
[illegible] stream functions
[illegible] lateral
[illegible] flow due to
[illegible] other
[illegible] limit of
[illegible] chosen arbitrarily
[illegible] conditions, in
[illegible] configurations
[illegible] two members in

[illegible] equations consist of the
[illegible] equations and the
[illegible] equations for the streamlike
[illegible] the vorticity transport equa-
[illegible] coordinate coordinates are given

$$[illegible] = [illegible] + \frac{1}{Re} \nabla^2 \eta \tag{7}$$

$$[illegible] = [illegible] + \frac{1}{Re} \nabla^2 \zeta \tag{8}$$

$$[illegible] = [illegible] + \frac{1}{Re} \nabla^2 \xi \tag{9}$$

[illegible] ξ, ζ are the components of the
[illegible] vector, $\vec{\Omega}$, in the x, y and z
[illegible], respectively. The differential
[illegible] for the streamlike functions are
[illegible] from the substitution of equa-
[illegible] into the following vorticity
velocity relations:

$$\eta = \frac{\partial w}{\partial y} - \frac{\partial v}{\partial z} \tag{10}$$

$$\xi = \frac{\partial u}{\partial z} - \frac{\partial w}{\partial x} \tag{11}$$

$$\zeta = \frac{\partial v}{\partial x} - \frac{\partial u}{\partial y} \tag{12}$$

This results in the following two dimensional Poissons equations:

$$\frac{\partial^2 \chi_1}{\partial x^2} + \frac{\partial^2 \chi_1}{\partial y^2} = \zeta^* - \zeta + \frac{\partial}{\partial y} \int_{x_o}^{x} \frac{\partial w_2}{\partial z} \, dx \tag{13}$$

$$\frac{\partial^2 \chi_2}{\partial x^2} + \frac{\partial^2 \chi_2}{\partial y^2} = \eta^* - \eta - \frac{\partial}{\partial y} \int_{z_o}^{z} \frac{\partial u_1}{\partial x} \, dz \tag{14}$$

$$\frac{\partial^2 \chi_3}{\partial x^2} + \frac{\partial^2 \chi_3}{\partial z^2} = \xi^* - \xi + \frac{\partial}{\partial z} \int_{x_o}^{x} \frac{\partial w_2}{\partial z} \, dx - \frac{\partial}{\partial x} \int_{z_o}^{z} \frac{\partial u_1}{\partial x} \, dz \tag{15}$$

where

$$\eta^* = \frac{\partial w_3}{\partial y} - \frac{\partial v_1}{\partial z} \tag{16}$$

$$\xi^* = \frac{\partial u_1}{\partial z} - \frac{\partial w_2}{\partial x} \tag{17}$$

$$\zeta^* = \frac{\partial v_2}{\partial x} - \frac{\partial u_3}{\partial y} \tag{18}$$

The governing equations (7)-(9) and (13)-(15) are solved for the vorticity components η, ξ, ζ and the streamlike functions χ_1, χ_2 and χ_3, respectively. The boundary conditions used for the solution of these equations are given for the viscous flow in a square duct. Because of symmetry, only one quarter of the square duct is considered in the following derivations. Th coordinate y along the straight duct is measured from the duct entrance, while x and z represent the coordinates in the cross sectional planes measured from the duct centerline as shown in Fig. 1.

Boundary Conditions

At the inlet station which extends far upstream of the duct entrace, the flow velocity is taken to be uniform ($v = v_I$, $u, w = 0$), leading to the following boundary conditions:

$$\eta = \zeta = \xi = 0$$

and

$$\frac{\partial \chi_1}{\partial y} = \frac{\partial \chi_2}{\partial y} = 0$$

At the duct boundaries, the no slip condition is used to obtain the boundary conditions for the vorticity components, while the zero flux condition is used to obtain the boundary conditions for the streamlike functions.

The streamlike function boundary conditions are simplified through the appropriate choice of the reference coordinates x_o, z_o in the lower limit of the integrals in equations (3)-(5). The following boundary conditions result when $x_o = z_o = 0$.

At $x = \frac{1}{2}$,

$$\eta = 0$$

$$\xi = -\frac{\partial v}{\partial x},$$

$$\zeta = \frac{\partial v}{\partial z}$$

$$\chi_1 = -\int_{x=0}^{x=\frac{1}{2}} v_I \, dx$$

and

$$\chi_3 = 0$$

At $z = \frac{1}{2}$

$$\eta = -\frac{\partial v}{\partial z}$$

$$\xi = \frac{\partial u}{\partial z}$$

$$\zeta = 0$$

$$\chi_2 = \int_{x=0}^{x=\frac{1}{2}} v_I \, dx$$

and

$$\chi_3 = 0$$

The rest of the boundary conditions are due to symmetry at the planes x = 0 and z = 0.

At x = 0

$$\frac{\partial \eta}{\partial x} = 0$$

$$\xi = \zeta = 0$$

and

$$\chi_1 = \chi_3 = 0$$

At z = 0

$$\eta = \xi = 0$$

$$\frac{\partial \zeta}{\partial z} = 0$$

and

$$\chi_2 = \chi_3 = 0$$

Fully developed flow conditions are applied at the duct exit.

$$\frac{\partial \eta}{\partial y} = \frac{\partial \zeta}{\partial y} = 0$$

$$\xi = 0$$

and

$$\frac{\partial \chi_1}{\partial y} = \frac{\partial \chi_2}{\partial y} = 0$$

Results and Discussion

The elliptic system of equations are solved using an iterative procedure. At each global iteration, the linear equations were solved by successive relaxation methods. Numerical computations in a straight duct with L/DRe = 0.1 were performed using a uniform grid with $\Delta x/DRe = \Delta z/DRe = 0.001$ and $\Delta y/DRe = 0.0033$. Due to symmetry, the computations were only carried out in one quarter of the duct for χ_1, χ_3, ζ and ξ since $\zeta(x,y,z) = -\eta(z,y,x)$ and $\chi_1(x,y) = -\chi_2(z,y)$. Relaxation parameters of 1.6 for χ_1, 1.9 for χ_3 and 0.4 for ζ and ξ were used in the inner iterations with a convergence criteria of $\varepsilon_\zeta = 1 \times 10^{-4}$, $\varepsilon_\xi = 1 \times 10^{-5}$, $\varepsilon_{\chi_1} = 1 \times 10^{-5}$, $\varepsilon_{\chi_3} = 5 \times 10^{-6}$ according to the following equation:

$$\frac{1}{M} \sum_{1}^{M} \left(|\omega_{i,j}^{m+1} - \omega_{i,j}^{m}| \right) \leq \varepsilon_\omega$$

The numerical solutions required 50 global iterations and a CPU time of 2 minutes and 13 seconds on AMDAHL 370 using an 11 x 11 x 14 uniform grid. The overall number of iterations was 357 for the vorticity equations and 179 for the streamlike function equations. The numerical solution domain extended 1.67 diameters upstream of the duct inlet, where the flow velocity was taken to be uniform and equal to one. The results of the numerical computations are presented at y/DRe = 0.0, 0.01 and 0.10. The through flow contours at the duct inlet are presented in Fig. 2. The flow development from a uniform through velocity to the profile of Fig. 2 at the duct inlet is accompanied by lateral flow displacements due to the secondary velocities. The secondary velocity contours at the duct inlet are shown in Fig. 3 for the vertical velocity component w. The ellipticity of the numerical solution is demonstrated in the velocity contours at the duct inlet, and in the velocity fields up to 0.83 diameters upstream of the duct inlet. Figure 4 shows the contours for the secondary velocity component, w, at y/DRe = 0.01. A comparison of Figs. 3 and 4 reveals the change in both the magnitude and the location of the maximum secondary velocities along the duct. The development of the secondary velocity component, w, along the plane of symmetry, x = 0, is presented in Fig. 5. One can see that the maximum secondary velocities are found near the solid boundaries at the duct inlet. As the flow proceeds towards fully developed conditions, the secondary velocities decrease and the location of the maximum values moves toward the center of the duct. The results of the numerical computations at the duct exit are shown in Fig. 6 for the

through flow velocity contours.

The vorticity and streamlike function contours are shown in Figs. 7 through 11. The contours for the vorticity component ζ are shown at y/Dh = 0.0 and 0.1 in Figs. 7 and 8. Figures 9 and 10 show the contours of the streamlike function χ_3 at y/Dh = 0.0 and 0.01. The figures show a change in the sign of the streamlike function between these two sections. The contours for the streamlike function χ_1 at z/Dh = 0.0 are shown in Fig. 11. One can see that χ_1 reaches values less than -0.5 inside the duct near the walls.

The computed through flow velocity profile along the plane of symmetry, x = 0, are compared with the experimental measurements of reference 18 in Fig. 12. One can see that the computed results are in good agreement with the experimental measurements. The computed through flow velocity development along the duct centerline are compared with the experimental measurements of reference 18 in Fig. 13. The agreement between the computed results and the experimental data as shown in Figs. 12 and 13 is very satisfactory, in view of the uniform coarse grid used in the numerical calculations.

Conclusions

This paper presents a new method for the three-dimensional elliptic solution of the Navier-Stokes equations which is based on the streamlike-function vorticity formulation. The computed results for the three-dimensional viscous flow in a square duct are presented and compared with experimental measurements. The results demonstrate that the streamlike function can successfully model viscous effects in the three dimensional flow field computations. Since the same formulation has been successfully used in inviscid rotational flows, to model secondary flow development due to inlet shear velocity under the effect of curvature, one can conclude that the present method can be effectively developed to obtain efficient numerical elliptic solutions of internal viscous flow in curved passages.

Acknowledgement

This work was sponsored by U.S. Air Force Office of Scientific Research under Contract No. 80-0242

The authors wish to express their appreciation to Mr. M. Mansour for his help in performing the numerical computations.

References

1. Patankar, S.V. and Spalding, D.B., "A Calculation Procedure for Heat, Mass and Momentum Transfer in Three-Dimensional Parabolic Flows," Int. Journal of Heat and Mass Transfer, Vol. 15, 1972, pp. 1787.

2. Caretto, L.S., Curr, R.M. and Spalding, D.B., "Two Numerical Methods for Three-Dimensional Boundary Layers," Computer Methods in Applied Mechanics and Engineering, Vol. 1, 1973, pp. 39.

3. Briley, W.R., "Numerical Method for Predicting Three-Dimensional Steady Viscous Flow in Ducts," Journal of Computational Physics, Vol. 14, 1974, pp. 8-28.

4. Buggeln, R.C., McDonald, H., Kreskovsky, J.P. and Levy, R., "Computation of Three-Dimensional Viscous Supersonic Flow in Inlets," AIAA Paper No. 80-0194, 1980.

5. Pratap, V.S. and Spalding, D.B., "Fluid Flow and Heat Transfer in Three Dimensional Duct Flows," Int. Journal of Heat and Mass Transfer, Vol. 19, 1976, pp. 1183-1188.

6. Roberts, D.W. and Forester, C.K., "A Parabolic Computational Procedure for Three-Dimensional Flows in Ducts with Arbitrary Cross-Sections," AIAA Paper No. 78-143, 1978.

7. Moore, J. and Moore, J.G., "A Calculation Procedure for Three-Dimensional Viscous, Compressible Duct Flow. Part II - Stagnation Pressure Losses in a Rectangular Elbow," Journal of Fluids Engineering, Vol. 101, December 1979, pp. 423-428.

8. Briley, W.R. and McDonald, H., "Solution of the Multi-Dimensional Compressible Navier-Stokes Equations by a Generalized Method," Journal of Computational Physics, Vol. 24, 1977, p. 372.

9. Beam, R.M. and Warming, R.F., "An Implicit Factored Scheme for the Compressible Navier-Stokes Equations," AIAA Journal, Vol. 16, 1978, p. 393.

10. Hah, C., "A Navier-Stokes Analysis of Three-Dimensional Turbulent Flows Inside Turbine Blade Rows at Design and Off-Design Conditions," ASME Paper No. 83-GT-40, 1983.

11. Williams, G.P., "Numerical Integration of the Three-Dimensional Navier-Stokes Equations for Incompressible Flow," Journal of Fluid Mechanics, Vol. 37, Part 4, 1969, pp. 227-250.

12. [illegible], S.F., "The Numerical Solution of the Navier-Stokes Equations for a Three-Dimensional Laminar Flow in Curved Pipes Using Finite Difference Methods," Journal of Engineering Mathematics, Vol. 12, No. 4, October 1978, pp. 303-323.

13. Axis, A. and Halluma, J.D., "Numerical Solution of the Three-Dimensional Equations of Motion for Laminar Natural Convection," The Physics of Fluids, Vol. 10, No. 2, 1967, pp. 314-324.

14. Mallinson, G.D. and Davis, G. DeVahl, "Three-Dimensional Natural Convection in a Box. A Numerical Study," Journal of Fluid Mechanics, Vol. 83, Part 1, 1977, pp. 1-31.

15. Hamed, A. and Abdallah, S., "Stream-like Function: A New Concept in Flow Problems Formulation," Journal of Aircraft, Vol. 16, No. 12, December 1979, pp. 801-802.

16. Abdallah, S. and Hamed, A., "The Elliptic Solution of the Secondary Flow Problem," Journal of Engineering for Power, Vol. 105, No. 3, 1983, pp. 530-535.

17. Hamed, A. and Liu, C., "Three Dimensional Rotational Compressible Flow Solution in Variable Area Channels," AIAA Paper No. 83-0259, 1983.

18. Goldstein, R.J. and Kreid, D.K., "Measurement of Laminar Flow Development in a Square Duct Using a Laser-Doppler Flow Meter," Journal of Applied Mechanics, December 1967, pp. 813-818.

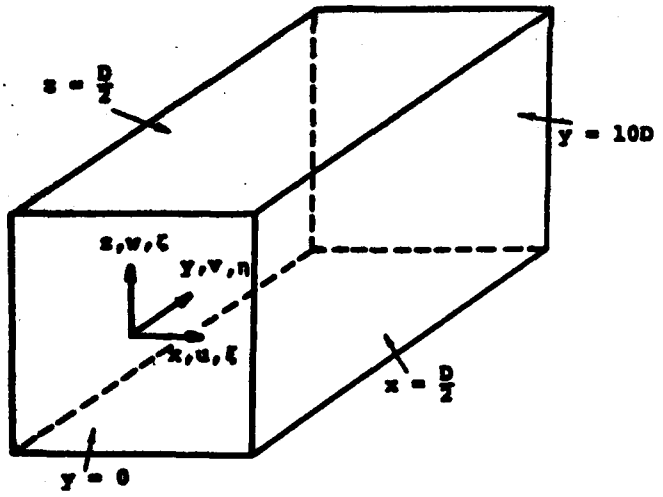

Fig. 1. Coordinate System in the Duct.

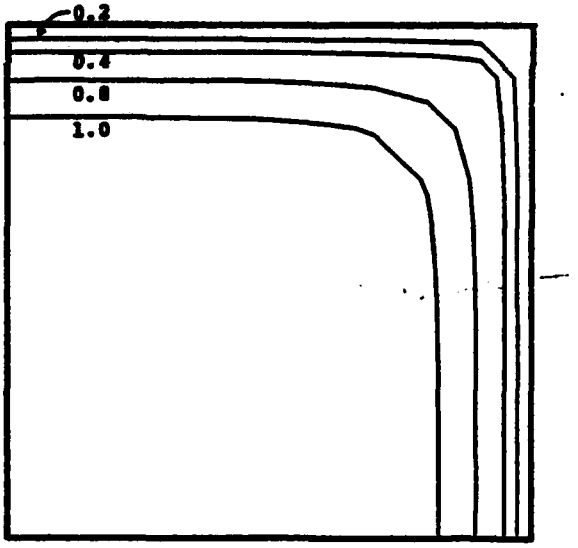

Fig. 2. Through Flow Velocity Contours at the Duct Inlet (y/DRe = 0.00).

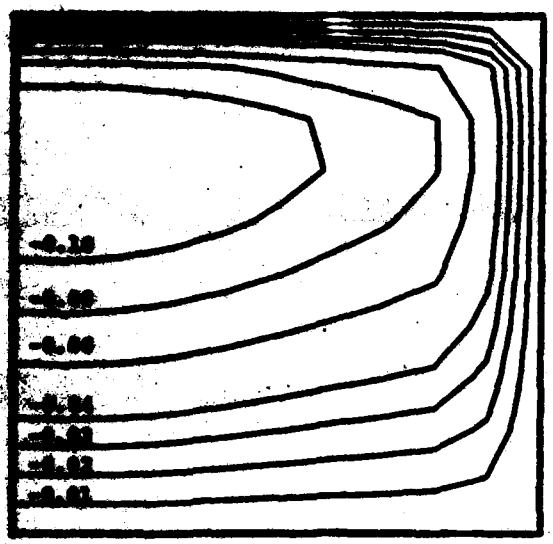

Fig. 3. Secondary Velocity Contours at the Duct Inlet (y/DRe = 0.00).

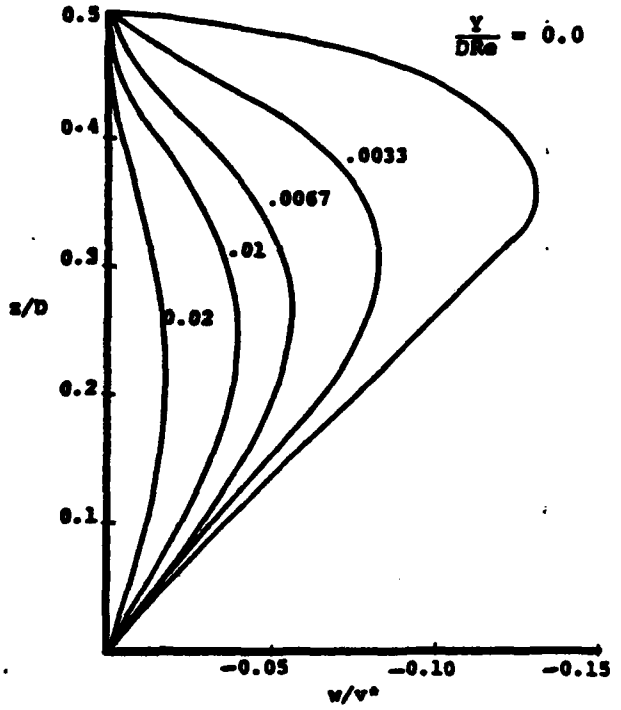

Fig. 5. The Development of Secondary Flow Velocity Profile at the Central Plane, x = 0.0.

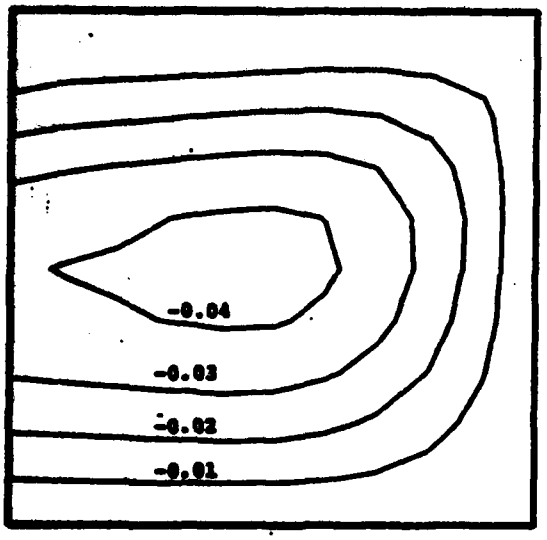

Fig. 4. Secondary Velocity Contours at y/DRe = 0.01.

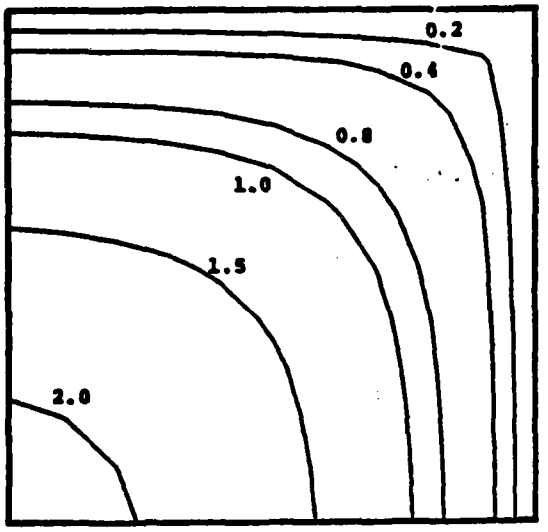

Fig. 6. Through Flow Velocity Contours at y/DRe = 0.1.

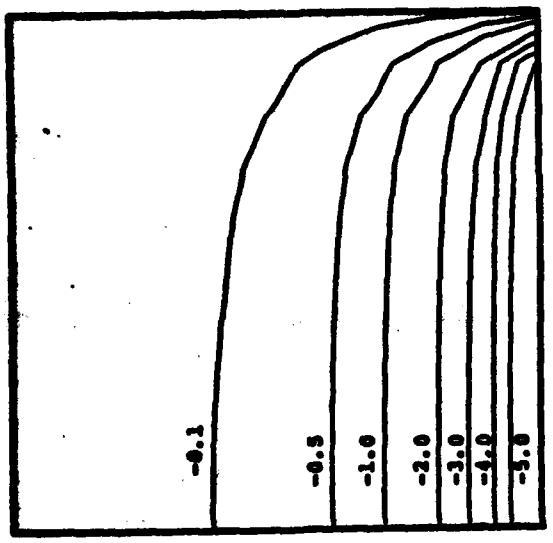

Fig. 7. Vorticity, ζ Contours at the Duct Entrance (y/DRe = 0.0).

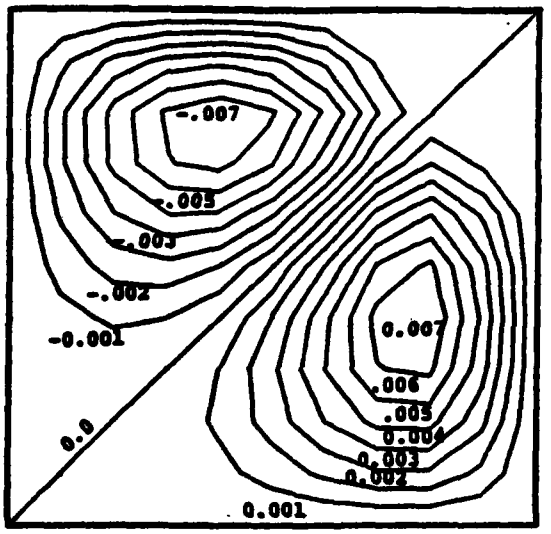

Fig. 9. Streamlike Function, χ_3 Contours at the Duct Inlet (y/DRe = 0.0).

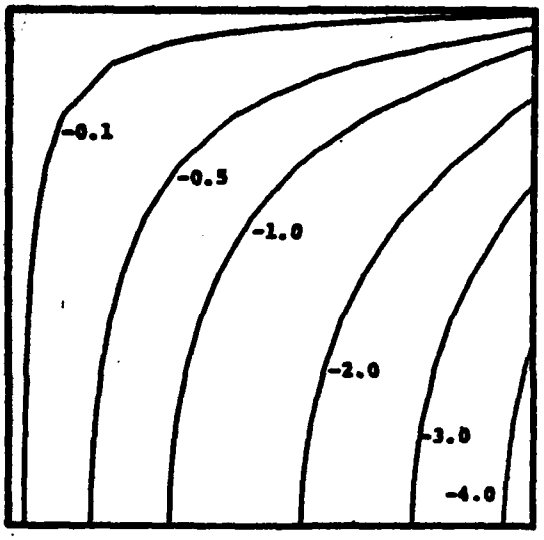

Fig. 8. Vorticity, ζ Contours at y/DRe = 0.1.

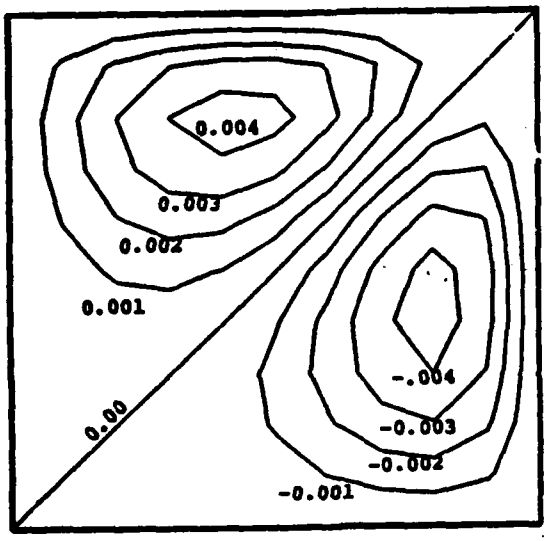

Fig. 10. Streamlike Function, χ_3 Contours at y/DRe = 0.01.

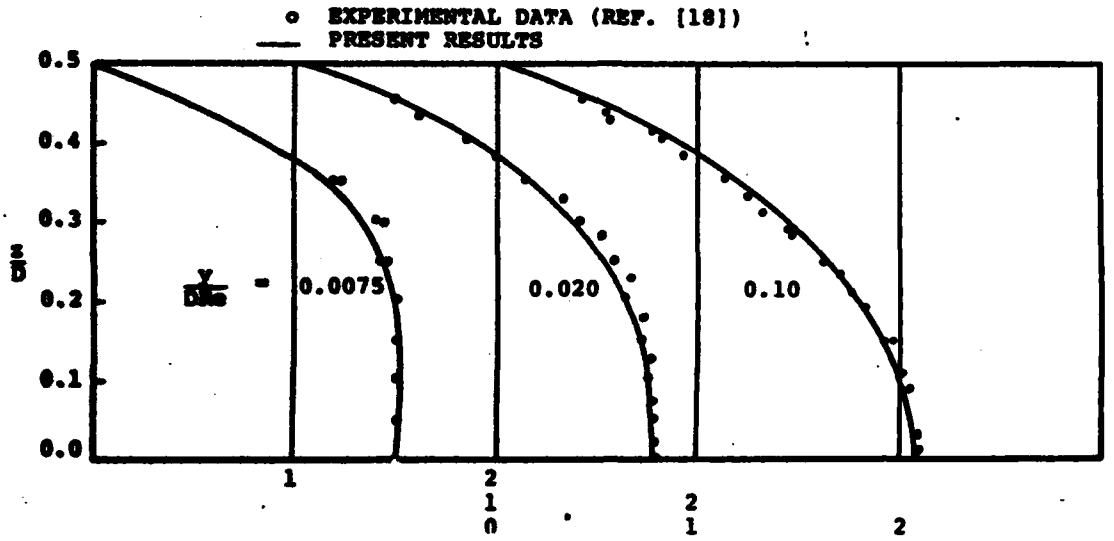

Fig. 11. Streamlike Function, χ_1 Contours at z = 0.

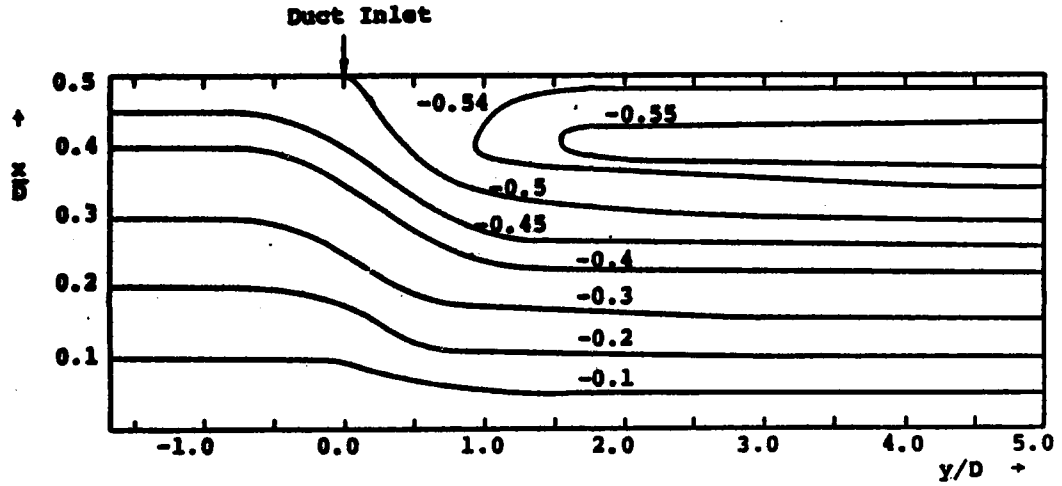

Fig. 12. Development of the Through Flow Velocity Profile at the Central Plane x = 0.

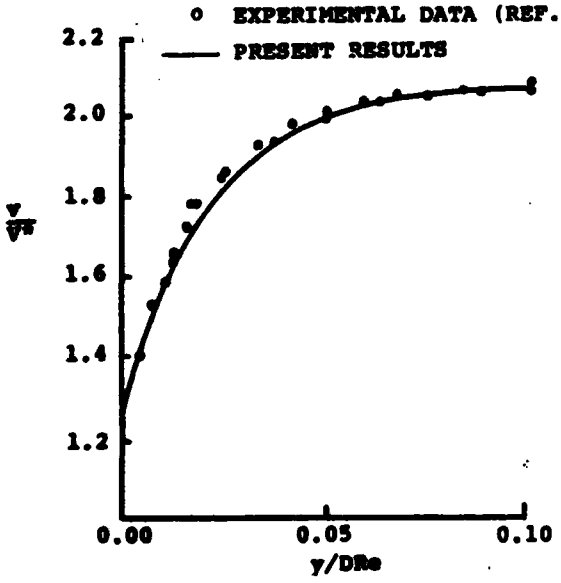

Fig. 13. Through Flow Velocity Development Along the Duct Centerline.

Appendix 5

The Elliptic Solution of 3-D Internal Viscous Flow Using the Streamlike Function

THE ELLIPTIC SOLUTION OF 3-D INTERNAL VISCOUS FLOW USING THE STREAMLINE FUNCTION

A. Hamed
Dept. of Aerospace Engineering and Applied Mechanics
University of Cincinnati
Cincinnati, Ohio U.S.A.

and

S. Abdallah
Applied Research Laboratory
Pennsylvania State University
State College, Pennsylvania
U.S.A.

1. INTRODUCTION

The prediction of the complex 3-D flow field in turbomachinery blade passages continues to be the subject of many viscous and inviscid flow studies. Recently developed 3-D inviscid methods [1-2] are capable of predicting 3-D flow characteristics such as secondary flows [3]. While the secondary flow is caused by vorticity which is produced by viscous forces, these inviscid methods cannot predict the viscous produced losses in the blade passage. Internal viscous flow solution methods have been developed using parabolized Navier-Stokes equations. While these methods are very fast, their application is limited due to their inabilities to simulate downstream blockage and strong curvature effects. Partially parabolized methods maintain the advantages of the parabolized methods in that the streamwise diffusion of mass, momentum and energy are still neglected but the elliptic influence is transmitted upstream through the pressure field. These well developed methods are not discussed here since the reader can refer to the extensive review of Davis and Rubin [4] and Rubin [5]. Our following discussion will be limited to the fully elliptic methods for the solution of the 3-D Navier-Stokes equations for internal flows.

Aziz and Hellums [6] developed the vector potential-vorticity formulation, and used it to solve the problem of laminar natural convection. This approach is an extension of the well known 2-D stream function vorticity formulation to 3-D problems. The equation of conservation of mass is identically satisfied through the definition of the vector potential. In this formulation, the resulting governing equations consist of three 3-D Poisson equations for the vector potential and three vorticity transport equations. Williams [7] used a time marching method for the solution of the laminar incompressible flow field due to thermal convection

in a rotating annulus using primitive variables. In this [illegible] the pressure field is computed from the solution of a [illegible] equation with Neumann boundary conditions. Both [illegible] therefore require the solution of three parabolic transport equations. The first method requires in addition the solution of the 3-D Poisson equations with [illegible] boundary conditions along two boundaries and zero [illegible] conditions along the third boundary, while [illegible] only one additional 3-D Poisson equation for [illegible] boundary conditions over all the [illegible]. Reference [8] discussed the relative merits of these [illegible] in terms of CPU time, computer storage requirements and program development time when iterative and direct [illegible] are used in the solution of Poisson equation. [illegible] obtained an elliptic solution for viscous flow in a [illegible] pipe [9] and curved duct [10] from the governing [illegible] in primitive variables using a new finite difference [illegible]. Two problems were encountered in the application of [illegible] method to through flow calculations; the tendency of the [illegible] to flutter and a loss of mass between the duct inlet and exit in the computed results. More recently, Dodge [11] [illegible] a velocity split procedure in which the velocity is separated into viscous and potential components, and the pressure field is determined from the potential velocity component. The governing equation for the viscous velocity vector component is obtained from the momentum equation with the pressure gradient expressed in terms of the derivatives of the velocity potential vector component, while the governing equation for the velocity potential vector component is obtained from continuity. Beyond this formulation, Dodge's numerical solution procedure is partially parabolic since he neglected the streamwise diffusion of momentum in pursuing a marching solution for the viscous velocity components. The analysis itself, in terms of the type of the governing equations and their boundary conditions, is comparable to the velocity pressure formulation since the governing equation for the velocity potential is a 3-D Poisson equation. Dodge did not discuss the boundary conditions for the velocity potential. He only mentioned that it can be complex and that he used zero potential gradient normal to the wall in his numerical solution. Other formulations that can lead to elliptic solution, were described in references [5] and [8], however they will not be discussed here since they have not yet been applied to 3-D flow computations.

In summary, existing elliptic solvers for the Navier-Stokes equations require the solution of one or three 3-D Poisson equations in addition to the three momentum or the three vorticity transport equations. In the case of the velocity pressure formulation, the velocity vector is evaluated from the momentum equation and the continuity equation is satisfied indirectly in the pressure equation. The convergence of the iterative numerical procedure would be very

[illegible] are not used for the solution of the [illegible] equations with Neumann boundary conditions for the [illegible]. On the other hand, the continuity equation [illegible] implicitly in the vector potential-vorticity [illegible], but it leads to three 3-D Poisson equations for [illegible] potential equations. Convergence of the iterative [illegible] does not present a problem in this case, since Dirichlet [illegible] are imposed on parts of the boundary, but computer [illegible] requirements are greatly increased by two additional [illegible].

[illegible] work represents a new formulation for the [illegible] equations that leads to a very economical [illegible]. The formulation is based on the use of [illegible] functions [12] to identically satisfy the [illegible] for 3-D rotational flows. In addition to [illegible] transport equation, the present formulation [illegible] in 3-D Poisson equations with Dirichlet boundary conditions [illegible] stream-like functions. The presented method [illegible], in that inviscid flow solutions can be obtained [illegible] limit where Re → ∞. In fact, numerical solutions [illegible] obtained for inviscid rotational incompressible [13] and compressible [14] flows in curved ducts and it was observed that the method predicts the secondary flow [illegible] due to inlet vorticity. The validity of the [illegible] predicting secondary flow which are indirectly [illegible] through the effects of viscosity have been demonstrated for inviscid flow [13, 14]. The following work represents an extension of this formulation to viscous flow problems. The analytical formulation is developed for general 3-D flows but the results of the computation are presented for the simple viscous flow problem of a uniform entrance flow in a [illegible] duct. The final goal is to develop a method for predicting the three dimensional flow field, and the losses in internal flow fields with large surface curvature and significant downstream effects as in the case of turbine blade passages.

2. ANALYSIS

The governing equations are the vorticity transport equation and the equation of conservation of mass, which are given below in nondimensional vector form for incompressible flow [15]

$$\frac{\partial \bar{\Omega}}{\partial t} + (\bar{V}\cdot\nabla)\bar{\Omega} - (\bar{\Omega}\cdot\nabla)\bar{V} - \frac{1}{Re}\nabla^2\bar{\Omega} = 0 \qquad (1)$$

and

$$\nabla\cdot\bar{V} = 0 \qquad (2)$$

where

$$\bar{\Omega} = \nabla \times \bar{V} \tag{3}$$

The Reynolds number ($Re = \frac{V^* D}{\nu}$), appears in the equations as a result of normalizing the velocities by V^*, the space dimensions by D and the vorticity by V^*/D, where ν is the kinematic viscosity.

Equations (1-3) are written in Cartesian coordinates as follows.

Vorticity Transport Equations

$$\frac{\partial \eta}{\partial t} = -\bar{V}\cdot\nabla\eta + \bar{\Omega}\cdot\nabla u + \frac{1}{Re}\nabla^2\eta \tag{4}$$

$$\frac{\partial \xi}{\partial t} = -\bar{V}\cdot\nabla\xi + \bar{\Omega}\cdot\nabla v + \frac{1}{Re}\nabla^2\xi \tag{5}$$

$$\frac{\partial \zeta}{\partial t} = -\bar{V}\cdot\nabla\zeta + \bar{\Omega}\cdot\nabla w + \frac{1}{Re}\nabla^2\zeta \tag{6}$$

where η,ξ,ζ are the components of the vorticity vector, $\bar{\Omega}$, in the x, y and z directions, respectively; u,v,w are the components of the velocity vector $\bar{V}$.

Equation of Conservation of Mass

$$\frac{\partial u}{\partial x} + \frac{\partial v}{\partial y} + \frac{\partial w}{\partial z} = 0 \tag{7}$$

Vorticity Velocity Relations

$$\eta = \frac{\partial w}{\partial y} - \frac{\partial v}{\partial z} \tag{8}$$

$$\xi = \frac{\partial u}{\partial z} - \frac{\partial w}{\partial x} \tag{9}$$

$$\zeta = \frac{\partial v}{\partial x} - \frac{\partial u}{\partial y} \tag{10}$$

The Streamlike Function Formulation

Three streamlike functions [12] $\chi_h(x,y)$, $\chi_v(y,z)$, $\chi_c(x,z)$ are defined to identically satisfy the equation of conservation of mass in the case of internal rotational flows [13, 14]. The velocity field is determined from the streamlike functions according to the following relations:

Streamlike Functions Velocity Relations

$$u_h = \frac{\partial \chi_h}{\partial y} - \int_{x=0}^{x} \frac{\partial w_v}{\partial z}\, dx \tag{11}$$

$$v_h = -\frac{\partial \chi_h}{\partial x} \tag{12}$$

$$w_v = -\frac{\partial \chi_v}{\partial y} - \int_{z=0}^{z} \frac{\partial u_h}{\partial x}\, dz \tag{13}$$

$$v_v = \frac{\partial \chi_v}{\partial z} \tag{14}$$

$$u_c = -\frac{\partial \chi_c}{\partial z} + \int_{x=0}^{x} \frac{\partial w_v}{\partial z}\, dx \tag{15}$$

$$w_c = \frac{\partial \chi_c}{\partial x} + \int_{z=0}^{z} \frac{\partial u_h}{\partial x}\, dz \tag{16}$$

where the subscripts h, v and c refer to solutions on the horizontal, vertical and cross-sectional planes respectively with

$$u = u_h + u_c, \quad v = v_h + v_v \quad \text{and} \quad w = w_v + w_c \tag{17}$$

Equations (11-17) satisfy the equation of conservation of mass (7) identically.

Streamlike Functions Equations

Substituting equations (11)-(17) into equations (8)-(10) one obtains

$$\frac{\partial^2 \chi_h}{\partial x^2} + \frac{\partial^2 \chi_h}{\partial y^2} = \zeta^* - \zeta + \frac{\partial}{\partial y} \int_{x=0}^{x} \frac{\partial w_v}{\partial z}\, dx \tag{18}$$

$$\frac{\partial^2 \chi_v}{\partial z^2} + \frac{\partial^2 \chi_v}{\partial y^2} = \eta^* - \eta - \frac{\partial}{\partial y} \int_{z=0}^{z} \frac{\partial u_h}{\partial x}\, dz \tag{19}$$

$$\frac{\partial^2 \chi_c}{\partial x^2} + \frac{\partial^2 \chi_c}{\partial z^2} = \xi^* - \xi + \frac{\partial}{\partial z} \int_{x=0}^{x} \frac{\partial w_v}{\partial z}\, dx - \frac{\partial}{\partial x} \int_{z=0}^{z} \frac{\partial u_h}{\partial x}\, dz \tag{20}$$

where

$$\eta^* = \frac{\partial w_\zeta}{\partial y} - \frac{\partial v_h}{\partial z} \tag{21}$$

$$\zeta^* = \frac{\partial u_h}{\partial z} - \frac{\partial w_y}{\partial x} \tag{22}$$

$$\xi^* = \frac{\partial v_y}{\partial x} - \frac{\partial u_\zeta}{\partial y} \tag{23}$$

The governing equations (4)-(6) and (18)-(20) are solved for the vorticity components η,ξ,ζ and the streamlike functions χ_h, χ_y and χ_ζ, respectively. The boundary conditions used for the solution of these equations are given for the viscous flow in a square duct. The inlet station is extended far upstream where uniform incoming flow is assumed (Fig. 1). This case simulates flow in cascades with zero turning where periodic conditions apply over the extended boundaries up to the duct entrance. Because of symmetry, only one quarter of the square duct is considered in the derivation of the boundary conditions. The coordinates x and z are measured from the duct centerline and y from the duct entrance as shown in Fig. 1.

DUCT GEOMETRY AND DIMENSIONS

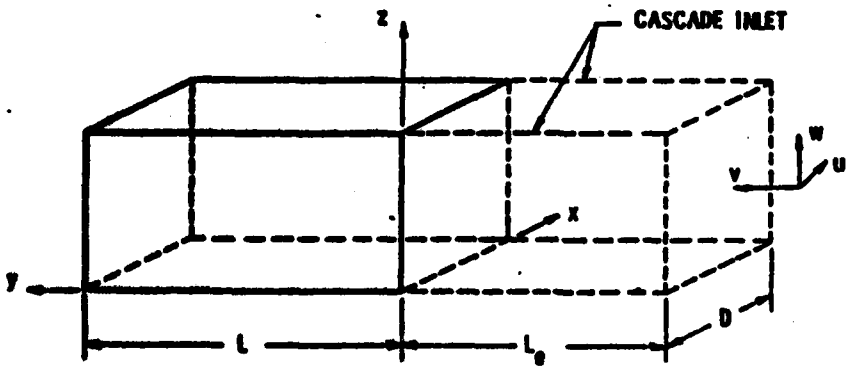

Fig. 1. A Schematic of the Duct with Cascade Entrance.

Boundary Conditions for the Streamlike Functions

i. [illegible] boundaries:

Referring to Fig. 2, the boundary conditions for [illegible] are obtained from the substitution of the no [illegible] into equations (11)-(17). The symmetry condi- [illegible] used to determine the rest of the boundary condi- [illegible] = 0. In addition the following condition [illegible] at the duct boundaries

$$\frac{\partial \chi_c}{\partial x} + \frac{\partial \chi_h}{\partial y} + \frac{\partial \chi_v}{\partial z} = 0$$

The above equation is used in the determination of the streamlike functions in the planes coinciding with the duct boundaries.

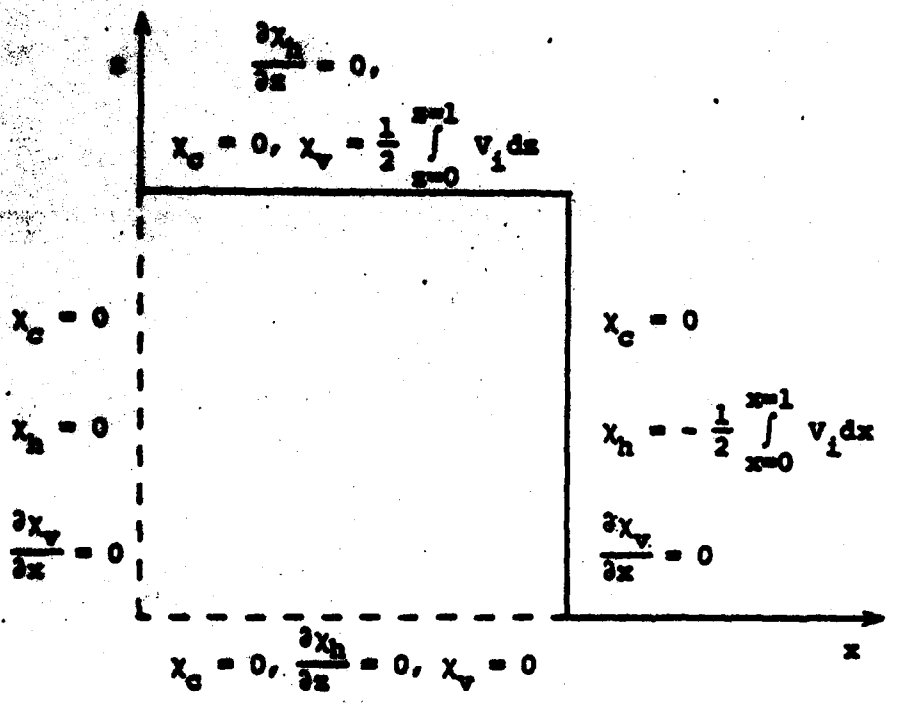

Figure 2

ii. Along the cascade entry:

Figure 3 shows the boundary conditions for the stream-like functions at the extension of the duct boundaries. The conditions at the planes of symmetry are unchanged.

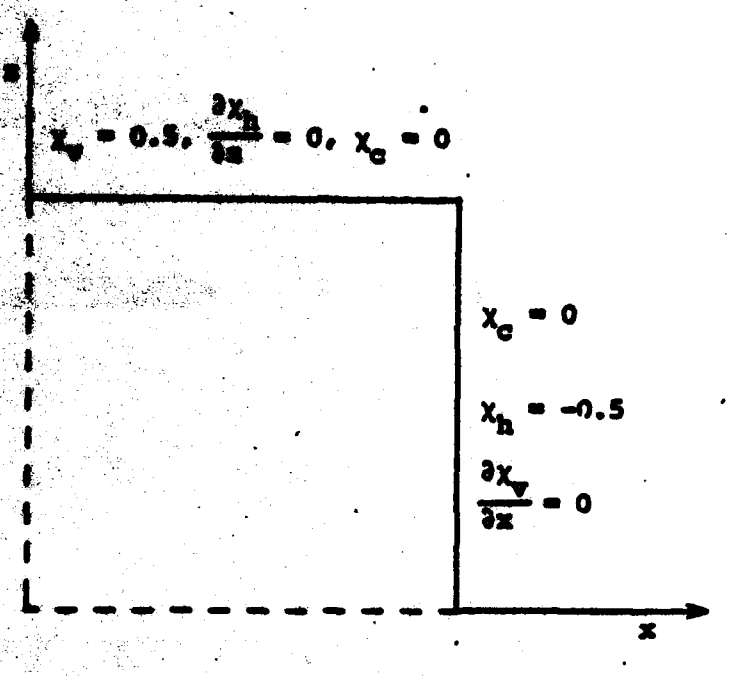

Figure 3

iii. <u>At the inlet station:</u>

The following relations satisfy the inlet condition u = v = 0

$$\frac{\partial \chi_h}{\partial y} = 0$$

$$\frac{\partial \chi_v}{\partial y} = 0$$

iv. <u>At exit:</u>

Fully developed flow conditions are assumed, leading to

$$\frac{\partial \chi_h}{\partial y} = 0$$

$$\frac{\partial \chi_v}{\partial y} = 0$$

Boundary Conditions for the Vorticity Components

At the Duct Boundaries:

The no-slip condition is satisfied through the vorticity symmetry conditions. The symmetry conditions are used along the vertical and horizontal central planes to determine the values of the boundary conditions shown in Fig. 4.

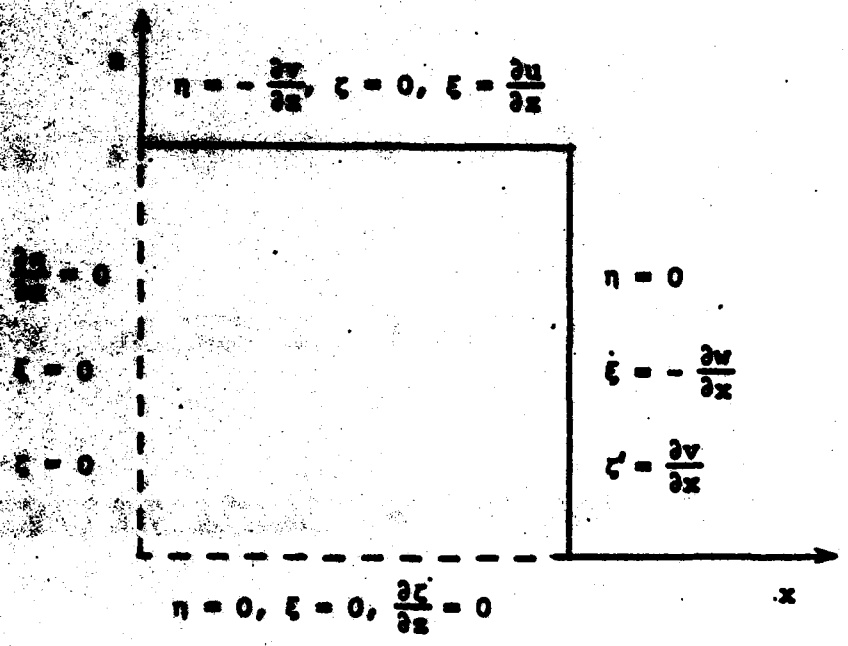

Figure 4

ii. Along the cascade entrance

Figure 5 shows the boundary conditions at the extension of the duct boundaries.

iii. At the inlet station:

$\xi = 0$

$\eta = 0$

$\zeta = 0$

iv. At exit:

Fully developed flow conditions are assumed, leading to:

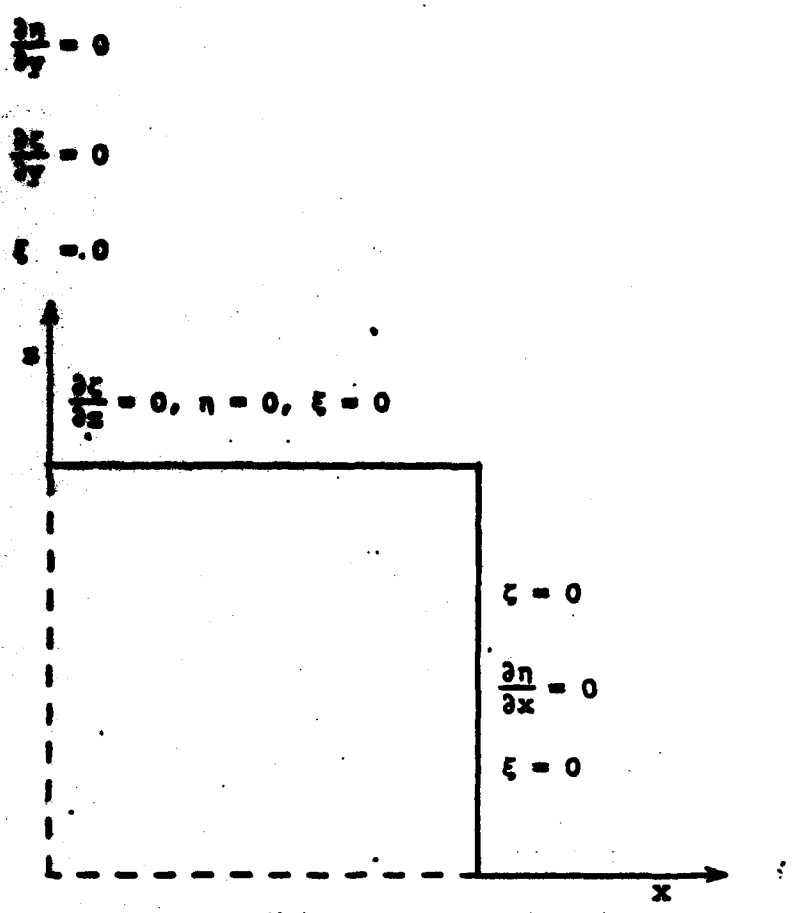

Figure 5

3. RESULTS AND DISCUSSION

The results of the numerical computations are presented in one quarter of a square duct. In this case, only two of the vorticity equations [eqs. (4) and (5)] and two of the streamlike function equations [eqs. (19) and (20)] are solved, since $\chi_h = \chi_v$ and $\zeta(x,y,z) = -\eta(z,y,x)$. Referring to Fig. 1, the solution was obtained for Re = 50 in a duct with L/DRe = 0.1 and Le/DRe = 0.01 using SOR and a (11 x 11 x 34) grid.

Figures 6a and 6b show the through flow velocity contours at the duct entrance and exit. The influence of the cascade entering on the elliptic solution is demonstrated in contours of Fig. 6a.

The contours for the secondary velocity component, w, are shown at y/DRe = 0.0 and 0.0075 in Figs. 7a and 7b. From these figures, one can see a large change in both the magnitude and the location of the maximum secondary velocities along the duct. The development of the through flow velocity profiles along the plane of symmetry, x = 0, is shown in

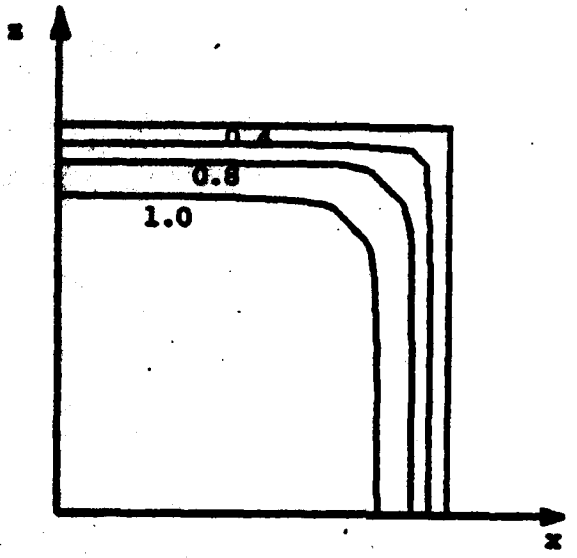

Fig. 6a. Through Flow Velocity Contours at the Duct Entrance.

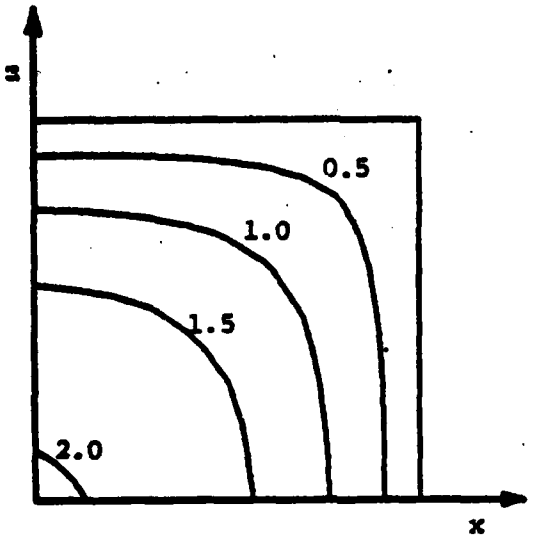

Fig. 6b. Through Flow Velocity Contours at the Duct Exit ($y/D_{Re} = 0.1$).

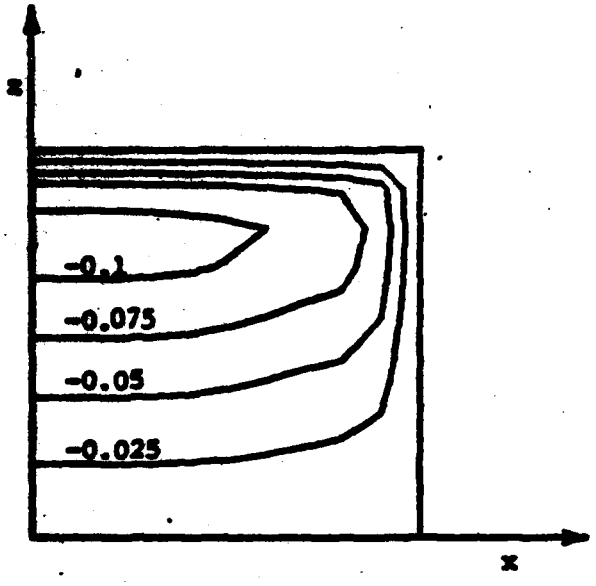

Fig. 7a. Secondary Velocity Contours at y/DRe = 0.0

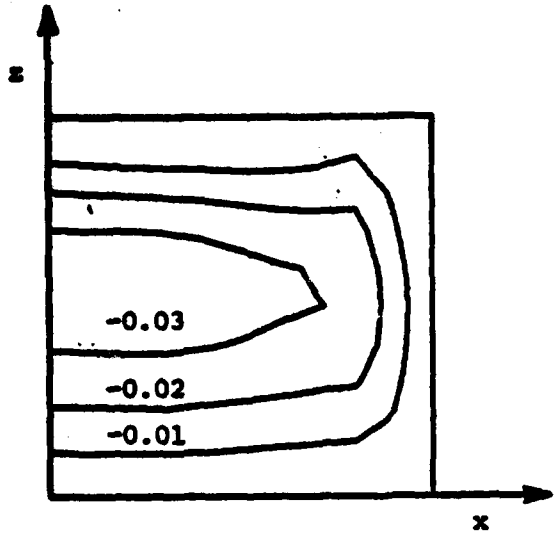

Fig. 7b. Secondary Velocity Contours at y/DRe = 0.0075

Fig. 8 for the computed results and the experimental measurements of reference [16]. One can see that the computed results are in good agreement with the experimental measurements at y/DRe = 0.0075 and 0.02, but that the computed through flow velocities at y/DRe = 0.1 did not reach the experimentally measured fully developed profile.

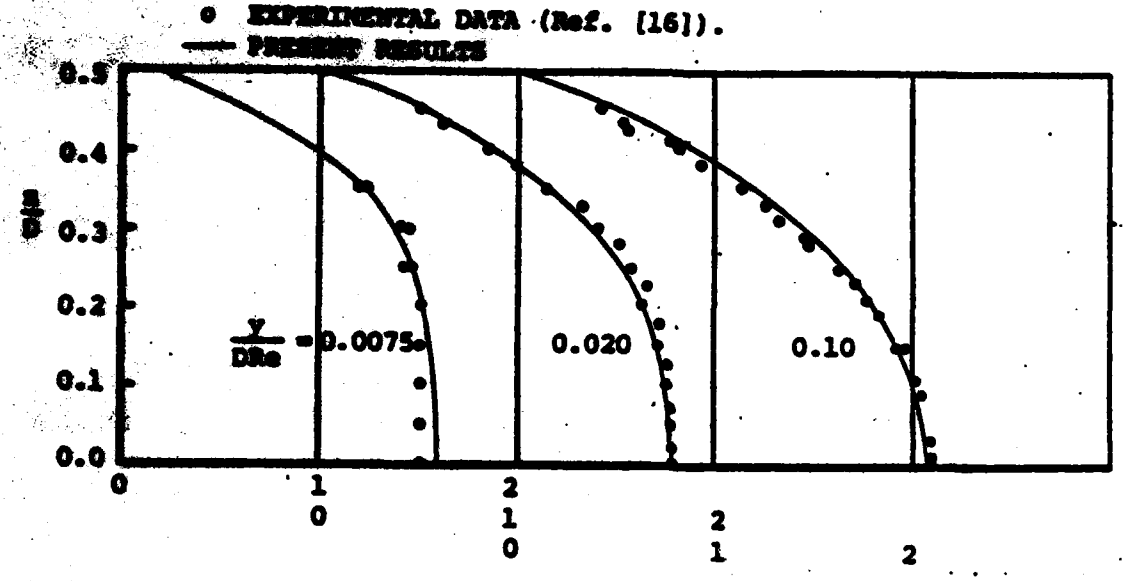

Fig. 8. Development of the Through Flow Velocity Profile at the Central Plane x = 0.

Figure 9 shows the development of the secondary velocity component, w, along the duct plane of symmetry, x = 0. No experimental measurements are available for comparison with the computed secondary velocities. Figure 9 shows that the maximum secondary flow is initially located near the solid boundaries, then moves towards the center of the duct and decreases as the flow proceeds towards fully developed conditions. The computed through flow velocity development along the duct centerline are compared with the experimental measurements of reference [16] in Fig. 10. One can see in this figure that the elliptic solution predicts an increase in the centerline through flow velocity in the cascade entry region preceding the actual duct entry. Figure 10 shows that the computations slightly underestimate the centerline velocity. Considering the coarse grid used in the numerical computations [(11 x 11 x 34) grid points in the duct], the agreement of the computed results with the experimental data as shown in Figures 8 and 10 is very satisfactory.

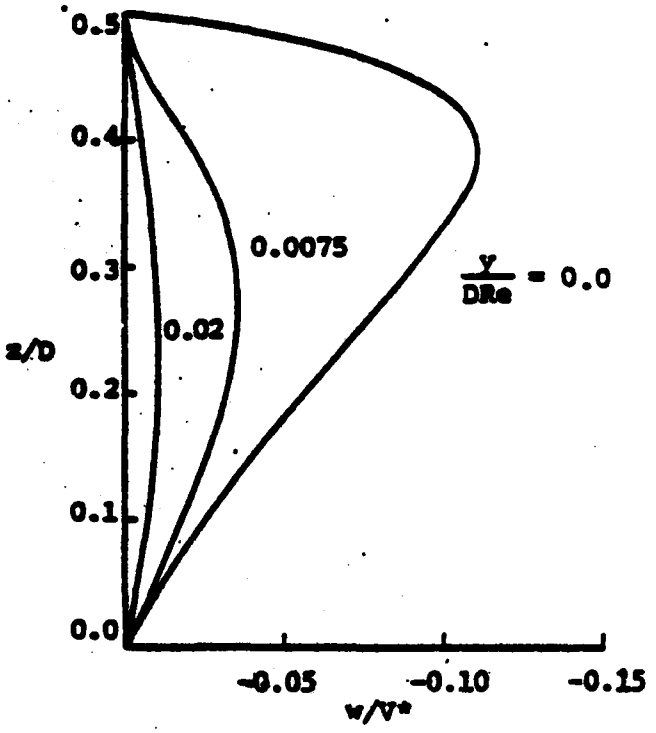

Fig. 9. The Development of Secondary Flow Velocity Profile at the Central Plane x = 0.

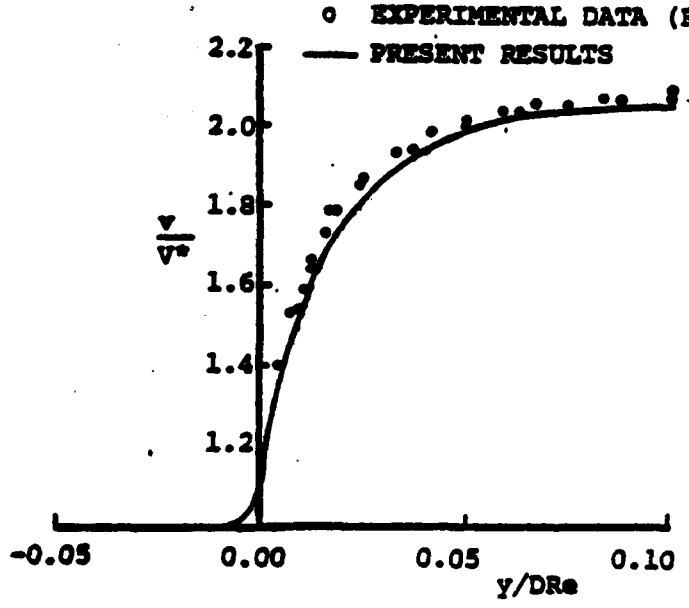

Fig. 10. Through Flow Velocity Development Along the Duct Centerline.

6. SUMMARY

This paper presents a fast efficient method for the 3-D incompressible solution of the Navier-Stokes equations. It is based on the streamline-function vorticity formulation which leads to 3-D Poisson equations with Dirichlet boundary conditions for the three streamline functions, in addition to the vorticity transport equations. The method is more economical than existing Navier-Stokes elliptic solvers, yet does not have the limitations of the parabolized and partially parabolized procedures. It offers a useful tool for the numerical solutions of 3-D internal viscous flow fields where surface curvature and downstream effects are significant, as in turbine blade passages. The results of the computations are presented for the viscous flow in a constant area duct, as a corner stone for more general future applications.

ACKNOWLEDGEMENT

This work was supported by the Air Force Office of Scientific Research under Grant No. 80-0242.

REFERENCES

1. DENTON, J.D., "A Time Marching Method for Two and Three Dimensional Blade-to-Blade Flows," ARC R&M 3775, 1975.

2. FAMOLARI, M. and GOLASURDO, G., "Three-Dimensional Inviscid Compressible Rotational Flows - Numerical Results and Comparison with Analytical Solutions," ASME Flow in Primary Non-Rotating Passages in Turbomachines, ASME Symposium, pp. 141-149, 1979.

3. BARBER, T. and LANGSTON, L.S., "Three Dimensional Modelling of Cascade Flow," AIAA Paper 79-0047, 1979.

4. DAVIS, R.T and RUBIN, S.G., "Non-Navier-Stokes Viscous Flow Computations," Computers and Fluids, Vol. 8, 1982, pp. 101.

5. RUBIN, S.G., "Incompressible Navier-Stokes and Parabolized Navier-Stokes Solution Procedures or Computational Techniques," VKI Lecture Series on Computational Fluid Dynamics, 1982.

6. AZIZ, A. and HELLUMS, J.D., "Numerical Solution of the Three Dimensional Equations of Motion for Laminar Natural Convection," The Physics of Fluids, Vol. 10, No. 2, February 1967, pp. 314-324.

[illegible], G.P., "Numerical Integration of the Three-[illegible]dimensional Navier-Stokes Equations for Incompressible [illegible] Flow," Journal of Fluid Mechanics, Vol. 37, Part 4, [illegible], pp. 737-750.

[illegible], F.J., Computational Fluid Dynamics, Hermosa, [illegible], New Mexico, 1972.

[illegible], D.E., "The Numerical Solution of the Navier-Stokes [illegible] for a Three-Dimensional Laminar Flow in Curved [illegible] Using Finite Difference Methods," Journal of [illegible] Mathematics, Vol. 12, No. 4, October 1978, pp. 303-323.

[illegible], D.E., "The Solution of the Three-Dimensional [illegible]-Stokes Equations Using a New Finite Difference [illegible]," Int. Journal of Numerical Methods in Engineering, Vol. 10, 1976, pp. 1299-1308.

[illegible], P.R., "Numerical Method for 2-D and 3-D Viscous [illegible]," AIAA Journal, Vol. 15, No. 7, 1977, pp. 961-965.

[illegible], A. and ABDALLAH, S., "Streamlike Function: A New Concept in Flow Problems Formulation," Journal of Aircraft, Vol. 16, No. 12, December 1979, pp. 801-802.

[illegible], S. and [illegible], A., "The Elliptic Solution of the Secondary Flow Problem," ASME Paper No. 82-GT-242, 1982.

[illegible], A. and LIU, C., "Three Dimensional Rotational Compressible Flow Solution in Variable Area Channels," AIAA Paper No. 83-0259, 1983.

PEYRET, R. and TAYLOR, T., "Computational Methods for Fluid Flow," Springer Series in Computational Methods, Springer-Verlag, New York, Heidelberg, Berlin, 1983.

GOLDSTEIN, R.J. and KREID, D.K., "Measurement of Laminar Flow Development in a Square Duct Using a Laser-Doppler Flow Meter," Journal of Applied Mechanics, December 1967, pp. 813-818.

[redacted]

H	duct height
L	duct length
Re	Reynolds number
t	time
u,v,w	velocity components in x, y and z directions
$\vec{q}$	velocity vector
u_0	normalising velocity at inlet
x,y,z	Cartesian coordinates
χ_x,χ_y,χ_z	streamline functions
ν	kinematic viscosity
$\vec{\omega}$	vorticity vector
ξ,η,ζ	vorticity components in x, y and z directions

[redacted]

c	refers to cross sectional plane
h	refers to horizontal plane
i	refers to inlet plane
v	refers to vertical plane

Appendix 6

LVD Measurements of Three-Dimensional Flow Development in a Curved Rectangular Duct with Inlet Shear Profile

AIAA-1984-1621

Measurements of Three-Dimensional Flow Development in a Curved Rectangular Duct with Thick Upper Profile

S. Sharma and M. Mobin, Dept. of Aerospace Engineering
Applied Mechanics, Univ. of Cincinnati, Cincinnati, OH.

AIAA 17th Fluid Dynamics, Plasma Dynamics, and Lasers Conference
June 25-27, 1984/Snowmass, Colorado

LDV MEASUREMENTS OF THREE-DIMENSIONAL FLOW DEVELOPMENT IN A CURVED RECTANGULAR DUCT WITH INLET SHEAR PROFILE

A. Hamed* and M. Malak**

Department of Aerospace Engineering and Applied Mechanics
University of Cincinnati
Cincinnati, Ohio 45221

Abstract

The results of an experimental investigation of the three-dimensional flow development in a highly curved duct with inlet shear profile are presented. The three components of the air velocity in a curved duct with a rectangular cross section are measured using Laser Doppler Anemometry. Significant through velocity contour rotations are reported with secondary velocity development of magnitudes up to 0.25 of mean inlet velocity in the 90° turning angle curved duct.

Introduction

The secondary flow affects the overall turbomachinery performance through its influence on the angle and the energy distribution of the flow leaving the blade rows. A deviation in the exiting flow angles from those predicted by the blade element analysis results from the secondary velocities. The secondary losses are also caused by the redistribution of the low energy flow by the same secondary velocities. These cross velocities are associated with the secondary velocity development in the streamwise direction through the turning of the flow with nonuniform inlet conditions in the blade passages.

Secondary flow in compressor and turbine cascades has been the subject of several theoretical and experimental investigations. In most of the experimental secondary flow investigations, the flow measurements have been limited to cascade inlet and exit conditions to provide empirical correlations for secondary flow losses and exit flow angles.

Langston[1] obtained detailed measurements showing the general characteristics of the end wall flow downstream of the saddle point and upstream of the turbine cascade passages. Moore[2] measured the total pressure and flow directions downstream of the turbine cascade trailing edge. Several investigators measured the development of secondary flow in curved ducts[4-7] from a fully developed inlet velocity profile. These studies demonstrate the secondary flow development in the absence of added complexities of the cascade blade leading edges.

In the present work detailed measurement of the three flow velocity components are obtained in a curved duct with a nearly linear shear flow inlet profile produced using a grid of parallel rods with varying spacing. Under these conditions, the development of the secondary velocities associated with the passage vortex is not limited to the boundary layer region near the wall, but extends instead through the whole passage sections. The experimental measurements of this complex flow field are based on the use of a two-color back scatter Laser Doppler Velocimeter.

EXPERIMENTAL SET-UP

The experimental set-up is shown schematically in Fig. 1. It consists of the tunnel, the seeding particle atomizer, the LDV, optical and data acquisition systems.

Tunnel

The high pressure air supply from the storage tanks is regulated to a lower pressure before entering the 12" diameter settling chamber. A 1.5" thick honeycomb of 0.187" cell and 0.003" wall thickness is placed in a 4" diameter PVC tube to condition the flow. The latter extends 18" inside the chamber and blends smoothly into a 22.75" long rectangular channel preceding the curved duct. The duct is shown schematically in Fig. 2 and consists of a 90° bend of 6" mean radius and a 2" x 4" rectangular cross-section. The duct walls are made of plexiglass. The thickness of the curved wall is equal to 1/8" while the plane walls are 3/4" thick. The curved duct is connected to straight ducts downstream and upstream where the shear flow is produced using a grid of parallel rods with varying spacing. The grid imposes a resistance to the flow that varies across the section so as to produce variation in the flow velocity, without introducing an appreciable gradient in static pressure. The basic relations between rod size, spacing and the produced velocity gradient were derived first by Owen and Zienkiewicz[8] and modified later by Livesey and Turner[9] and by Elder[10] for more generalized profiles. The basic relations for a grid to generate a uniform

---

* Professor; Associate Fellow AIAA.
** Graduate Research Assistant; Student Member AIAA.

[illegible] flow are given by the following equa-

$$[illegible] \quad (1)$$

[illegible] is the duct diameter

[illegible] is the mixing ratio

[illegible] is the duct height

[illegible] is the resistance parameter

[illegible] is the shear parameter.

The linear velocity profile produced by a [illegible] according to the above [illegible] and placed in a uniform velocity [illegible], U_o, is given by:

$$U = U_o + \lambda \left(y - \tfrac{1}{2} h\right) \quad . \quad (2)$$

The grid was designed according to [illegible] to produce a uniform shear [illegible] of 0.45 when placed in a [illegible] flow. A schematic of the [illegible] generating grid which was de-[illegible] with 0.375 inch diameter wires, is shown in Fig. 1, with the coordinate system and secondary velocity components.

A 6-jet atomizer was used to seed the flow with propylene glycol particles. The atomizer was connected to a secondary air supply to produce particles of 2 micron mean diameter at 1×10^5 particles/cm^3. The atomizer was connected to the back of the settling chamber through a flexible tube of 1.25" diameter.

Laser and Optics

A two-color 5 watts argon-ion Spectra Physics, model 164-09 Laser is used in the backward scatter mode to measure two simultaneous velocity components of a single particle. The laser beams are brought into one common measuring volume using a transmitting lens of 250 mm focal length. The crossing angle for the incident 1.5 mm diameter beams was 11.05 degrees. The measuring volume is approximately ellipsoidal in shape with the geometrical parameters shown in Table 1.

A 40 MHz Bragg cell and downmixer were used in one of the colors to obtain frequency offsets ranging between one and [illegible] MHz in the secondary velocity measurements. The maximum doppler frequency was 3 MHz for the secondary velocities, and 10 MHz for the through flow velocity.

The laser and optical systems are mounted on a table designed such that [illegible] can be traversed in the [illegible] direction, as well as along and [illegible] to the laser and optical [illegible] in the horizontal plane. The whole [illegible] is mounted on a platform that rotates [illegible] the curved duct vertical axis. This [illegible] degree of freedom is used to [illegible] measurements through the outer curved wall. Finally the mountings of the sending and receiving optics are designed to allow for rotation around the optical axis up to 90°, in order to obtain the measurements of the two velocity components in any specified direction.

TABLE 1

LDV CHARACTERISTICS

	Blue	Green
Wavelength	0.448 μm	0.5145 μm
Fringe spacing	2.534 μm	2.672 μm
Diameter of measuring volume at the $1/e^{-2}$ intensity location,	0.1045 mm	0.1097 mm
Length of measuring volume at the $1/e^{-2}$ intensity location,	1.08 mm	1.134 mm
Number of stationary fringes	41	41

Two signal processors and a DIGITAL MINC 11/23 computers were used on line to acquire synchronized data for the simultaneous measurements of the two velocity components.

RESULTS AND DISCUSSION

The high pressure air supply from air storage tanks was regulated to a pressure of 2.0684×10^5 N/m^2 gauge (30 psig) at the orifice meter, using a pressure regulating valve, to give an air mass flow of 0.1143 kg/sec (0.252 lb/sec). This corresponds to Reynolds number of 1.3×10^5, based on the height of the duct and the mean inlet velocity of 20 m/sec (66 ft/sec), upstream of the shear velocity generator.

The experimental velocity measurements were obtained at sections B, C, D and E as shown in Fig. 2. Sections C and D are located in the curved duct at the 45° and 75° turning angles, while the first and last measuring stations B and E are located in the straight portions of the tunnel. A quarter inch spacing between the measuring points in the radial direction and also in the direction normal to the duct plane walls was kept in the measurements at all four cross sections. The velocity measurements were, therefore, obtained at 105 points of a 7 x 15 grid in every section. In order to determine the three velocity components at each measuring point the measurements were obtained once with the Laser-optics axis perpendicular to the duct plane wall, then repeated with the Laser-optics axis perpendicular to the curved wall. The first set of measurements provided the through flow velocity U, in the direction normal to the tunnel cross-

sections, and the radial velocity components, V_x, while the second set of measurements give the third velocity component V_y and also the through flow velocity U. The through flow velocities from the two sets of measurements were compared to determine the repeatability of the data after the duct is rotated 90° relative to the settling chamber. The difference between these two values was not found to exceed 3.5% in the reported measurements. The results of the experimental measurements of the three velocity components normalized with respect to the mean flow velocity U_b, upstream of the shear generating grid, are presented in Figures 4 through 11.

The profiles of the normalized through flow velocity (U/U_b) are presented at seven concentric cylindrical surfaces between the duct inner and outer curved walls at sections B, C, D and E in figures 4, 5, 6 and 7 respectively. One can see that the shear generating grid produced the desired linear velocity variation in the z direction except in the region near the upper wall where the velocity gradient is higher. This deviation was due to the influence of the distance of the last grid wire from the upper wall. This factor was not found to have significant effect near the lower wall where the wire grid spacings are smaller. Other shear velocity generating grids with different wire diameters (0.039" and 0.125") have been investigated. The forementioned effect was even more pronounced in the case of larger wire diameter grid. On the other hand, the velocity profiels produced by the grids of the smaller wire diameter were found to produce velocity variations along the wire length. Careful examination of the grid revealed non-uniformities in the wire spacings in this direction, which was found difficult to control. Figures 5 through 7 demonstrate the change in the through flow velocity profile with the duct turning angle. Initially, the flow accelerates along the inner wall and decelerates along the outer wall to approach potential free vortex velocity distribution. This can be seen by comparing the velocity profiles in Figures 4 and 5, at x = 1.75" and x = 0.25" respectively. Later on the flow decelerates along the inner wall and accelerates along the outer wall. This pattern is reinforced by the secondary flow velocity development, which tend to transfer the slower moving flow towards the inner wall as can be seen by comparing the profiles at x = 1.75" in Figures 6 and 7.

The profiles of the normalized secondary velocity in the radial direction (V_x/U_b) are also presented at seven concentric cylindrical surfaces which are equally spaced at 0.25" between the inner and outer curved walls of the duct. Figure 8 combines all the profiles at sections C,D and E, as the LDV measurements did not indicate any significant secondary velocities at section B. On the other hand, the profiles for the normalized secondary velocity for the normalized secondary velocity in the vertical direction (V_y/U_b) are presented at 15 parallel planes which are equally spaced at 0.25" between the duct plane walls as shown in Fig. 9. The same symbols which were used for the through flow velocity profiles at sections C, D and E are also maintained in presenting the measured secondary velocities in Figures 8 and 9. The vertical component of the secondary velocity, V_z, was not measured at section D-D, due to the deterioration of the quality of the duct curved outer wall after obtaining the measurements at the other sections. The maximum secondary velocity components were measured at section E-E and were found to be 0.264 in the radially inward direction near the duct upper wall and 0.138 in the vertically upward direction near the duct inner wall. These values are also normalized by the inlet flow velocity, U_b, before the shear generating grid.

The two measured secondary velocity components were combined to produce the secondary flow patterns at sections C and E which are shown in Figures 10 and 11, respectively. From these figures the development of the passage vortex due to the nearly linear shear inlet flow profile can be observed throughout the duct cross-sections. The secondary velocities associated with this vortex tend to move the slower flow in the lower duct sections towards the inner curved wall and the faster flow in the upper duct sections, towards the outer curved wall. One can see from Gig. 10 that, the center of the passage vortex at the 45° turning angle is nearly in the middle between the inner and outer curved walls but closer to the duct upper wall at Y = 0.62h. A close examination of Figures 10 and 11 reveals that the center of the passage vortex moves towards the duct lower wall and also in the outward radial direction as the flow turning angle increases from 45° to 90° between sections C and E.

CONCLUSIONS

LDV measurements were presented for the three velocity components of the flow in a rectangular curved duct with shear inlet velocity profile. Secondary velocities of magnitudes greater than 25% of the main velocity, were measured after the 90° flow turning angle. The results demonstrate the passage vortex development throughout the duct cross-sections with the flow turning angles. These experimental results, can therefore be used to validate both viscous and inviscid codes for internal three dimensional rotational flow fields.

ACKNOWLEDGEMENT

This research was sponsored by the U.S. Air Force Office of Scientific Research under Grant No. 80-0242.

REFERENCES

1. Langston, L.S., "Crossflows in a Turbine Cascade Passage," Trans. ASME, Journal of Engineering for Power, Vol. 102, October 1980, pp. 866-874.

2. Moore, J., "Flow Trajectories, Mixing and Entropy Fluxes in a Turbine Cascade," AGARD-CP-351.

3. Melling, A. and Whitelaw, J.H., "Turbulent Flow in a Rectangular Duct," Journal of Fluid Mechanics, Vol. 78, Part 2, 1979, pp. 289-315.

4. McMillan, O.J., "Mean Flow Measurements of the Flow Field Diffusing Bend," NASA CR 3634, November 1982.

5. Humphrey, J.A.C., Taylor, A.M.K. and Whitelaw, J.H., "Laminar Flow in a Square Duct of Strong Curvature," Journal of Fluid Mechanics, Vol. 83, Part 3, 1977, pp. 509-527.

6. Humphrey, J.A.C., Whitelaw, J.H. and Yee, G., "Turbulent Flow in a Square Duct with Strong Curvature," Journal of Fluid Mechanics, Vol. 103, 1981, pp. 443-463.

7. Lasser, R., "Measurements of Secondary Flows Within a Cascade of Curved Blades and in the Wake of the Cascase," ASME Paper No. 83-GT-24.

8. Owen, P.R. and Zienkiewicz, H.K.,"The Production of Uniform Flow in a Wind Tunnel," Journal of Fluid Mechanics, Vol. 2, 1957, pp. 521-531.

9. Livesey, J.L. and Turner, J.T., "The Generation of Symmetrical Duct Velocity Profiles of High Uniform Shear," AIAA Journal, Vol. 4, 1966, pp. 1490-1491.

10. Elder, J.W., "Steady Flow Through Non-Uniform Gauges of Arbitrary Shape," Journal of Fluid Mechanics, Vol. 5, 1959, pp. 355-368.

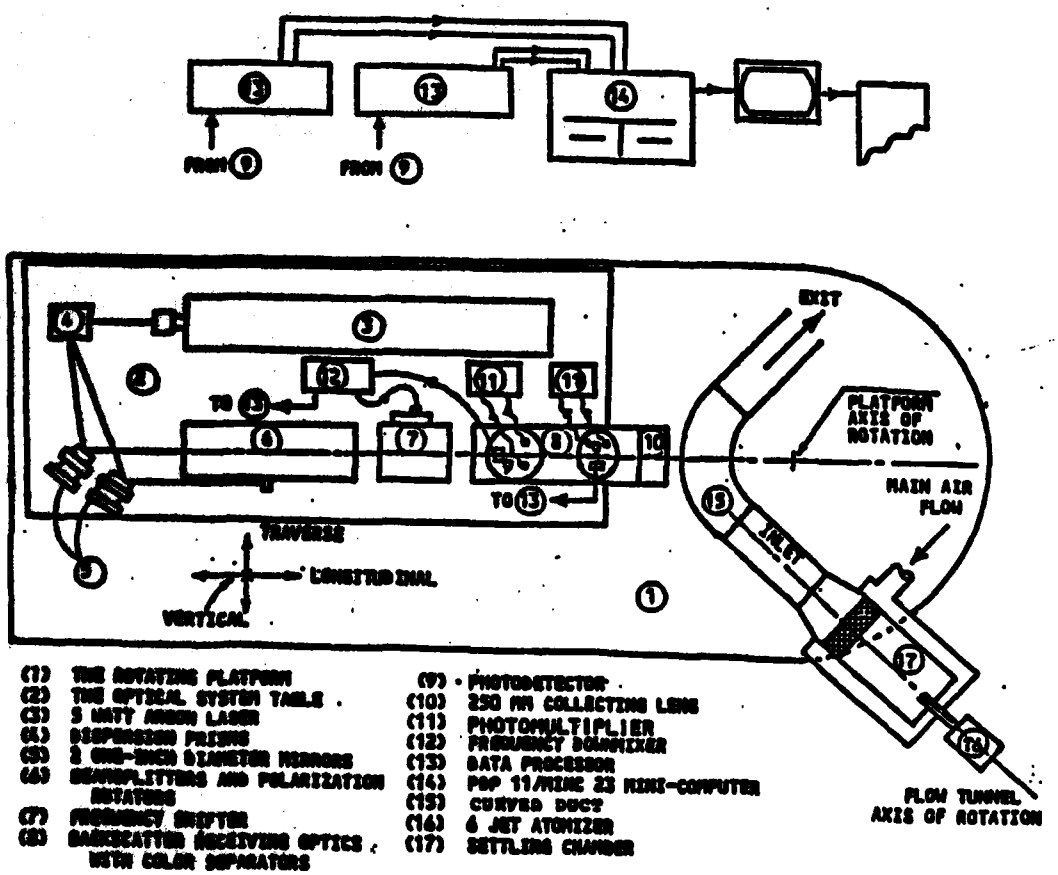

FIG. 1. SCHEMATIC SHOWING THE EXPERIMENTAL SET-UP.

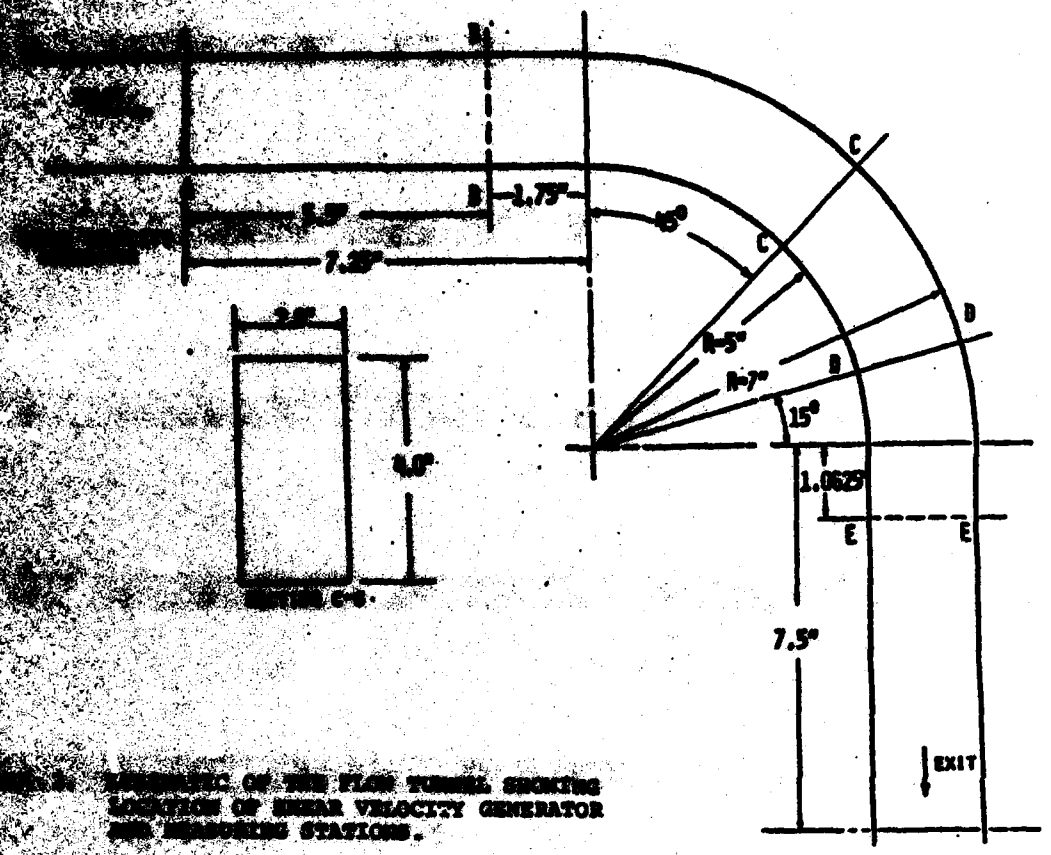

[illegible] SCHEMATIC OF THE FLOW TUNNEL SHOWING LOCATION OF SHEAR VELOCITY GENERATOR AND MEASURING STATIONS.

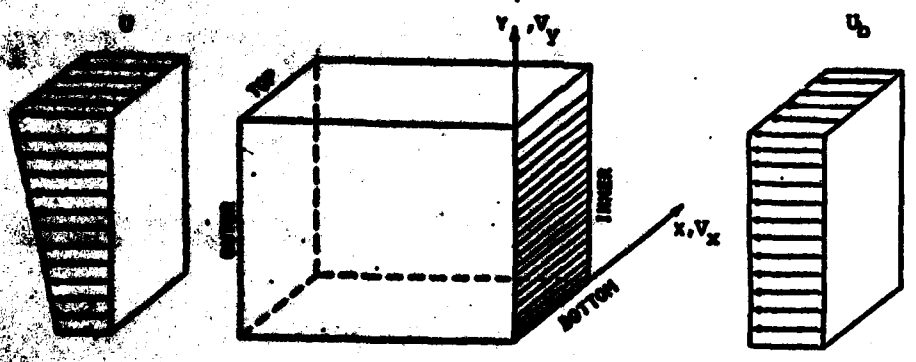

[illegible] THE SHEAR VELOCITY GENERATOR AND COORDINATE SYSTEM

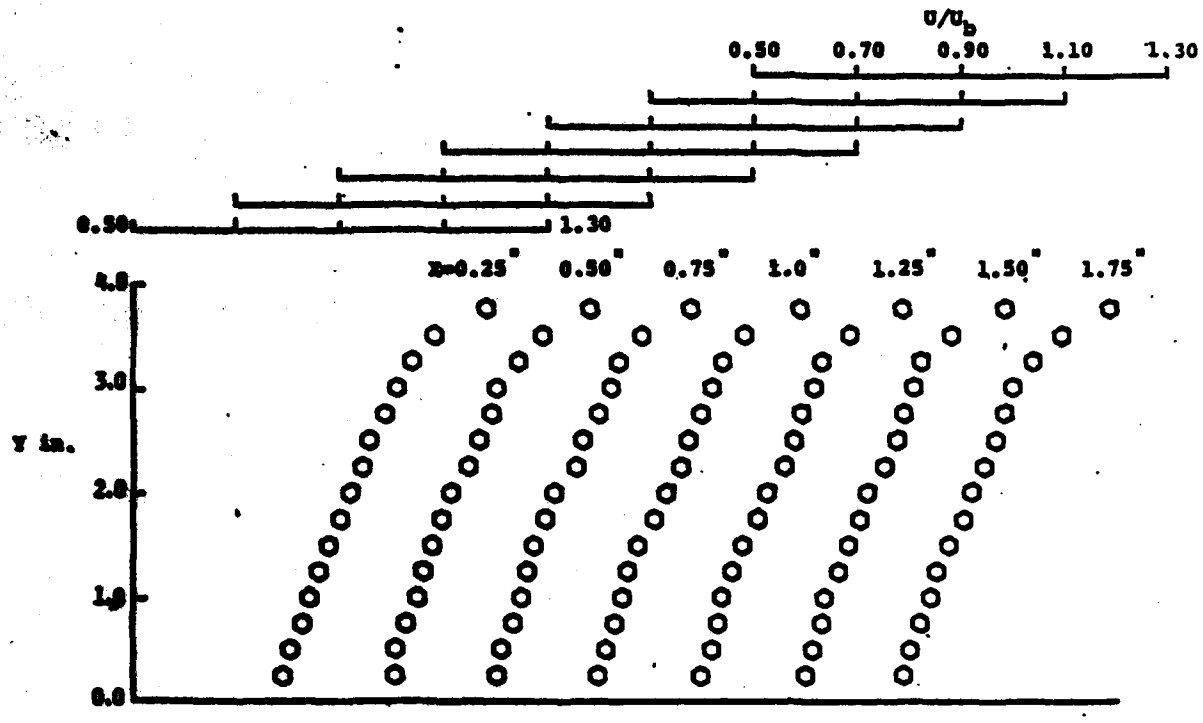

FIG. 4. NORMALISED THROUGH FLOW VELOCITY AT SECTION B-B

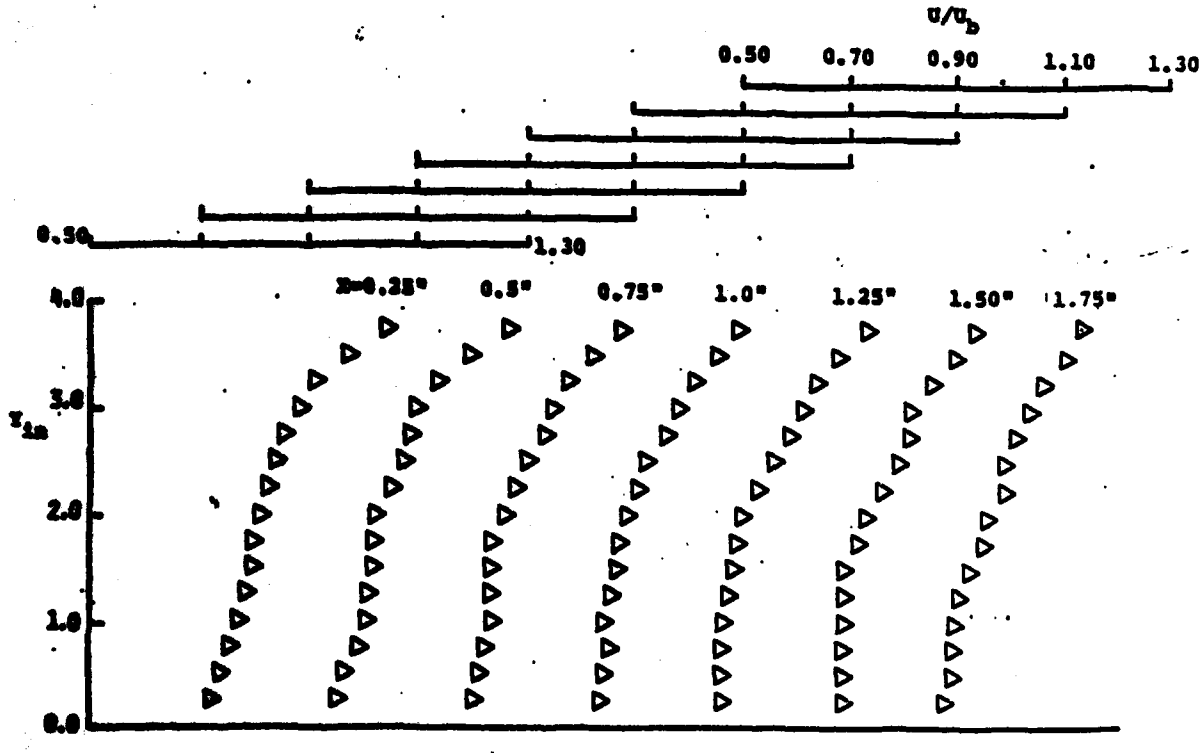

FIG. 5. NORMALIZED THROUGH FLOW VELOCITY AT SECTION C-C

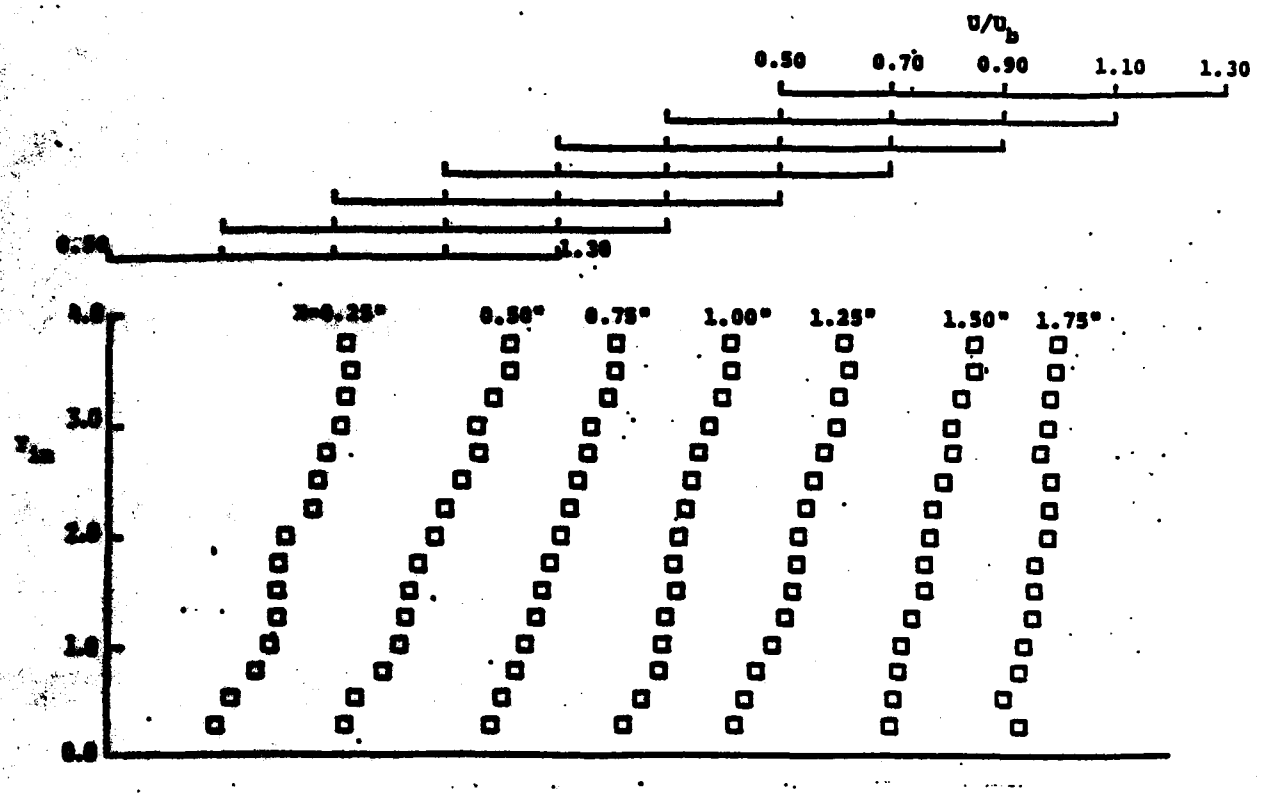

FIG. 6. NORMALISED THROUGH FLOW VELOCITY AT SECTION D-D

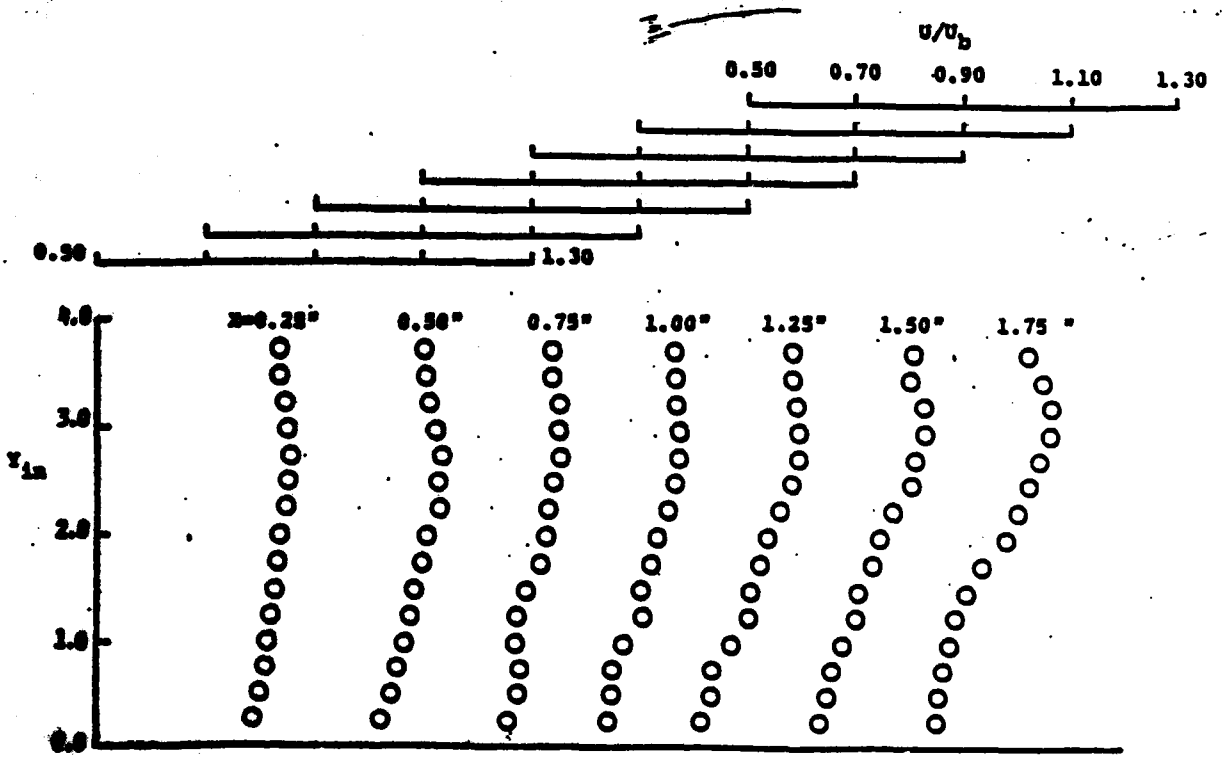

FIG. 7. NORMALISED THROUGH FLOW VELOCITY AT SECTION E-E

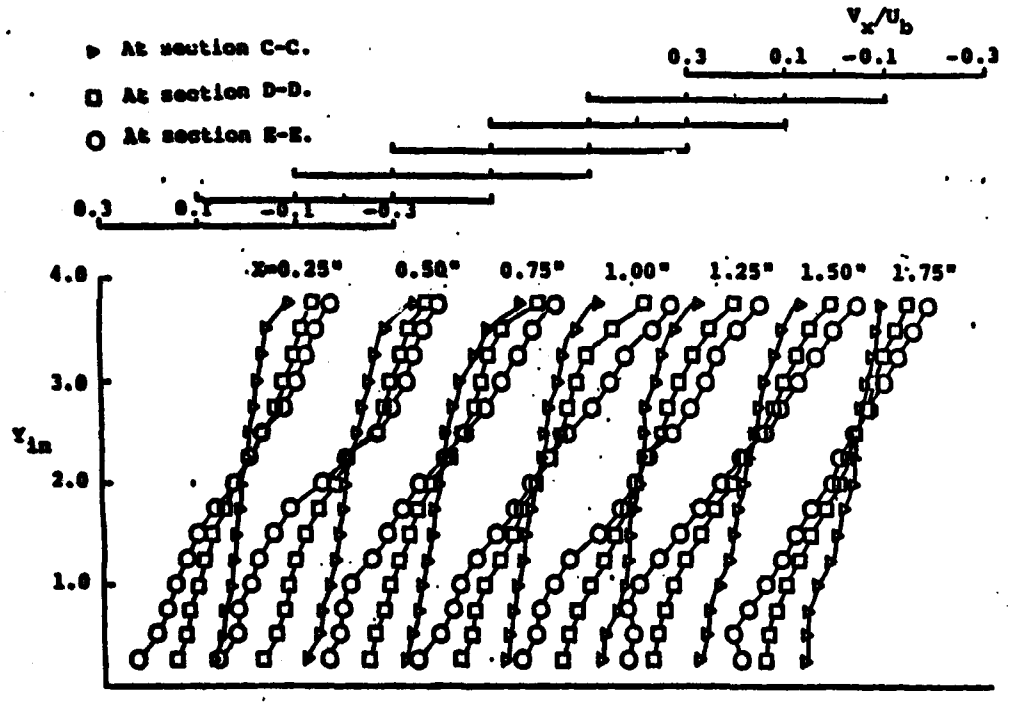

FIG. 8. NORMALIZED SECONDARY FLOW VELOCITY COMPONENT IN RADIAL DIRECTION

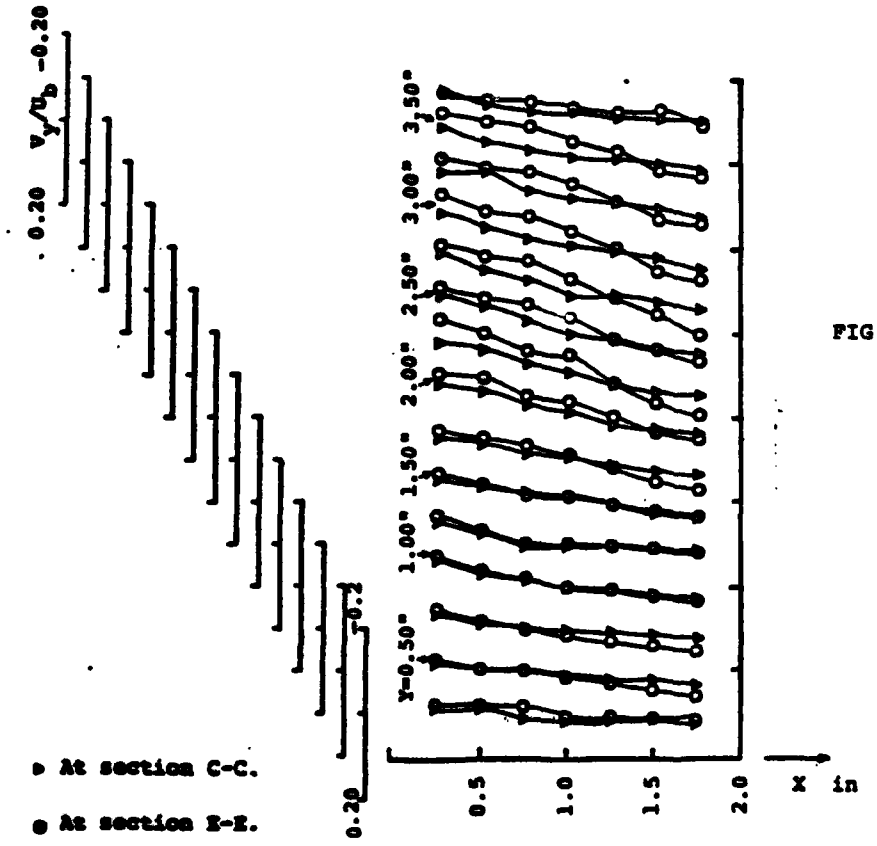

FIG. 9. NORMALIZED SECONDARY FLOW VELOCITY COMPONENT IN THE VERTICAL DIRECTION

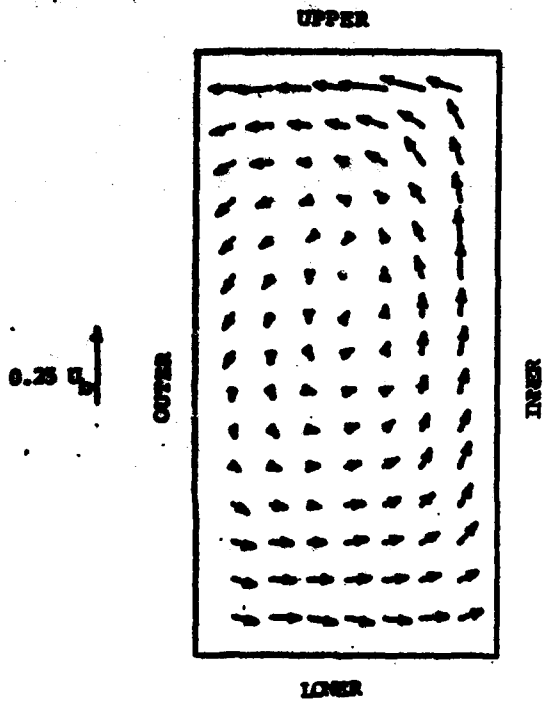

FIG. 10. SECONDARY FLOW VELOCITY AT SECTION C-C

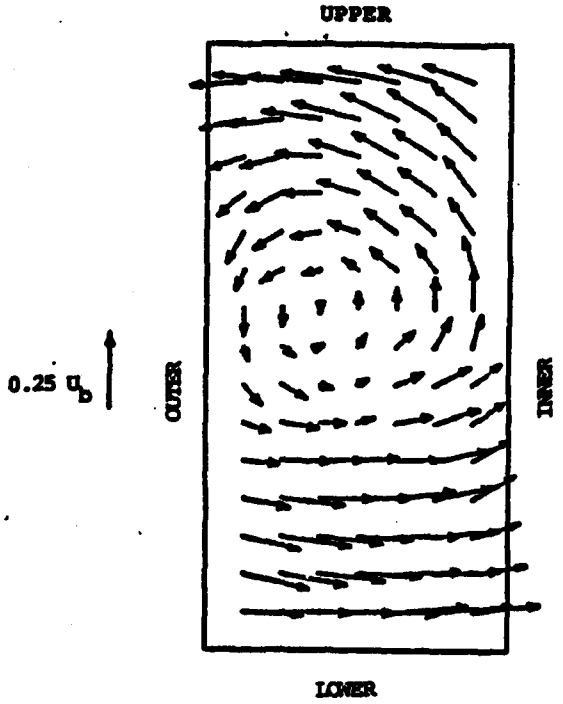

FIG. 11. SECONDARY FLOW VELOCITY AT SECTION E-E

END

FILMED

1-85

DTIC